January 2018

Channel Fading Statistics For Real-Time Data Transmission In Emergency Call Systems And Unmanned Aerial Systems

Yunrui Li
Wayne State University, yunrui.li@wayne.edu

CHANNEL FADING STATISTICS FOR REAL-TIME DATA TRANSMISSION IN EMERGENCY CALL SYSTEMS AND UNMANNED AERIAL SYSTEMS

by

YUNRUI LI

DISSERTATION

Submitted to the Graduate School

of Wayne State University,

Detroit, Michigan

in partial fulfillment of the requirements

for the degree of

DOCTOR OF PHILOSOPHY

2018

MAJOR: ELECTRICAL ENGINEERING

Approved By:

_____

Advisor Date

_____

_____

_____

_____

ACKNOWLEDGEMENTS

I would like to thank my advisor, Dr. John Liu, for his guidance and nurturing. He provided everything I needed for my research and experiment. I will be always grateful for his encouragements and support, not only for my research, but also for the difficulties in life. Without his patience and encouragements, I would not be able to accomplish the research I have achieved. I also would like to thank my Ph.D. committee members, Dr. Harpreet Singh, Dr. Ivan Avrutsky, and Dr. Shiyong Lu, for their valuable guidance and suggestions. I would like to express my deepest appreciation to my wife and my parents for their encouragement and support during my difficult times. The years I spent in the laboratory along with Dr. Jacob Brandenburg are sweet.

TABLE OF CONTENTS

LIST OF TABLES

LIST OF FIGURES

CHAPTER 1 INTRODUCTION

1.1 Background and Motivation

In our current society, mobile real-time communication is becoming increasingly vital, especially in emergency situations, such as car accidents, life-threatening medical situations, hurricanes or earthquakes. The European Union (EU) has been committed to deploying a pan-European in-vehicle emergency call (eCall) system to enhance road safety. The eCall system transmits real-time emergency data via an in-band modem of the cellular voice channel. The in-band modem can also be used for real-time unmanned aerial system (UAS) tracking, command and control. Recently the UAS industry has been experiencing steady growth. UASs have been used in numerous applications including infrastructure inspection, wildfire management, disaster monitoring, mapping, wind estimation, filmography, traffic control, and search, and rescue and medical aid [1, 2]. The Federal Aviation Administration (FAA) requires a radio link between the UAS and the operator for real-time UAS ID tracking, command and control [3].

The EU delegated the Third Generation Partnership Project (3GPP) to standardize the technical specifications of the eCall data transmission. After careful study, the 3GPP group selected the in-band modem solution operating through the voice channel of 2G/3G cellular network and public switched telephone network (PSTN) for the emergency data transmission [4]. This is the best choice and the right technical approach to minimize the delay of emergency data transmission. The digital cellular voice channel is circuit-switched, and the signal transmission is real-time. The capacity of the digital cellular voice channel is sufficient for emergency data communication [4]. In 2G/3G cellular networks, the voice channel is of higher priority than data channels. Additionally, the voice channel

coverage is much wider than the coverage of data channels.

In case of a traffic accident, even if the driver and the passengers are unconscious and unable to make a call, the in-vehicle system (IVS) can autonomously detect the accident, dial the European unified emergency call number 112, and report the location of the vehicle, through transmitting the emergency data to the Public Safety Answering Point (PSAP) [5]. To ensure timely, accurate and reliable emergency data transmission, on April 28, 2015, an eCall regulation was approved by the European Parliament to finalize the legislative process for the EU eCall deployment. The regulation requires all new passenger cars and light vans in the EU market to be provided with an eCall device by March 31, 2018 [6].

Road traffic accidents bring severe social and economic losses not only to EU, but also cause enormous losses in other countries across the globe. It is commonly accepted that comparing road fatality rates among different countries can provide good indication about safety levels in such countries. In the 2015 World Health Organization (WHO) report Global Status Report on Road Safety [7], around 26,000 individuals, in the EU, lost their lives in traffic accidents, in 2013 only. The traffic fatality rate was about 52 per million inhabitants, which was the lowest fatality rate in the world at the time. The United States reported 34,064 traffic fatalities on the road, during the same year, resulting in approximately 106 deaths per million people; i.e. nearly twice that of the EU. WHO estimated that the number of road deaths, in China, was about 261,000 in 2013, yielding a rate of 188 deaths per million people. In 2013, the world's average traffic fatality rate was 174 per million inhabitants. The total number of traffic fatalities reached 1.25 million in the world's 180 countries and regions; most of which were in low-income developing countries. The

data also indicated that casualties due to road traffic accidents have an enormous impact on the global economy. Traffic accident casualties cause substantial social and economic losses at up to 3% of the global Gross Domestic Product (GDP) losses. Successful deployment of the eCall system would benefit the EU. Moreover, establishing eCall as an international standard would also have a significant global impact [8].

The EU eCall system can be activated automatically or manually to call an emergency center and route rescue services swiftly to an accident site [4, 9]. In the event of an accident, an IVS autonomously initiates an emergency call to the appropriate PSAP via activation of in-vehicle sensors. Additionally, the passengers of the vehicle can also press an emergency button to make the call. Once a voice connection is established, the IVS transmits a minimum set of data (MSD), including the vehicle identification number (VIN), the time, vehicle location, driving directions, and other relevant information to the PSAP. After successfully receiving the data, a PSAP operator begins speaking with passengers in the vehicle. The PSAP operator organizes the necessary rescue services and oversees the entire process, until it is concluded. The foreseen advantage is that the PSAP obtains the precise accident location and vehicle type rapidly; thus enabling the rescue service to reach the accident's victims in a timely manner, and ultimately, save more lives in Europe.

The eCall system is foreseen to cut rescue time by 60% in urban areas and 50% in rural parts of the EU [10, 11]. The quicker response would save thousands of save thousands of lives and decrease the severity of injuries. Clearly, the eCall system has great social impact, regarding reducing human suffering, in addition to the economic impact through reducing costs of health care and other related costs [12, 13].

1.2 Literature Review

Car manufacturers and governments have always valued the use of in-vehicle emergency call systems to enhance road safety. In 1996, General Motors (GM) launched the OnStar mobile emergency communication services in the USA employing in-band modem to transmit emergency data from vehicle to the call center. In 1997, BMW started to offer emergency communication services using the short message service (SMS) for emergency data transmission. Other automotive manufacturers have followed the practice, and the automotive telematics has become popular worldwide. In 2002, the European Commission (EC) established the eSafety initiative, which recommended the use of advanced information and communication technology to implement intelligent vehicle safety systems to improve road safety [14]. In 2004, a memorandum of understanding (MoU) was issued by the eCall Driving Group to provide the definition, framework, and feasibility of in-vehicle eCall systems [15]. In 2005, the EC commissioned the European Telecommunications Standards Institute (ETSI) Mobile Standards Group (MSG) to begin the standardization for the eCall system.

In 2006, the global system of mobile telecommunications (GSM) Europe conducted a comprehensive assessment of MSD transmission solutions including Short Message Service, User to User Signaling, Unstructured Supplementary Service Data, GSM Circuit-Switched Data, Dual Tone Multi-Frequency (DTMF), and In-band Modem technologies. GSM Europe concluded that the in-band modem is the only suitable solution. The cellular voice channel has higher priority for acquiring channels, is more reliable and provides wider coverage and faster connection establishment than cellular data channels. These properties can be exploited in low bit-rate, high priority emergency applications that require

data to be transmitted immediately. Moreover, this solution does not require modifying the cellular or PSTN networks. The 3GPP began standardizing an in-band modem specification for the eCall system with the delegation of the European Commission and ETSI [16].

The 3GPP standardization organization began to select eCall in-band modems in 2007. In the first phase, the 3GPP evaluated cell phone text telephony modem (CTM) [17] according to the eCall service requirements. The CTM did not meet all the requirements of the eCall system. In the second phase, several in-band modem solutions were then tested in the laboratory. Based on those testes, the official selection was made in August, 2008. It was established that Qualcomm's solution met the eCall requirements per these laboratory tests. With the strong support of the EU government, the first international standard in telematics was released by the 3GPP standard group as TS 26.267, 26.268, 26.269 in 2009. The 3GPP standardization group completed the appropriate verification, characterization, and modem specifications. From March 2009 to June 2018, the 3GPP group updated the technical specifications of the eCall in-band modem and released multiple versions from Version 2.0 to Version 15.0. As previously mentioned, the European Commission adopted proposals to enforce mandatory IVS installment in all new passenger cars and light commercial vehicles models, by March 31, 2018 [18].

A testbed was designed and built by our team to study the performance of the EU eCall system [19]. Extensive experimental work has been performed using the testbed. It was found that deep fading still exists in the voice channels of the GSM and the CDMA2000 system after power control. Such fading is not negligible. For emergency data transmission, the fading can cause severe performance degradation in signal detection, demodulation, and decoding. It must be measured carefully and accounted for in the system

performance evaluation, especially for emergency data transmission through digital cellular voice channel for systems like the 3GPP TS 26.267

In [20], the authors discussed the eCall system requirements and the selection process of the in-band modem solution by the 3GPP. The in-band modem solution proposed by Qualcomm was selected after comparing three proposals through PC-to-PC computer simulations. However, many realistic factors in the digital cellular network were not considered in the selection process, such as echo canceller, noise canceler, handover and the effects of transcoding between codecs, implemented in digital cellular networks and PSTN.

The authors of [21] obtained the bit error rate (BER) and signal-to-distortion power ratio (SDR) for the EU eCall modem through a GSM adaptive multi-rate (AMR) vocoder and additive white Gaussian noise (AWGN) channel. The uncoded BER was determined by simulation using C code of various GSM vocoders. The authors also attempted to find an optimal receiver filter for the PSAP demodulator. It was shown that the AMR vocoder could cause significant SNR degradation to the 3GPP in-band modem output signal. For example, when the AMR vocoder rate is 4.75 kbps, the SDR at the vocoder output is 4 dB for the robust modulation mode or 3.9 dB for the fast modulation, causing the demodulation error rate to be 0.041 or 0.14, respectively.

Some field test results were reported in Finland [22]. The work also reported that the success rate of the MSD transmission varied significantly at different test sites. In effect, temporal variations of signal power have effects on the success rate of MSD transmission. The success rate of the MSD varied from 71% to 100%, among the countries that attended the Harmonized eCall European Pilot (HeERO) project. The report pointed

out that there is a great potential to increase the MSD success rate and decrease the MSD transmission delay, in practical operating conditions. In [23], the authors applied the Gilbert-Elliott model to the voice channel and obtained the capacity bounds for in-band modem data transmission through the voice channel. They also proposed an improved detection scheme invoking Weibull and Chi-square distributions.

In other efforts, authors evaluated the multiple frequency-shift keying (M-FSK) modulation scheme on transmitted data over the cellular voice channels [24]. A desktop computer connected to a mobile phone was used to transmit the M-FSK modulation signal while another desktop computer connected to another mobile phone received the modulated signal and demodulated the information. The test model featured public land mobile network (PLMN)-PLMN architecture. Optimal modulation parameters and data transfer rates were determined in a series of experiments, using this model. Data transmission was optimal using a 16-FSK modulation scheme and corresponding transmission speed was between 80 to 250 bits/s, and the bit error rate without error coding was less than 10^{-2}. This testbed model differs distinctly from the eCall PLMN-PSTN architecture. The EU eCall data rate is 1500 bits/s or 750 bits/s, which is faster than the 16-FSK modulation used in the test.

An autoregressive model of speech production was applied to design the modulation and demodulation scheme for data transmission in [25]. The author analyzed speech signal characteristics based on the autoregressive modeling principle. A speech-like modulation signal was generated and transmitted through the voice channel of the GSM system. The autoregressive model was also used to analyze the demodulator which demodulated the incoming modulation signal. The results showed that the performance of the proposed

modulation scheme was better than that of the FSK modulation scheme in general, but the performance of the FSK modulation showed superior performance, when the transmission rate was less than 250 bits/s.

The EU eCall emergency data is, ideally, transferred from IVS to PSAP via the GSM voice channel within four seconds to ensure that the driver receives timely assistance [26]. The technical specifications under Qualcomm's modem solution allow for MSD to be transmitted within four seconds successfully in some test cases. However, these tests were performed in a laboratory environment, and thus do not adequately reflect real-world channel characteristics. The test scenario included running IVS and PSAP on two computers connected via Ethernet to evaluate modem performance under the influence of various codecs, e.g., GSM full rate (GSM-FR) vocoder and AMR vocoder for voice coding in GSM and UMTS networks. The impacts of echo cancellers or noise cancellers, switching, possible execution errors, and transcoding effects between codecs using mobile versus fixed telephone networks were not measured in the test. Although the delay is extended to 20 seconds under the newest standards, according to the NXP Semiconductors road trial and HeURO road test results, current methods do not guarantee a 20-second-maximum delay [27].

Multipath propagation fading between cellphone antenna and base transceiver station (BTS) radio receiver without power control was studied in [28, 29]. Anti-fading techniques have been employed to decrease the impact of fading [30], which include power control [31, 32], diversity [33], interleaving and channel coding [34], etc. The received analog voice signal through the cellular voice channel meets the quality requirements for voice transmission, but it is still unknown whether fading has impacts on the in-band modem

solution significantly. Existing technical specification [4] and core standards only describe requirements, architecture, and simulation conformance tests on the EU eCall system. The 3GPP eCall conformance tests and previous data modulation schemes treated the digital voice channel, as if it were an AWGN channel.

To ensure successful deployment of eCall, core standards [35, 26, 36] of the system had been released in 2011 The latest standards were updated in 2015. The standard EN 15722 [35] defines the eCall MSD format. The standard EN 16072 [36] gives a detailed description of the eCall operating requirements, while the standard EN 16062 [26] introduced the eCall high-level application requirements (HLAP), using 2G/3G voice channel of the circuit-switched networks. Fading has rendered the original goal of the EU eCall standard impossible, meaning MSD transmission delay under four seconds is impossible to attain.

Data transmission through the cellular voice channel is very challenging and demands more research to understand the channel. The EN15722:2015 standard defines the emergency data as the MSD which is a packet of 140 bytes. In the eCall system requirements, it is written that “The MSD should typically be made available to the PSAP within 4 seconds, measured from the time when end to end connection with the PSAP is established.” (Section 4.2, 3GPP TS 26.267, Version 15.0.0, July 2018 [4]). This requirement has remained unachievable since the publication of the first version of the standard in 2009. The road test results presented by Harmonized eCall European Pilot (HeERO) project showed that counting all of the MSD packets successfully delivered, the delay of the MSD transmission had a mean of 13 seconds and the minimum duration of 8 seconds, while the success rate of the MSD delivery was 71% for long number [37]. Since this system is for emergency

communications, the 29% failure in MSD delivery needs to be improved. More extensive research needs to be performed to understand the channel, before the requirement of delay in the standard can be met.

In our experiments, it was found that although the GSM system employs power control for its voice channel, heavy fading still exists in the output signal of the GSM voice channel. This fading affects the success rate of MSD transmission. The impact of fading, in the GSM voice channel output on the performance of the EU eCall MSD transmission, is still to be well investigated and yet to appear in the literature.

1.3 Dissertation Organization

The remainder of this dissertation is organized as follows.

Chapter 2 gives an overview of the EU eCall system architecture and channel model. The eCall system requirements and architecture are discussed in detail followed by the mathematical system model of the channel and the relation between the transmission power control interval and MSD packet duration.

Chapter 3 describes the hardware design of the in-vehicle system and the measurements and experimental design for the fading statistics.

Chapter 4 presents the fading statistics of the eCall system. Signal power measurements and fading in the GSM voice channel, as determined experimentally, are reported. Our statistical analysis of the data and a discussion on the cumulative fading distribution of the voice channel with power control in the GSM system are also provided in this chapter.

Chapter 5 derives analytical expressions for error probability performance. The numerical results of the eCall in-band modem performance are presented in this chapter.

Chapter 6 provides the synchronization frame generation, transmission, and detection

for the up-link channel in the 3GPP eCall system. Timing synchronization detection procedure and algorithm for the in-band modem are introduced. Finally, data analysis and performance evaluation are discussed in this chapter.

Chapter 7 presents a testbed for full duplex real-time UAS communications using the eCall data transmission channel. The testbed is used to measure the power of signals received by the UAS in flight for the downlink and by the receiver in the operation center for the uplink, respectively. A novel method is proposed to measure the power of cellular networks and obtain fading statistics for full duplex real-time UAS communications. The channel fading statistics for the UAS communication are obtained.

Chapter 8 summarizes the dissertation and discusses future research directions related to this dissertation.

CHAPTER 2 SYSTEM ARCHITECTURE AND CHANNEL MODEL

In the event of an accident, the eCall system automatically or manually establishes an emergency voice call between the IVS and a nearby PSAP center via the cellular network. The IVS transfers a data message denoted as the eCall MSD to the PSAP over the in-band modem of the cellular voice channel. The MSD, as discussed above, can be transmitted immediately following the connection of the voice call.

2.1 System Requirements and Architecture

2.1.1 The Emergency Call System Requirements

The primary objective for the implementation of the eCall in-band modem is to transmit emergency data swiftly and reliably. The key eCall requirements can be summarized as follows [38, 39]:

- The PSAP should successfully receive the MSD within four seconds which is calculated from the call establishment.
- Both the voice and data from the IVS should be sent to the same PSAP or the same emergency call center.
- An emergency call may be initiated automatically or manually by the driver or the passengers.
- The size of the MSD shall not exceed 140 bytes.
- The PSAP can request the IVS to send the MSD through pull mode or the IVS send a transmission request through push mode.
- The PSAP can send a command to the IVS to terminate the emergency call.
- The MSD shall be appended with at least 28 cyclic redundancy check (CRC) bits.

• The PSAP shall send an acknowledgment when the MSD is successfully detected, if necessary, the IVS shall retransmit the MSD.

• The deployment of the eCall system should minimize the changes to the cellular and PSTN networks.

2.1.2 The Emergency Call System Architecture

Figure 1 shows the overall architecture of the eCall system including IVS, PLMN, PSTN, and PSAP. The IVS is used to initiate emergency calls and transmit MSD. The IVS is comprised of a Global Positioning System (GPS) receiver, an IVS modem, and a GSM module. The GPS receiver provides the vehicle coordinates, time, speed, and direction. The GPS information and vehicle information are then packaged into the 140-byte MSD packet and sent to the transmitter of the IVS modem. The modulated MSD information or voice information are transmitted through the voice codec, radio modem, and GSM antenna to the PSAP. The PSAP demodulates and decodes the received uplink signal and then obtains the MSD data.

Once the emergency call is established, the IVS transmits an ”INITIATION” signal which consists of a synchronization tone of 500 Hz and data bits modulated by the in-band modem. The ”INITIATION” signal followed by the modulated MSD signals are sent to the PSAP through the digital cellular voice channel. The microphone in the IVS is muted during the transmission of the MSD to minimize noise and interference. The PSAP receiver detects the signal, performs demodulation and decoding for the MSD. If the decoding is successful, the PSAP sends an acknowledgement (ACK) signal to the IVS. Upon receiving the ACK signal, the IVS switches to talking mode for people in the vehicle to talk with

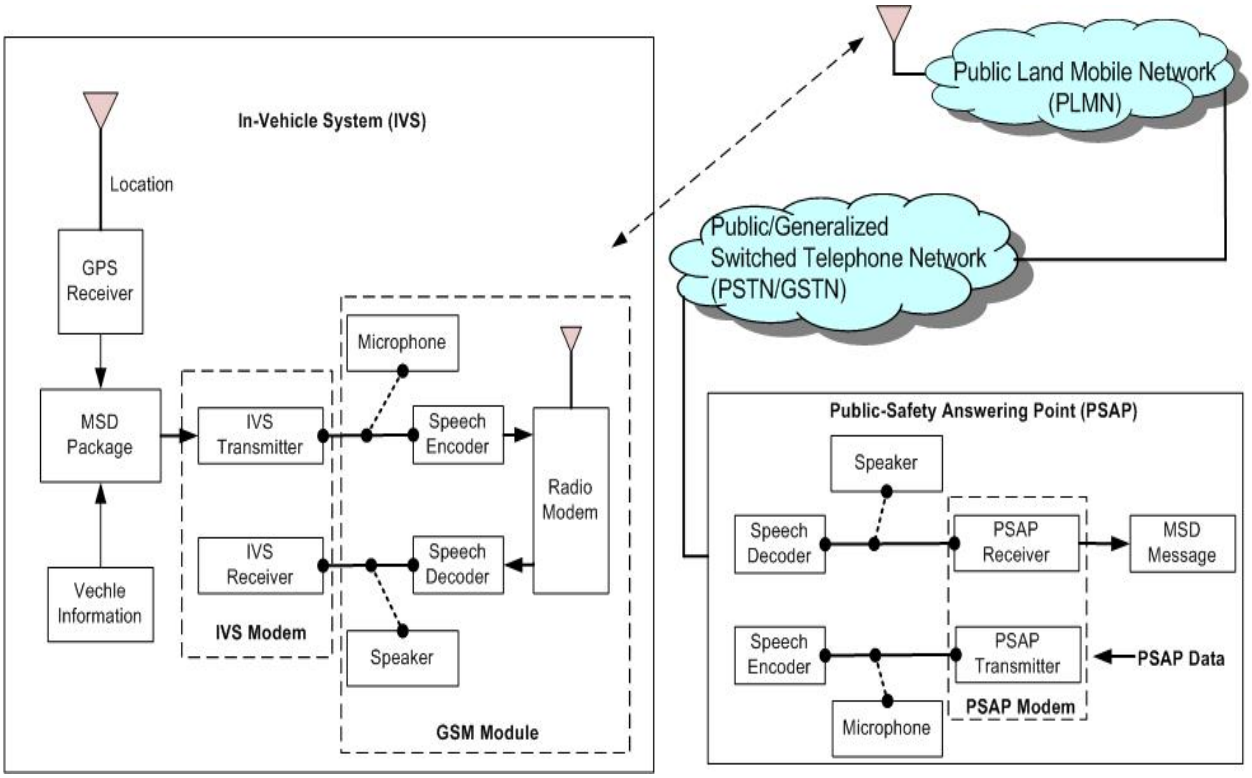

Figure 1: The eCall system architecture.

the person at the PSAP for further assistance.

The PSAP architecture of the eCall system is shown in Figure 2. The MSD signal arrives at the PSAP center through the voice channel of the PLMN and PSTN after the emergency call is connected between the IVS and the PSAP. The MSD signal is assigned by the switch of the PSAP center to an idle PSAP operator line. Then MSD information is displayed on the operator's computer after passing the PSAP modem, at the same time, the MSD and the voice signal is stored in a database of the PSAP center. The database of the PSAP Center can also be connected to the database of the third-party service point (TPSP) center to provide information Third-party service centers include hospitals, police stations, fire departments, and other commercial services. Third-party service centers include hospitals, police stations, fire departments, and other commercial services.

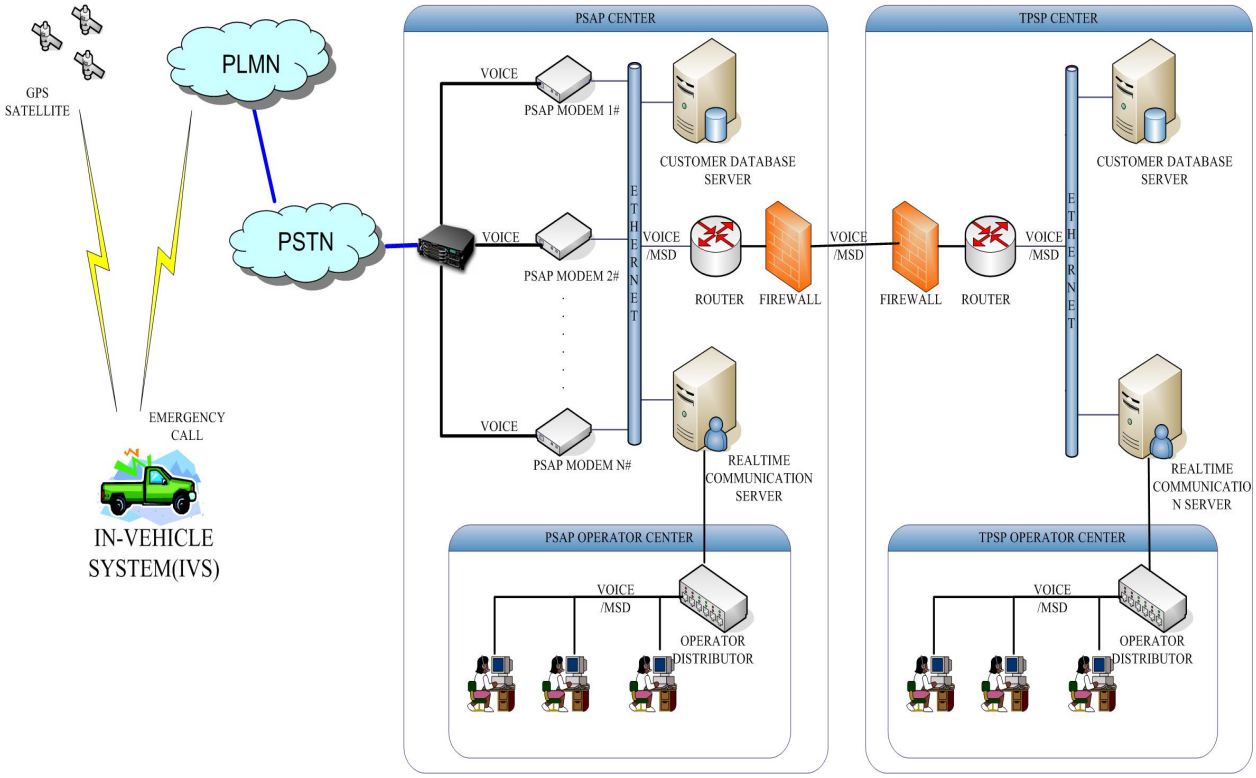

Figure 2: The PSAP architecture of the eCall system.

2.2 Channel Model

Figure 3 shows a block diagram of the uplink channel in the 3GPP eCall system. The electronic control unit (ECU) in the IVS continually monitors a trigger signal from the airbag control module or emergency button in the vehicle. When an accident occurs, the airbag control module broadcasts an emergency signal through the controller area network (CAN) bus. Once triggered, the ECU reads the VIN, GPS coordinates, time stamp, type of vehicle, number of passengers, and other relevant information and forms the MSD accordingly. The IVS dials 112 to establish an emergency call, and the MSD is fed into the IVS data modem at the same time. The IVS mutes the voice of the microphone to prevent the noise and passenger voice interfering with the MSD transmission for the duration of the EU eCall data transmission.

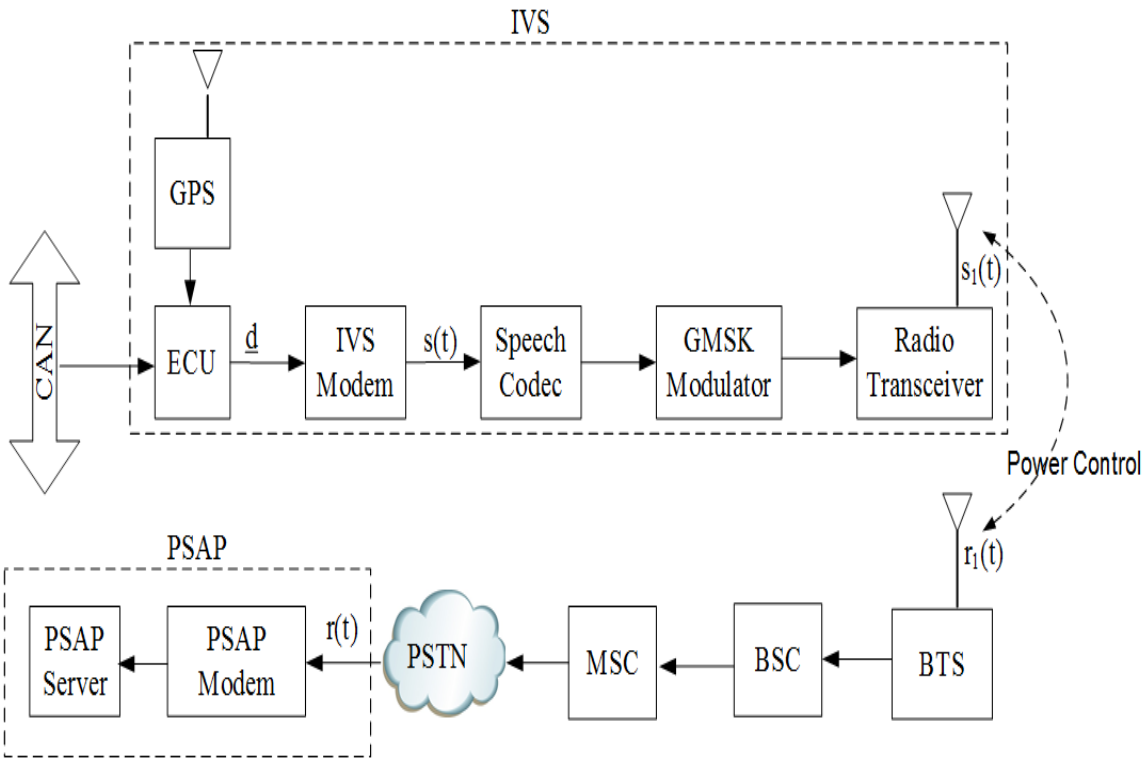

Figure 3: Block diagram of the uplink channel in the 3GPP eCall system.

The maximum size of the MSD is 140 bytes represented by 1120 binary bits. The binary bit stream $\underline{d}$ of the MSD is used to calculate the CRC parity bits. The CRC encoder output 1148 bits CRC appended MSD to a Turbo encoder [40]. The coding rate is 1/3, and the Turbo encoder generates 3456 bits MSD packet with 12 trellis bits. A hybrid automatic repeat request (HARQ) scheme is also applied to the channel coded bits to create eight different redundancy versions (RV). Each RV with 1380 bits are then modulated into symbols $\{d_m\}$ with three bits per symbol. Symbols are fed into an in-band modulator in the modem and modulated into uplink waveform $s_m(k)$ with 2 ms each symbol for the fast mode and 4 ms for the robust mode at 8 kHz sampling rate [38]. Therefore, the modulation rate is 1500 bits/s for the encoded binary data stream, not accounting for the 260-ms synchronization frames and 140-ms muting gaps. The modulation scheme employed in

the EU eCall is bipolar pulse position modulation (BPPM). These transmitted symbols can be written as [41]

$$s_m(k) = (-1)^m g\left[\left(k - A\left\lfloor\frac{m}{2}\right\rfloor (mod\ (F_s T_s))\right)\right], \quad m \in \{0, 1, ..., M-1\} \tag{2.1}$$

where $g(t)$ is the pulse shaping function,

$$g(t) = \begin{cases} 1 - \beta + \frac{4\beta}{\pi}, & t = 0 \\ \frac{\beta}{\sqrt{2}}[(1+\frac{2}{\pi})\sin(\frac{\pi}{4\beta}) + (1-\frac{2}{\pi})\cos(\frac{\pi}{4\beta})], & t = \pm\frac{T_s}{4\beta} \\ \frac{\sin[\pi\frac{t}{T_s}(1-\beta)] + 4\beta\frac{t}{T_s}\cos[\pi\frac{t}{T_s(1+\beta)}]}{\pi\frac{t}{T_s}[1-(4\beta\frac{t}{T_s})^2]}, & \text{otherwise} \end{cases} \tag{2.2}$$

The spectral expression of g(t) is

$$G(f) = \begin{cases} T_s, & 0 \le |f| \le \frac{1-\beta}{2T_s} \\ \frac{T_s}{2}\{1 + \cos[\frac{\pi T_s}{\beta}(|f| - \frac{1-\beta}{2T_s})]\}, & \frac{1-\beta}{2T_s} \le |f| \le \frac{1+\beta}{2T_s} \\ 0, & |f| > \frac{(1+\beta)}{2T_s} \end{cases} \tag{2.3}$$

$$A = \begin{cases} m, \ \ m \in \{0, 1, ..., M/2-1\} \\ M - 1 - m, \ \ m \in \{M/2, M/2+1, ..., M-1\} \end{cases}$$

$\lfloor x \rfloor$ is the floor function, the sampling rate F_s is equal to 8000 Hz, and the symbol time T_s is 2 ms in the fast mode or 4 ms in the robust mode, and M = 8 is the number of symbols.

Data transmission over the voice channel of the 2G/3G network is a challenging task since the speech codecs of the cellular networks with a strong speech signal compression [42]. The speech frames are 20-ms duration. The IVS modem output signal $s(t)$ is fed into the speech encoder, which is a highly non-linear device and can cause severe distortion to the MSD signal. The speech codec output signal is then modulated by the Gaussian Minimum Shift Keying (GMSK) modulator for transmission through the radio transceiver. There are multiple propagation paths between the IVS antenna and cellular tower antenna. The impulse response of the channel can be expressed as [30, 43]

$$c(t;\tau) = \sum_{k=1}^{L} \alpha(t)\delta(t-\tau_k) \tag{2.4}$$

where $\alpha(t)$ is the attenuation factor of the kth path and τ_k is the time delay of the kth path. The received signal $r_1(t)$ can be written as

$$r_1(t) = \sum_{k=1}^{L} \alpha(t)s_1(t-\tau_k) + n(t) \tag{2.5}$$

where $n(t)$ is the noise generated by the wireless channel.

As shown in Figure 3, $s_1(t)$ is the output signal of the radio transceiver and $r_1(t)$ is the received signal after multipath propagation from mobile station (MS) to BTS. Amplitude variations in the received signal occur randomly over time and location, so the multipath propagation results in signal fading. Fading phenomena can increase interference and reduce voice channel quality. Power control is used to adjust the transmission power of the BTS and MS to preserve call quality and reduce the overall network interference and power consumption [44]. The uplink and downlink transmission power can be changed

by the BTS and MS every 480 ms. For each 480 ms, changes in transmission power are random over time. Assume the gain of power control is $A(t)$, which depends on the environment and moving speed of the vehicle. The received signal by the PSAP modem after the power control is $r(t)$:

$$r(t) = A(t)r_1(t) \tag{2.6}$$

where A(t) is a variable of a time-varying gain variable.

The signal $r(t)$ after the BSC, MSC and PSTN network is the input signal of the PSAP receiver. The PSAP receiver samples and records $r(t)$ at an 8 kHz sampling rate, and stores 16 bits for each sample. The PSAP continuously monitors the speech signal from a telephone recording box. Once a synchronization tone and synchronization preamble are detected, the PSAP modem proceeds to demodulate and decode the full MSD. The PSAP modem sends negative acknowledgment (NACK) message during transmitting MSD. If the CRC check succeeds, an ACK message is forwarded to the IVS. The IVS receiver must detect any ACK and then stop the MSD transmission as necessary.

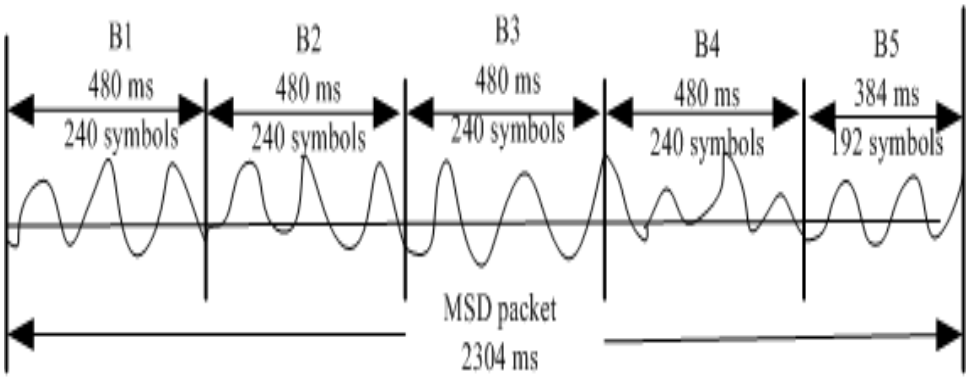

Figure 4: Relation between transmission power control interval and MSD packet duration.

The voice channel used to transmit the MSD has fading, and the SNR of the signal received by the PSAP center is a time-varying random variable. The transmission power control interval ΔT is 480 ms, and the symbol time T_s is 2 ms for the fast modulator mode. That is 240 symbols or 720 binary bits for each power control interval. As shown in Figure 4, fading may affect one block of 720 bits during the 480 ms. To make sure every bit in such a system is received correctly, it is critical to measure fading statistics of the voice channel with power control.

The multipath propagation results in signal fading with random amplitude variations in the received signal. Fading phenomena can reduce voice signal strength. The GSM system employs power control to adjust the transmission power of the BTS and the mobile station (MS) to preserve the quality of the voice call and reduce the overall network interference in a time-varying mobile channel [45, 46, 47]. The BTS and MS measure the received signal quality (RxQual) and received signal level (RxLev) every 480 ms [48]. The transmission power will be increased or decreased according to the value of the RxQual and RxLev. However, it should be noted that the RxQual and RxLev are not accurate and real-time metrics for voice quality. The power control interval in the GSM voice channel is 480 ms. This means that the transmission power is fixed during each power control interval. One symbol contains 3 bits coded data and the symbol time is 2 ms for fast modulation mode. As shown in Figure 4, fading can affect a block of 720 bits in the fast modulation mode or 360 bits in the robust modulation mode.

The existing power control technique in the GSM standard can keep the signal quality at an acceptable level for voice communication. However, the power control frequency is too slow for the MSD data transmission. Fading in the voice channel after power control

increases the BER and packet loss of the MSD transmission. Particularly, the fading is heavy in some regions with low signal strength, and it can affect demodulation of the MSD packet from symbol to symbol even for a block of 720 bits. Therefore, it is necessary to measure fading statistics of the GSM voice channel after power control and evaluate its impact on the MSD transmission.

CHAPTER 3 EXPERIMENT PLATFORM AND HARDWARE DESIGN

The existing power control techniques under the GSM standard can keep signal quality at an acceptable level for voice communication, but it is not fast enough for MSD data transmission, and fading still exists in the voice channel which affects the BER and packet loss. Fading is particularly strong in some regions with low signal strength and can affect demodulation of the MSD packet from symbol to symbol. It is necessary to obtain accurate fading statistics to develop effective techniques to mitigate these phenomena [19].

The power control interval between the BTS and MS is 480 ms, and the EU eCall symbol time or modulation frame is 2 ms in fast modulation mode. If the received MSD signal contains a deep fade during one power control period, it is not fast enough to compensate for power loss. The fading may affect up to 240 symbols or 720 bits of the MSD. The signal fading in this case may result in the MSD transmission failure. In this study, experiments were run to measure the channel characteristics, average fading duration, level crossing rate, and bit error performance of the EU eCall in-band modem channel.

3.1 The Measurement Apparatus

A testbed is designed and built to measure the fading characteristics of the voice channel in Figure 5. The system consists of an IVS, GSM network, PSTN network, telephone recording box, and PSAP software installed on a desktop computer. Data is processed after recording.

The IVS hardware platform contains a Freescale i.MX 6 board and a development board containing u-Blox GSM module LEON-G200 and GPS module LEA-6S with GPS antenna and GSM antenna in Figure 6. The central processor of the Freescale i.MX 6 is capable of generating continuous wave (CW) or the eCall modulated MSD signal $s(t)$ that

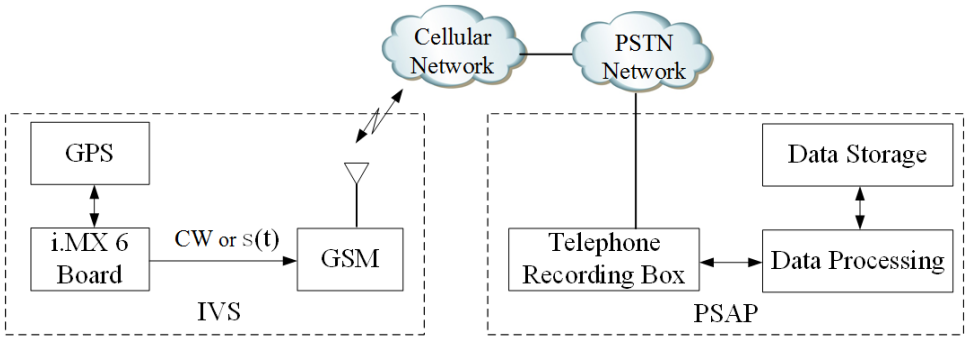

Figure 5: Block diagram of the experimental system.

are fed into a GSM voice codec. The output signal of the voice encoder is processed by the GSM baseband module and the radio module. The radio signal is transmitted through the GSM antenna and sent to a BTS of the GSM network. The signal received by the BTS is transmitted through the PSTN network and received by a telephone recording box located at the PSAP center. A sound card inside the PSAP records the received signal. The sound card digitizes the output waveform of the telephone recording box, and the digitized waveform files are stored on a computer hard drive.

The IVS modem was implemented on a Freescale i.MX 6 board [49] as shown in Figure 6. The left board mainly includes a Freescale i.MX 6 main processor running at 1 GHz, 1 GB Random Access Memory (RAM), 4 GB Flash memory, and Freescale audio codec chip SGTL5000. The IVS application software, testing continuous wave (CW) file, testing MSD data $s_m(k)$ are stored in Flash memory in this system. Upon the receipt of a trigger signal after the system is powered on, the processor sends an ATtention (AT) command to the GSM module through the universal asynchronous receiver/transmitter (UART) interface to begin calling the PSAP center. Once the voice channel is established, the CW or modulated MSD data $s_m(k)$ are sent to the GSM module through an Inter-IC Sound (I2S) interface. The output signal of the audio codec is then fed into the GSM voice codec;

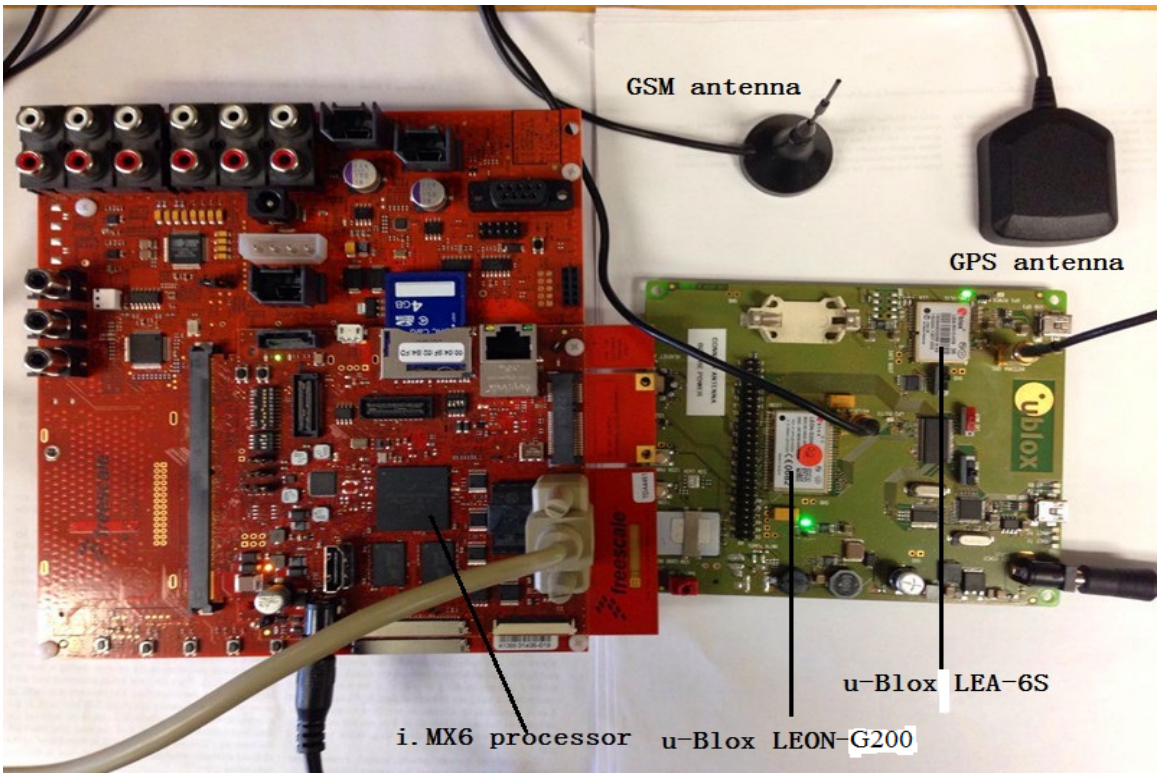

Figure 6: Hardware platform of the in-vehicle system.

the output signal of the voice encoder is processed by the GSM baseband module and the radio module. The radio signal is transmitted through the GSM antenna and sent to a BTS of the GSM network. The signal received by the BTS is transmitted through the PSTN network and received by a telephone recording box located at the PSAP center. The speech waveform is recorded by the PSAP's sound card, which digitizes the output waveform of the telephone recording box. The digitized waveform files are stored on a computer hard drive.

3.2 In-Vehicle System Design

A block diagram of the IVS hardware is shown in Figure 7. The IVS system includes an i.MX6 processor, power supply, FLASH, RAM, GSM module, GPS module, Audio Codec, 3-Axis Accelerometer, CAN Transceiver, emergency buttons, and touchscreen.

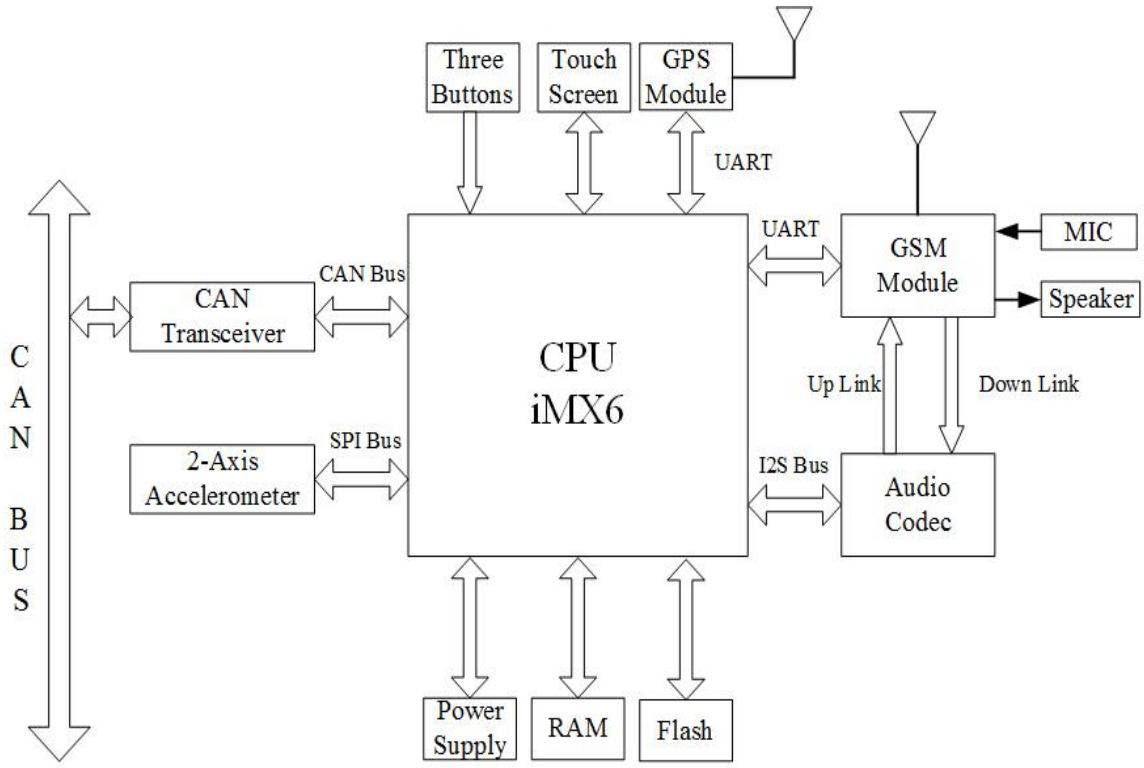

Figure 7: Block diagram of the IVS hardware.

The i.MX6 processor is a high-performance, high integration, and automotive-grade processor released by the Freescale Semiconductor. The processor passes the ACQ100 automotive grade chip test, which targets the increasingly stringent demands for infotainment and telematics markets. The i.MX6 processor can operate at speeds up to 1 GHz with a quad ARM Cortex-A9 core. The integrated chip also provides integrated power management. These features are useful for emergency call system as well as entertainment applications. The central processor extends 1 GB of RAM and 4GB of Nand Flash through the external memory interface. The Nand Flash stores Boot- Loader, an embedded operating system, and the IVS application and data. The RAM runs the application after the IVS system is initialized.

The power management module of the embedded system must meet the power-on

sequence and the power-down sequence to ensure a stable and reliable operation of the system. The NXP's power management integrated chip MMPF0100 is ideal for i.MX 6 Series application processors because the MMPF0100 is of programmable and configurable features and fully integrated power devices and external components. The MMPF0100 can also provide power for the entire IVS including application processors, memory, and system peripherals.

The i.MX6 processor continually monitors the signals from the emergency button, CAN bus, and 2-axis accelerometer when the system is in running mode. There are three buttons used for triggering an emergency service manually. The three buttons are physically connected with three general input/output (IO) port of the i.MX6 processor. When a user presses one of the buttons, the system should respond immediately. Thus, the processor configures the IOs as a high priority interrupt sources.

The i.MX6 integrates two CAN controllers. The IVS uses TJA1041A as a CAN transceiver to provides an interface between the i.MX6 processor and the CAN network of the vehicle. The TJA1041A is fully compliant with ISO 11898 and is designed for automotive high-speed CAN applications with very low power consumption and remote wake-up performance. The CAN transceiver can realize the differential transmission and receiving capability of the CAN controller [50]. The interface includes three electrical wiring, CANHIGH, CANLOW, and GND. The i.MX processor obtains the status of sensors, airbags, seat belts and other information of the vehicle by the protocol CAN2.0. The transmission speed is set to 500KBps. As shown in Figure 7.

The accelerometer is integrated for crash detection. The MMA6255 is a two-axis SPI-compatible accelerometer which is qualified AECQ100 standard. The central processor

configures the accelerometer and reads a real-time sensor data through SPI bus. There are four wires including CS, SCLK, MISO, and MOSI. The pin CS is chip selection; the pin SCLK provides a clock signal for the SPI bus, the pin MISO is the serial data input for the i.MX6 processor and the data output for the accelerometer sensor, the pin MOSI is the serial data output for the i.MX6 processor and data input for the accelerometer sensor.

The primary function of the GPS module is to get the current time, location and direction of the vehicle, and other information via satellites. The GPS module is a U-Blox NEO-7P module with precise point positioning technology. The i.MX6 processor connects to the GPS module via a UART interface which includes three electrical wiring, TX, RX, and GND. The processor controls the GPS module and reads the GPS information via a standard RS-232 protocol. The parameter of the UART port is configured as 115200 bps, no parity, eight data bits and one stop bit. The processor keeps reading the coordinate data and stores into a defined buffer, which is packaged with other information together into the minimum set of data. As shown in Figure 7.

The GSM module is used to make an outgoing call or answer an incoming call in case of an emergency situation. The LEON-G200 module offering full quad-band GSM / GPRS data and voice functionality meet AECQ100 standard. The GSM module combines power management unit, baseband, radio transceiver, and power amplifier in a single module, which could accelerate the development of the IVS. The interface is also used a serial port between the i.MX6 processor and the GSM module, which includes three electrical wirings, TX, RX and GND. The central processor controls GSM module through a standard RS-232 protocol. The processor sends AT commands to control the GSM module. Once the IVS is triggered automatically or manually, the processor will send an AT command

to call the PSAP center. When the emergency call is answered by the PSAP center, the i.MX6 processor will receive the response signal from the RX wire.

The audio codec SGTL5000 connects to the i.MX6 processor through I2S bus, and connects to the GSM module through analog signals. The SGTL5000 is a low power stereo codec from Freescale, which can achieve very high performance and ultra-low power functionality.

The output of IVS Modem is digital data with 16 bit, 8000 Hz sampling rate, little-endian PCM format. The processor sends the PCM data to the audio codec using the IIS bus. Then the SGTL5000 converts the PCM data to an analog signal output from the digital-to-analog converter of the audio codec. The output modulated signal is sent in analog to a digital converter in the GSM module. The MSD signal is sampled, digitized, and transmitted to the GSM voice band sample buffer before being sent to the frame-based voice band processing GSM block. An AMR player connected to the speech encoder is implemented before the uplink path's final block radio transmission. Similarly, on the downlink path, the speech decoder extracts speech signals from the starting block of the radio receiver and sends the downlink signals to the frame-based voice band processing block and voice band sample buffer.

3.3 Description of the Measurement Locations

Experiments were carried out in different propagation environments. A stationary experiment was conducted in the Communications Laboratory, Engineering Building; a series of mobile experiments was performed on the Freeway I-75, urban road, and rural road.

Case 1 involved stationary laboratory measurement within an environment where the

Figure 8: Measurement location 1: Laboratory of Engineering Building.

IVS transceiver was stationary and surrounded by tall buildings. The experiment was conducted at the Communications Laboratory located on the third floor of the Engineering Building. The IVS and GSM antenna were placed on a bench top in the laboratory while the GPS antenna was placed outside of the lab window. Tall buildings surround the Engineering Building; there is no line-of-sight propagation path between the IVS antenna and any cellular tower.

Case 2 was conducted on a local freeway with low traffic to collect data for a moving vehicle in average driving conditions. The experiment was performed between Exit 53 and Exit 83 of the freeway between 10 a.m. to 11 a.m. on Sundays. The IVS was installed inside of a car and the GSM and GPS antennas were placed on the roof of the car. There was at least one line-of-sight propagation path between the GSM antenna and a base station tower. The experiment was performed during a time when few other vehi-

Figure 9: Measurement location 2: Interstate-75 Freeway with low traffic.

cles were on the three-lane freeway; the test vehicle was driven from south to north in the middle lane in cruise control mode at speeds from 55 mph to 70 mph. Experiments were also conducted in heavy traffic conditions on Interstate-75 Freeway, but the test was run during a weekday rush hour. The measurement was carried out from 5 p.m. to 6 p.m. on Mondays at an average speed of about 30 mph.

Case 3 was conducted on a narrow, urban road surrounded by tall buildings with frequent interaction between motor vehicles and pedestrians. The vehicle speed on such roads is usually low. About 38% of all fatal road traffic accidents occur on urban roads in Europe. Figure 10 shows the downtown street where this experiment was run, where there are many 20-30 story buildings on either side. The signals sent from the IVS antenna cannot reach the neighborhood base transceiver station through a line-of-sight path. The radio signal includes shadow fading, diffraction, scattering, multipath fading, and other

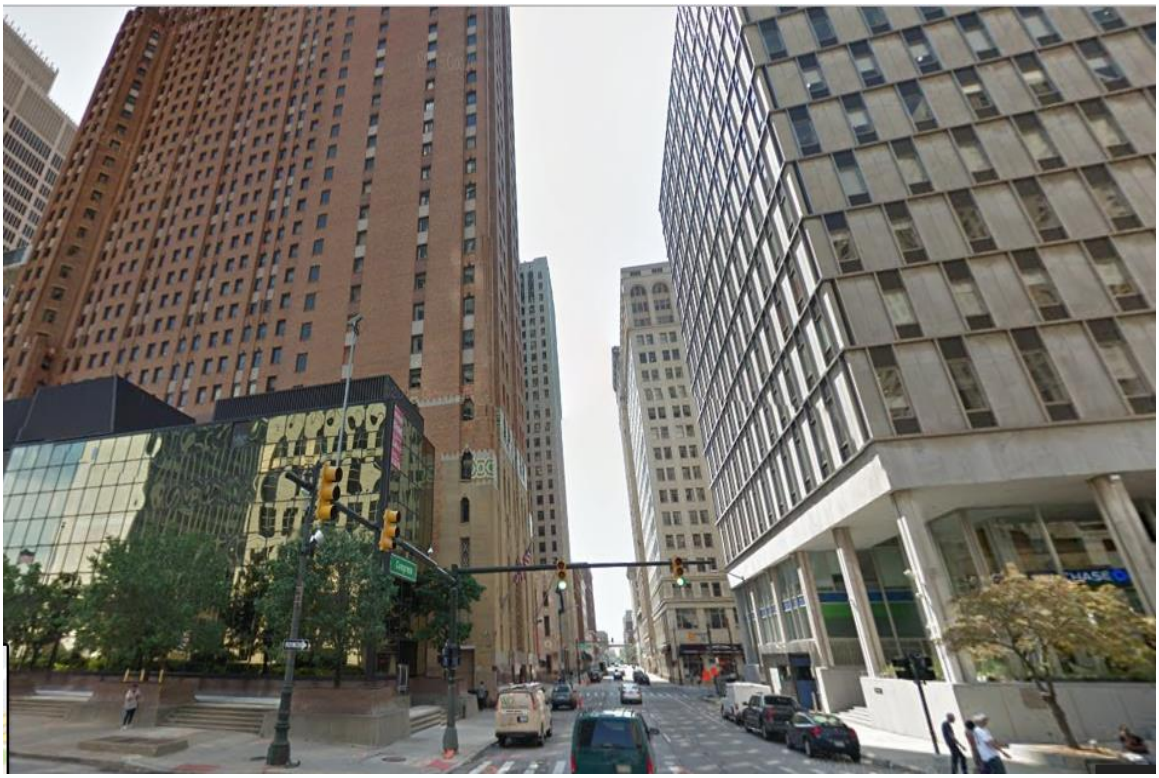

Figure 10: Measurement location 3: Urban roads of in Detroit City .

Figure 11: Measurement location 4: Rural roads in the north Michigan.

complications which impact GSM terminal signal strength and MSD transmission.

Case 4 was similar to Case 3 but was conducted on a rural road. Vehicles tend to move at higher speeds on rural roads than urban roads, but slower than on freeways. The fatality rate on rural roads is highest among all traffic environments. More than 55% of fatal accidents occur on rural roads. The rural road we tested only supports GSM signals; many rural areas do not support 3G or 4G data signals, and even the GSM signal strength is very weak. Both sides of the road are covered in trees about 20 m in height.

All experiments are based on T-mobile network. The carrier frequency of the GSM network uses 1900 MHz in the area. A vertical polarization antenna was used in the test, and the antenna height is 15 cm. The frequency range of the antenna is from 700 to 2100 MHz. The antenna was sucked on the top of a Sedan with 145 cm height. Data and waveform for the 4 test cases are analyzed and discussed in the next chapter.

CHAPTER 4 CHANNEL FADING MEASUREMENT AND STATISTICS FOR THE EMERGENCY CALL SYSTEM

4.1 Introduction

The signal received by the PSAP receiver is the sum of electromagnetic waves from different paths including reflection, diffraction and scattering [29, 30]. Signal transmission is affected by multipath fading and Doppler shift within the complexity of the wireless communication environment. Techniques for minimizing fading include equalization, diversity receiving, and channel error correction coding [51, 33]. The power distribution of the received signal needs to be obtained through experiments for different environments, so that proper modulation and coding can be selected accordingly to increase the MSD success rate and minimize MSD transmission delay. Fading statistics for the EU eCall channel is also required to evaluate the performance of the MSD transmission including detection, synchronization, modulation and coding. In this chapter, the cumulative distribution functions (CDF), level crossing rates (LCR) and average fade durations (AFD) are obtained for the CW signals received by the PSAP in different test cases. The results are compared with Rayleigh distribution.

4.2 Mathematical Modeling for Fading Channel

4.2.1 Envelope and Power Distribution

The IVS transmits a CW signal to the PSAP through a mobile channel. The baseband signal include $r_I(t)$ received in the in-phase channel and $r_Q(t)$ received in the quadrature channel, respectively. The signal envelope is

$$z(t) = |r(t)| = \sqrt{r_I^2(t) + r_Q^2(t)} \tag{4.1}$$

When $r_I(t)$ and $r_Q(t)$ are Gaussian random variables with zero-mean and variance σ^2, $z(t)$ is of Rayleigh distribution with probability density function (pdf) [52]

$$p(z) = \frac{z}{\sigma^2} \exp\left(\frac{-z^2}{2\sigma^2}\right) \tag{4.2}$$

The corresponding CDF of the received signal envelope is:

$$P(Z) = \int_0^Z p(z)dz = 1 - \exp\left(\frac{-Z^2}{2\sigma^2}\right) \tag{4.3}$$

Let Z_m be median value of $z(t)$. For Rayleigh distribution, one has $Z_m = 1.177\sigma$. The power of the received signal is traditionally normalized to the median in practice [53]. Let $x(t)$ be the normalized instantaneous power, which is

$$x(t) = 20 \log_{10} \frac{z(t)}{Z_m} \tag{4.4}$$

Given $z(t)$ with Rayleigh distribution, the instantaneous power $z^2(t)$ is of Chi-square distribution with 2 degrees of freedom.

As shown in Figure 3, the instantaneous power of the received signal is $r^2(t)$. We can obtain the average power of the signal received by the PSAP is

$$p_a(t) = \frac{1}{\triangle t} \int_t^{t+\triangle t} r^2(t)\, dt \tag{4.5}$$

where $\triangle t$ is a time window to calculate the instantaneous power for each calculation duration.

4.2.2 Level Crossing Rate and Average Fade Duration

The level crossing rate $L(Z)$ is defined as a rate at which the received signal envelope crosses a given level Z in the downward direction after the fading envelope is normalized to the root mean square (RMS) level [52, 54]. The number of crossings of the received signal envelope level Z over the interval [0, T] is

$$N(Z) = \int_0^{+\infty} \dot{z} p(Z, \dot{z}) d\dot{z} = \sqrt{2}\pi\rho f_m exp(-\rho^2) \tag{4.6}$$

where $\dot{z}$ is the derivative of $z(t)$ versus time, $p(Z, \dot{z})$ is the joint probability density function of z and $\dot{z}$ at $z = Z$, f_m is the maximum Doppler frequency and ρ is the value of the specified level Z which is normalized to the RMS level of the fading envelope. The level crossing rate is

$$L(Z) = \frac{N(Z)}{T} = \int_0^{-\infty} \dot{z} p(Z, \dot{z}) d\dot{z} \tag{4.7}$$

which is the LCR when the fades cross a threshold of level Z per second.

The average fade duration is the average time that the signal envelope stays below a given threshold level Z in the normalized signal amplitude [55]. Let t_i denote the fade duration of the ith fade below threshold level Z over a time interval $[0, T]$. Let

$$p\{z(t) < Z\} = \frac{1}{T} \sum_{i=1}^{n} t_i \tag{4.8}$$

The average fade duration is

$$\bar{t}(Z) = \frac{1}{TL(Z)} \sum_{i=1}^{L(Z)T} t_i \approx \frac{p\{z(t) < Z)\}}{L(Z)} \tag{4.9}$$

The average fade duration also can be expressed as a function of ρ and f_m, which is

$$\bar{t}(Z) = \frac{e^{\rho^2} - 1}{\rho f_m \sqrt{2\pi}} \tag{4.10}$$

The average fade duration of a faded signal helps to determine the number of data bits that may be affected during fading. It can also be linked to the BER according to the signal-to-noise ratio during fading. The statistics results of LCR and AFD are helpful for designing the modulation scheme, and selecting the symbol time and channel coding.

4.3 Experimental Procedure for Fading Statistics

The amplifier gains of the IVS, the telephone recording box, and the PSAP center were all set to 0 dB throughout the testing process as we measured the fading statistics of the voice channel. The received signal power yields the channel features of the GSM voice channel. The following two procedures were repeated for each experiment.

The procedure for sending and measuring CW signals is shown in Figure 12. The procedure for sending and measuring MSD is shown in Figure 13. The driver pressed the emergency button in the IVS to trigger an emergency call which was answered by the PSAP center. After the voice call was established, the IVS began to send CW signals at 500 Hz with a 20-second frame length. The IVS saved the CW waveform into the Secure Digital (SD) card of the IVS for comparison against the received waveform by the PSAP; the PSAP began to record and save data at an 8-kHz sampling rate, 16-bit, and little-endian mode on a hard drive. This process was repeated 500 times for each case, at the

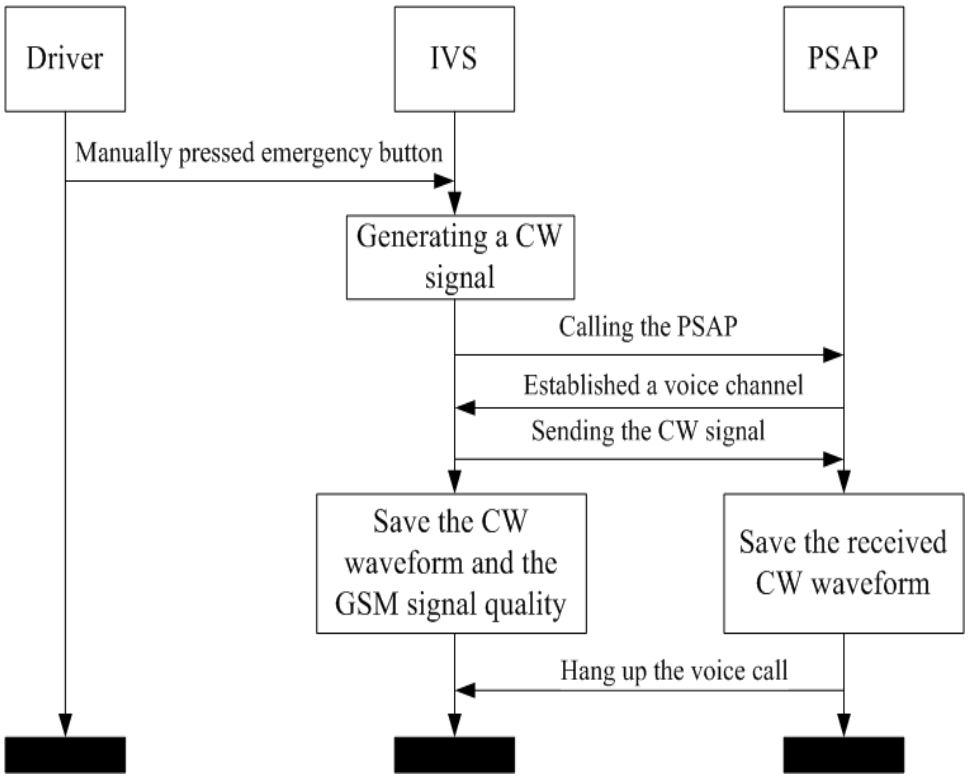

Figure 12: The procedure to measure CW signal strength.

end of which the PSAP hung up and complete the CW signal experiment procedure. The saved data and waveforms were then used to analyze the fading statistics of the GSM voice channel.

The measurement procedure of the EU eCall MSD is shown in Figure 13. In our experiment, the driver manually pressed the emergency button, then the IVS aggregated the MSD and initiated an emergency call. After the emergency call was answered and a voice channel was established, the PSAP sent a START command to the IVS. Then the IVS began to send a MSD containing the time, location, VIN, speed of the vehicle, the current GSM signal quality, and other information. The IVS and PSAP recorded the MSD waveform of each test sample. The decoded MSD was stored in a log file which contained MSD information as well as the PSAP modem input power and other data. The data and

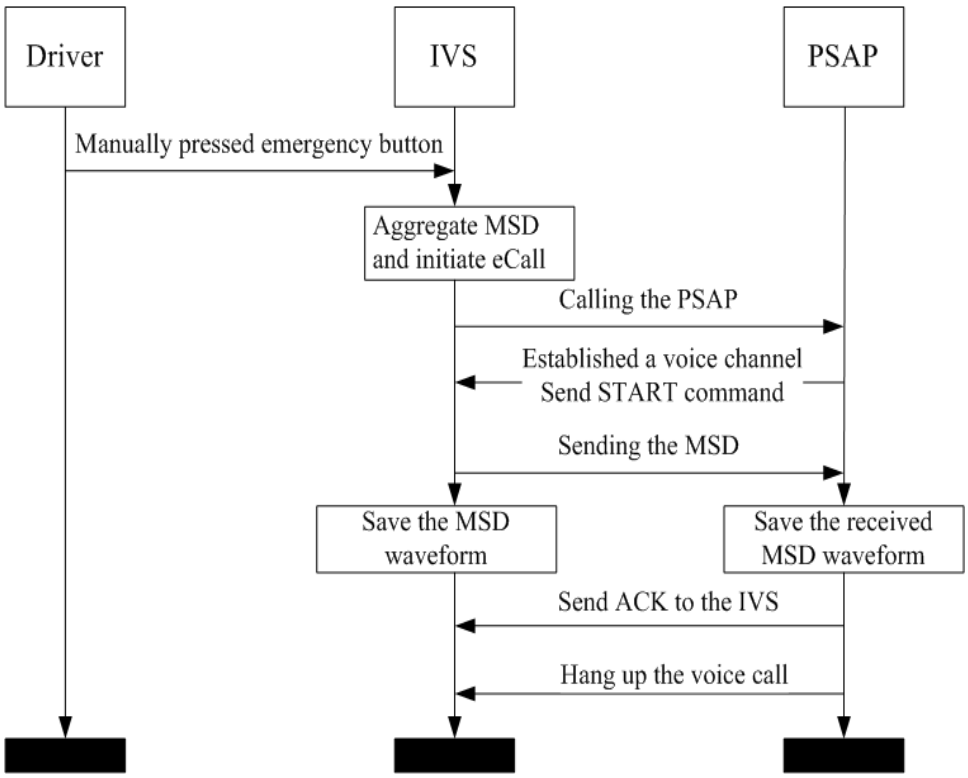

Figure 13: The measurement procedure of the EU eCall MSD.

waveforms were used to analyze the manner in which fading affected the MSD success rate at the same GSM signal quality.

4.4 Fading Statistics for the Emergency Call system

Figure 14 shows the MSD signal sent by the IVS and the received MSD signal at the input of the laboratory PSAP center. The average fade duration of a faded signal helps to determine the number of data bits that may be affected during fading. Figure 15 shows a 10 ms segment of CW signal received by the PSAP. It contained three deep fading durations t_1, t_2, and t_3 below -10 dB fading depth. The fading depth is the reduction from the received signal level to the RMS of the signal measured in dB. The fades fell below -10 dB on three occasions in 10 milliseconds. One of these fades was even lower than -20 dB. According to the LCR definition, the LCR of the signal is three crosses per 10

Figure 14: The MSD signal sent by the IVS and the received MSD signal at the input of the laboratory PSAP center.

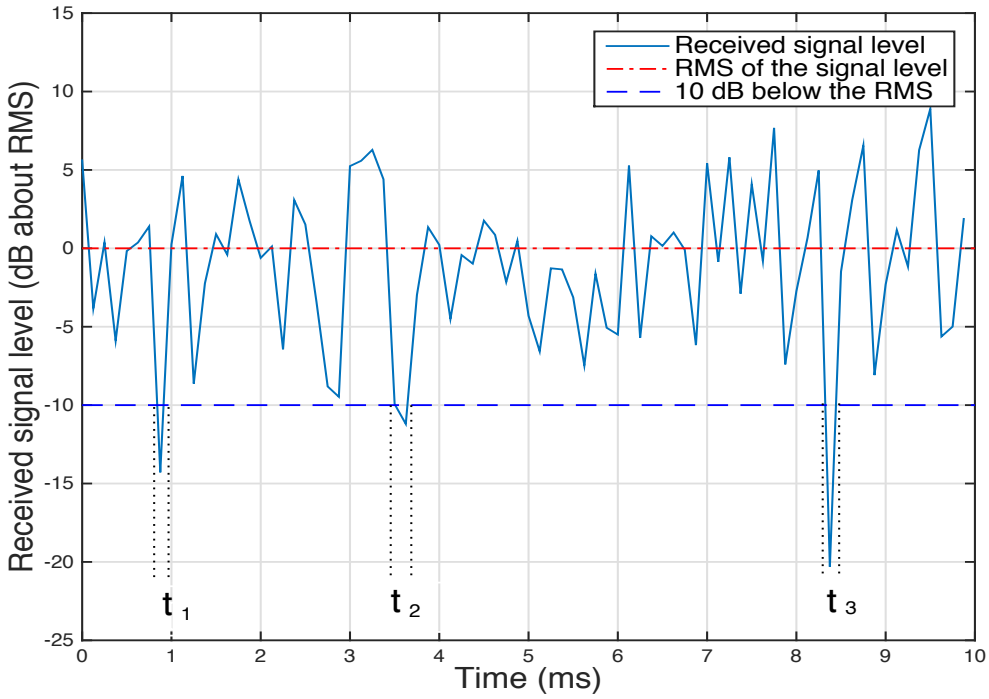

Figure 15: A segment of the received signal level for a GSM network. The RMS of the signal level is 0 dB. The signal crossed -10 dB for 3 intervals.

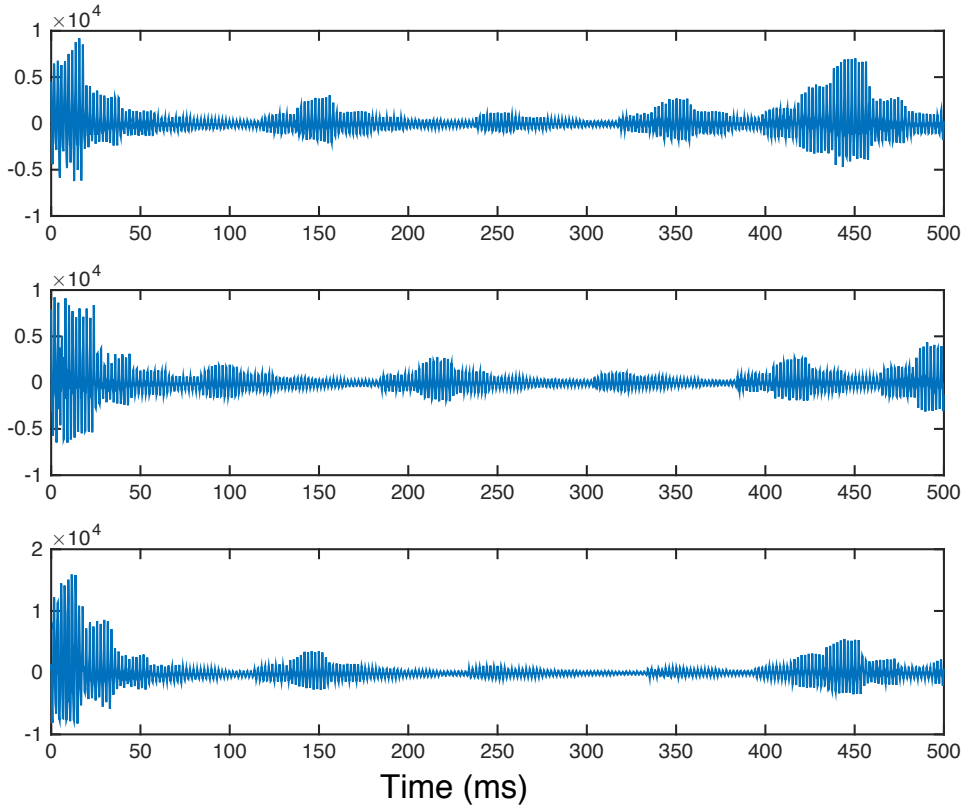

Figure 16: A segment of the signal received by the PSAP. The signal transmitted by the IVS was CW at 500 Hz. Deep fade existed at the start of the received signal.

ms (or 300 crosses/s). The AFD is (t_1 + t_2 + t_3) / 3, which is about 0.4 ms when the signal power stays below the threshold -10 dB. When a deep fade exists in the channel, the PSAP is likely to fail in demodulating and decoding the MSD. In this case, the PSAP center sends the NACK feedback message to the IVS and requests to resend the data packet. Therefore, the signal fading can increase the MSD transmission delay and even lead to MSD data transmission failure.

Figure 16 shows deep fade existed at the start of the received CW signal. There was deep fade in the time interval [40, 500] ms. The synchronization tone of the EU eCall is a 64-ms sinusoidal tone of frequency 500 Hz for the fast modulation mode. It is suggested

that the synchronization tone in the 3GPP TS 26.267 to be replaced by a synchronization tone of 600 ms at 2000 Hz for reliable synchronization.

Figure 17 shows a segment of the received CW signal power obtained in the laboratory, which contains many deep fading gaps, i.e., spaces in the middle of the received CW signal. Fading depth is the reduction from the normal received level, measured in dB. More than 40 fades in this experiment fell below -20 dB during 2500 seconds, with three of these fades being even lower than -25 dB.

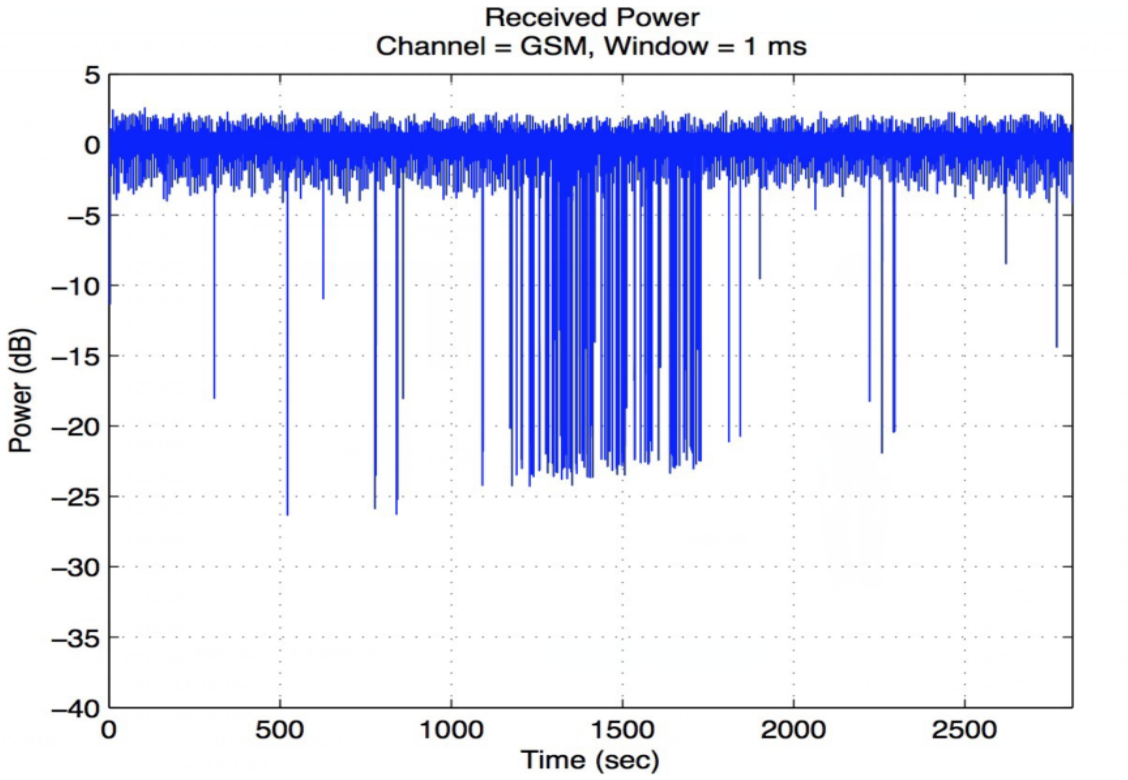

Figure 17: A segment of the received signal power.

Differences in fading depth are thought to be caused by decrease in signal quality, but the power control between the BTS and the MS can not rapidly compensate for the transmission power. When a deep faded signal exists in the channel, the PSAP is likely to fail to demodulate the MSD signal appropriately. In this case, the PSAP center sends

the IVS NACK feedback information to resend the data packets. Therefore, the signal fading can increase the average time of MSD transmission and even lead to MSD data transmission failure.

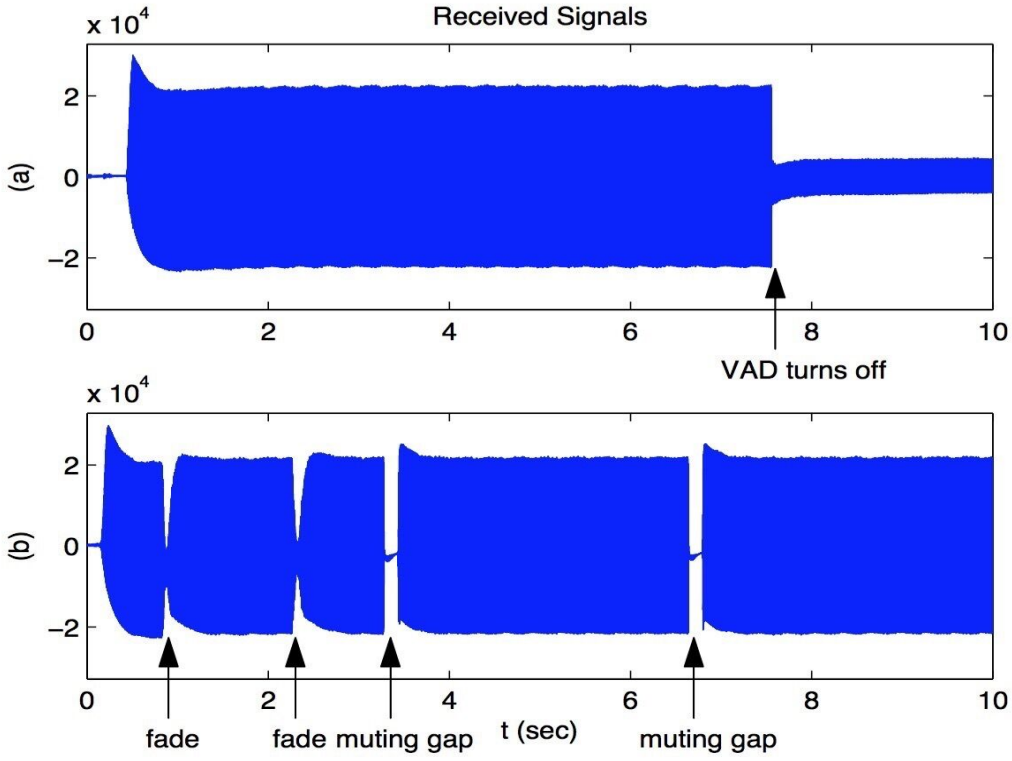

Figure 18: The received CW signal with fading gaps.

A 10-second received CW signal was used to assess the impact of the fading gap on MSD transmission as shown in Figure 18. Figure 18 (a) shows a received CW signal without fading gap. The waveform indicates that there was a jump when the received CW signal switched from on to off. According to the GSM codec standard, if there is no speech signal in the MS end, the voice channel will transmit no signal instead of generating a silence signal. Figure 18 (b) shows two fading gaps in the middle of the received CW signal within 4 seconds. Each fading gap interval is about 20 ms. There are 60 bits of the MSD to be affected in the fast mode. It is impossible to demodulate and decode the

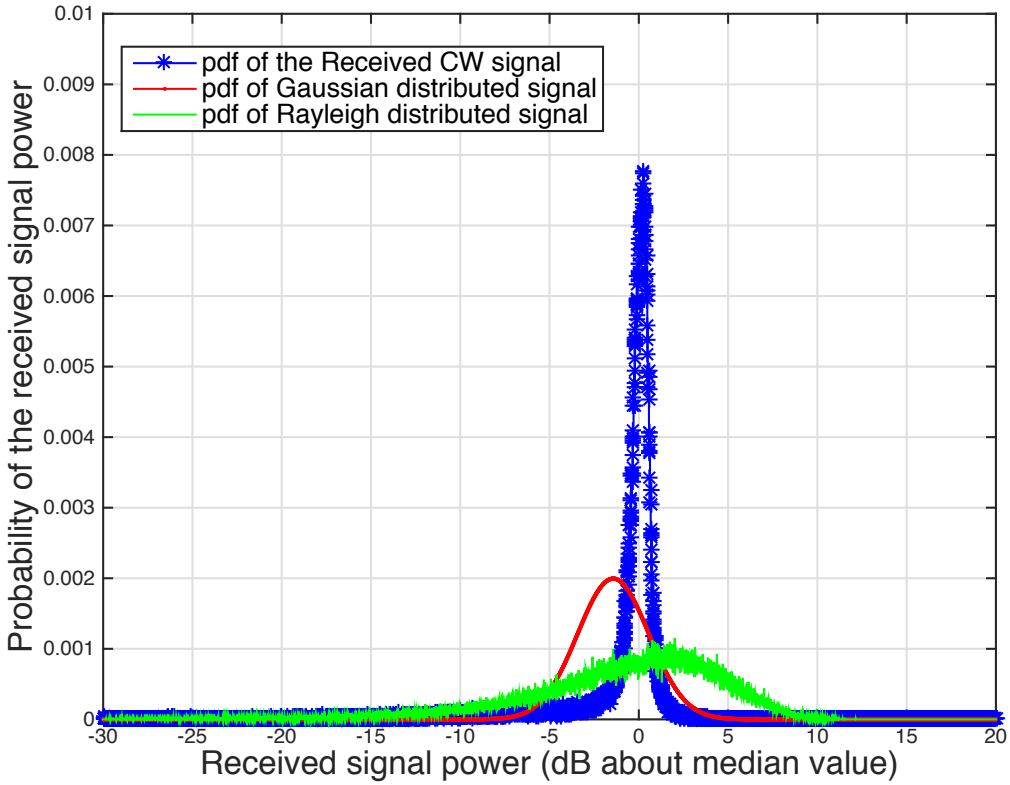

Figure 19: Probability density function of the received CW signal power versus Gaussian distribution and Rayleigh distribution. The data were obtained from the test case 2 with the transmitted CW signal at 500 Hz.

MSD with two fading gaps in 4 seconds, but the 3GPP eCall standard requires that the PSAP should successfully receive the MSD within 4 seconds from the time when the voice channel is established. To this effect, fading still exists in the voice channel of the GSM cellular system with power control; the fading will inevitably delay the MSD transmission time and reduce the MSD success rate. The IVS must retransmit the MSD repeatedly and switch to the robust mode.

Figure 19 shows the probability density function of the received CW signal power. The data was obtained from the test Case 2 with the transmitted CW signal at 500 Hz. Gaussian distribution and Rayleigh distribution with the same variance of the received signal

power are plotted for comparison. It can be seen that the power distribution of the received CW signal is neither Rayleigh nor Gaussian.

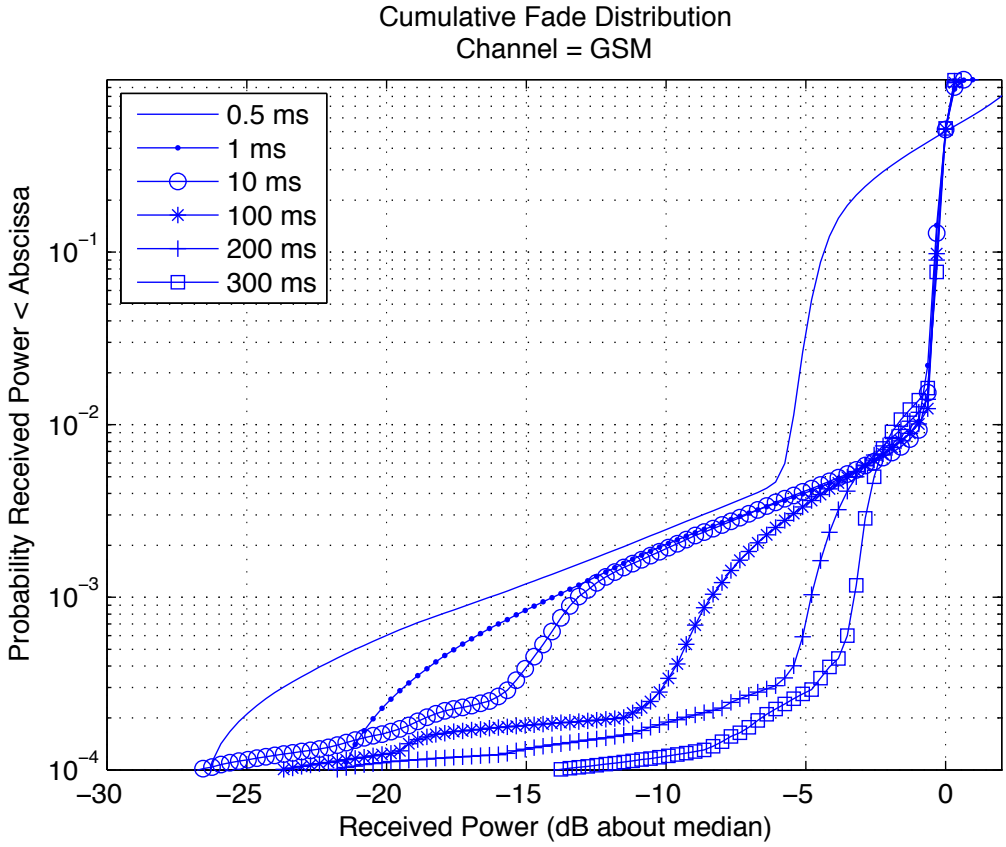

Figure 20: Cumulative fading distribution of different windows.

Cumulative distribution functions are plotted in Figure 20 to show the cumulative fading distribution of the GSM system voice channel. About 0.01% of the received power attenuated 27 dB, 0.1% attenuated over 16 dB, 1% attenuated over 5.8 dB and 10% attenuated over 4.8 dB. The GSM voice channel featured strong fading, which will increase data packet loss rate and reduces the data transmission success rate, as discussed above.

Figure 21 shows the CDFs of the CW signals at 500 Hz received by the PSAP in different test environments. The Rayleigh distribution is plotted for comparison. The data was collected in the laboratory, on the freeway, urban road and rural road. The fading

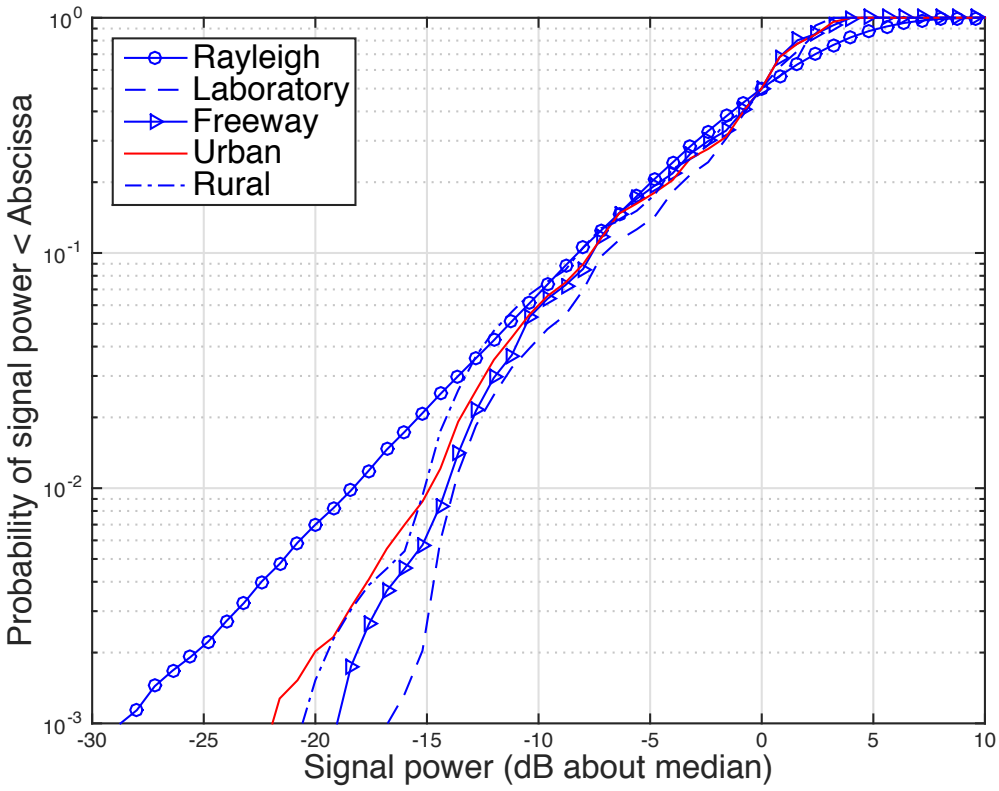

Figure 21: The CDFs of the CW signals at 500 Hz received by the PSAP in different test cases. The Rayleigh distribution is plotted for comparison.

cumulative distributions were compared to the Rayleigh distribution. When the probability was less or equal to 0.1%, the fading and attenuation was -22 dB on the urban road, -20.5 dB on the rural road, -19 dB on the freeway, and -16.7 dB in the laboratory, respectively. The maximum fade occurred on the urban road. When the probability was less or equal to 1%, the fading and attenuation was -14.8 dB on the urban road, -15.2 dB on the rural road, -14 dB on the freeway, and -13.6 dB in the laboratory, respectively. When the received signals were 10 dB below the median value, the probability was 7.1% on the rural road, 6.0% on the urban road, 5.8% on the freeway, and 4.3% in the laboratory, respectively. The results show that the signals received by the PSAP exist heavy fading, which will increase

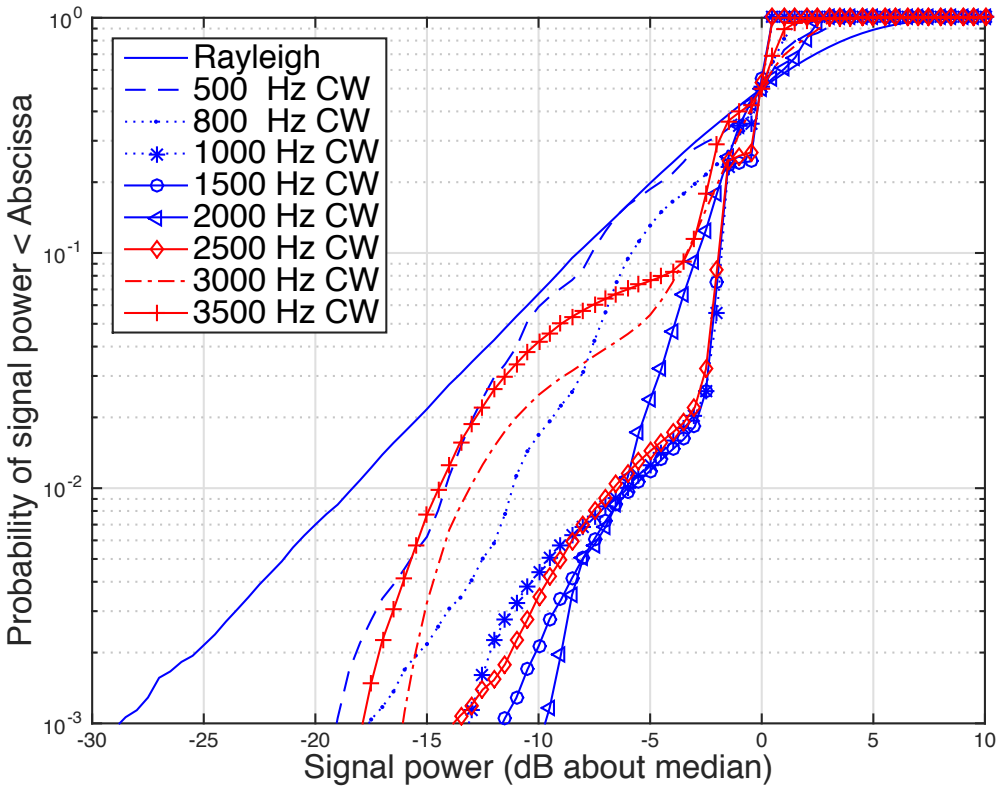

Figure 22: The CDFs of the CW signals received by the PSAP at different frequencies on the I-75 freeway. The Rayleigh distribution is plotted for comparison.

the data packet loss rate and reduce the data transmission success rate.

Figure 22 shows the CDFs of the CW signals received by the PSAP at different frequencies on the I-75 freeway. The Rayleigh distribution is plotted for comparison. When the probability was less or equal to 0.1%, the fading and attenuation was -19 dB for the 500 Hz CW signal, -17.5 dB for the 800 Hz CW signal, -13 dB for the 1000 Hz CW signal, -11.5 dB for the 1500 Hz CW signal, -9.5 dB for the 2000 Hz CW signal, -14 dB for the 2500 Hz CW signal, -16.2 dB for the 3000 Hz CW signal, -18 dB for the 3500 Hz CW signal, respectively. When the received signals were 10 dB below the median value, the probability was 5.9% for the 500 Hz signal, 1.6% for the 800 Hz signal, 0.45% for the 1000 Hz signal,

0.2% for the 1500 Hz signal, 0.08% for the 2000 Hz signal, 0.35% for the 2500 Hz signal, 2.5% for the 3000 Hz signal, 4.2% for the 3500 Hz signal, respectively. It can be seen that the fading of the 500 Hz CW signal and 800 Hz CW signal were more severe than the fading of the 1500 Hz CW signal and 2000 Hz CW signal. The worst fading occurred for the CW signal at 500 Hz which was the closest to the Rayleigh fading distribution.

In the 3GPP 26.267 standard, the synchronization tone for signal detection and synchronization is 500 Hz for the fast modulation mode and 800 Hz for the robust modulation mode. We recommend to move the synchronization tone from 500 Hz to 1500 Hz for the fast modulation mode and move the synchronization tone from 800 Hz to 2000 Hz for the robust modulation mode. This will give about 7.5 dB improvement in the fast modulation mode and 8 dB improvement in the robust modulation mode for signal detection and synchronization, respectively.

Level crossing rate is the number of fades for a given time interval. It shows how often the fades occur for a given threshold. Figure 23 shows the LCRs of the CW signals at 500 Hz received at different test locations. It can be seen that the LCR of the signal received on the rural road was the highest among the four test cases. The lowest LCR occurred in the laboratory. When the fade fell below -10 dB of the root mean square (RMS) of the received 500 Hz CW signal, the LCR was 3 fades per second on the rural road, 2.2 fades per second on the freeway, 3.3 fades per second in the laboratory, and 3.6 fades per second on the urban road, respectively.

Figure 24 shows the LCRs of the CW signals received by the PSAP at different frequencies on the I-75 freeway. When the received signal level was 10 dB below the RMS value, the LCR of the 500 Hz signal was 3.3 fades per second; the LCR of the 800 Hz

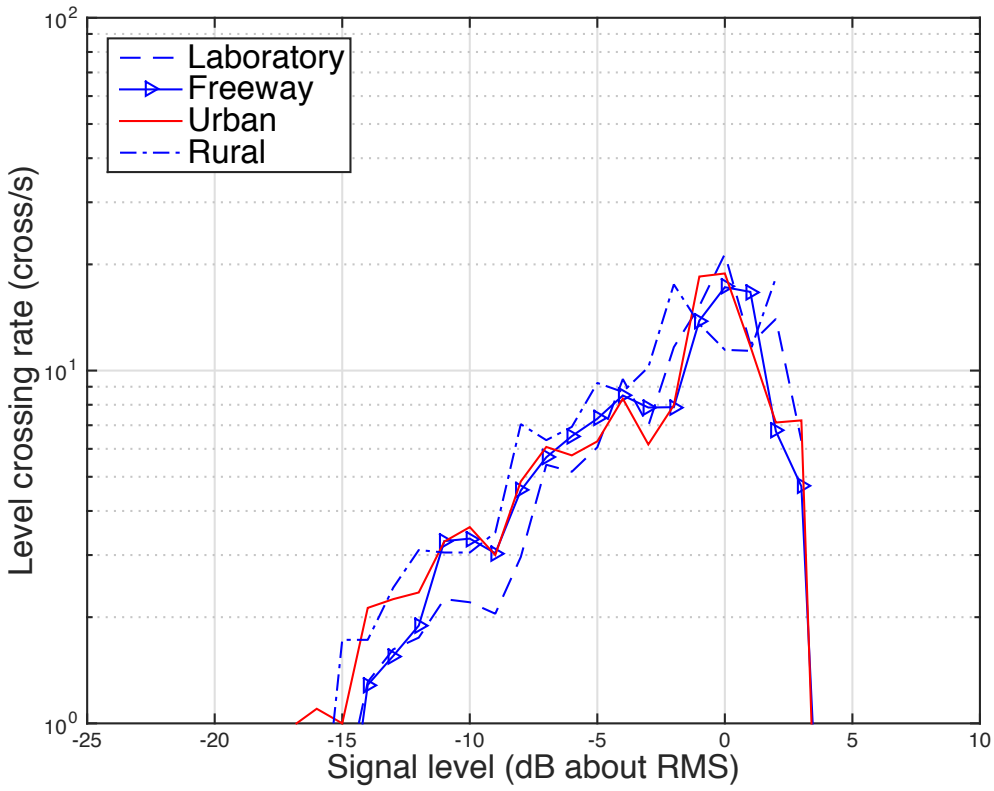

Figure 23: The level crossing rates of the CW signals at 500 Hz received by the PSAP in different test cases.

signal was 1.9 fades per second; the LCR was less than 1 fade per second for the CW signal at 1000 Hz or 1500 Hz or 2000 Hz; the LCR of the 2500 Hz signal was 1.2 fades per second; the LCR of the 3000 Hz signal was 1.9 fades per second; the LCR of the 3500 Hz signal was 3.3 fades per second. The maximum LCR occurred at 500 Hz and 3500 Hz CW signal.

Figure 25 shows the AFDs of the CW signals at 500 Hz received by the PSAP in different test cases. When the received signal level was -10 dB below the RMS value, the AFD of the received signal in the laboratory was 39 ms; the AFD of the received signal on the freeway was 36 ms; the AFD of the received signal on the urban road was 33 ms;

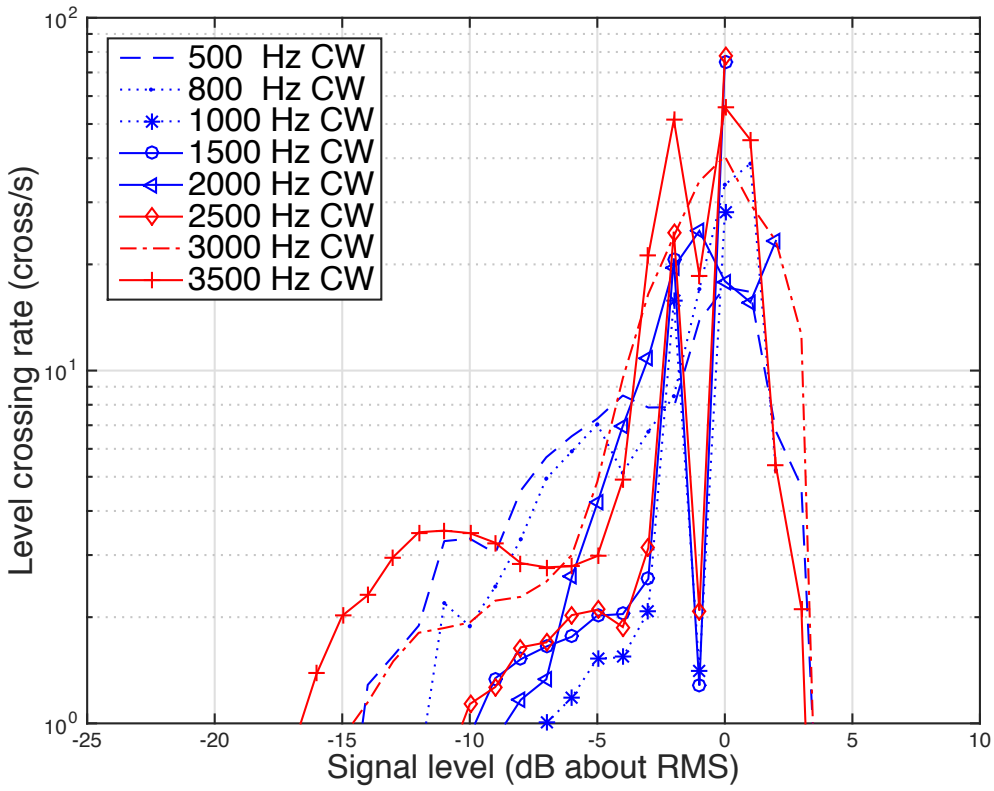

Figure 24: The level crossing rates of the CW signals received by the PSAP at different frequencies on the I-75 freeway.

the AFD of the received signal on the rural road was 48 ms. The maximum AFD occurred on the rural road. The symbol time is 2 ms for the fast modulation mode. One symbol represents 3-bit data. If a fade occurs during the MSD transmission, the 48 ms average fade duration may affect 24 symbols (or 72 bits) for the fast modulation mode. It is too difficult for the Turbo code in the 3GPP TS 26.267 standard to correct a burst of 72-bit errors within one MSD [38, 56].

Figure 26 shows the AFDs of the CW signals received by the PSAP at different frequencies on the I-75 freeway. When the received signal level was 10 dB below the RMS value, the AFD was 36 ms for the CW signal at 500 Hz, 18 ms for the CW signal at 800

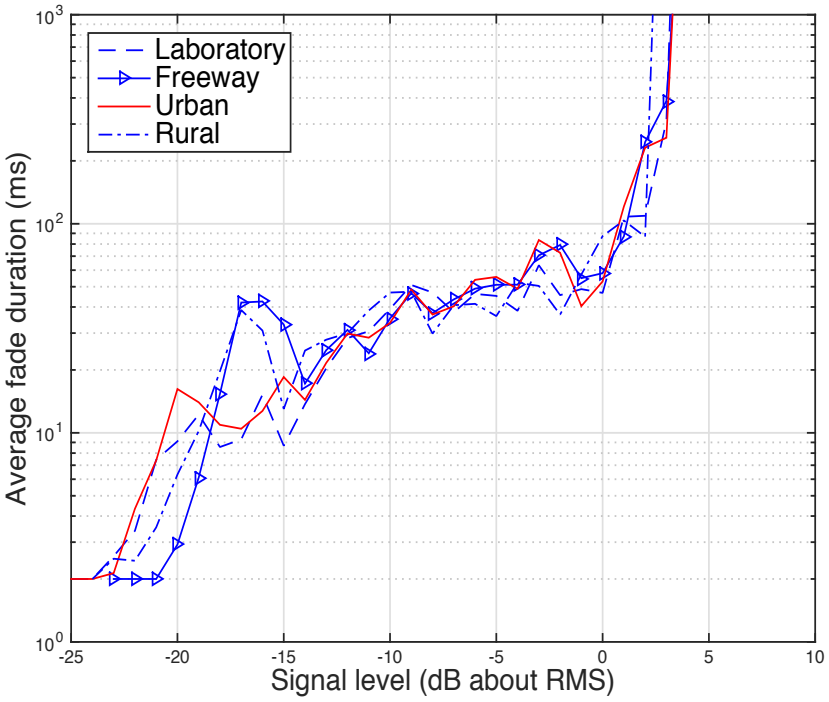

Figure 25: The average fade durations of the CW signals at 500 Hz received by the PSAP in different test cases.

Hz, 10 ms for the CW signal at 1000 Hz, 4 ms for the CW signal at 1500 Hz, 6 ms for the CW signal at 2000 Hz, 6 ms for the CW signal at 2500 Hz, 26 ms for the CW signal at 3000 Hz, 24 ms for the CW signal at 3500 Hz. The maximum AFD occurred at 500 Hz CW signal. In the frequency range [1000, 2500] Hz, the fading was much smaller.

The fading is less severe than the Rayleigh fading. It is not a Gaussian process either. Analyzing the distribution of the GSM signal fading after power control is nontrivial and worth further study. The fading varies with frequency. The CW signals at 500 Hz and 800 Hz for detection and synchronization experience severe fading. In the frequency range [1000, 2500] Hz, the fading is in the range [-13, -9.5] dB. The longest fading duration observed for the 500 Hz CW signal was 540 ms. The fading needs to be considered in the future revision of the 3GPP TS 26.267 standard.

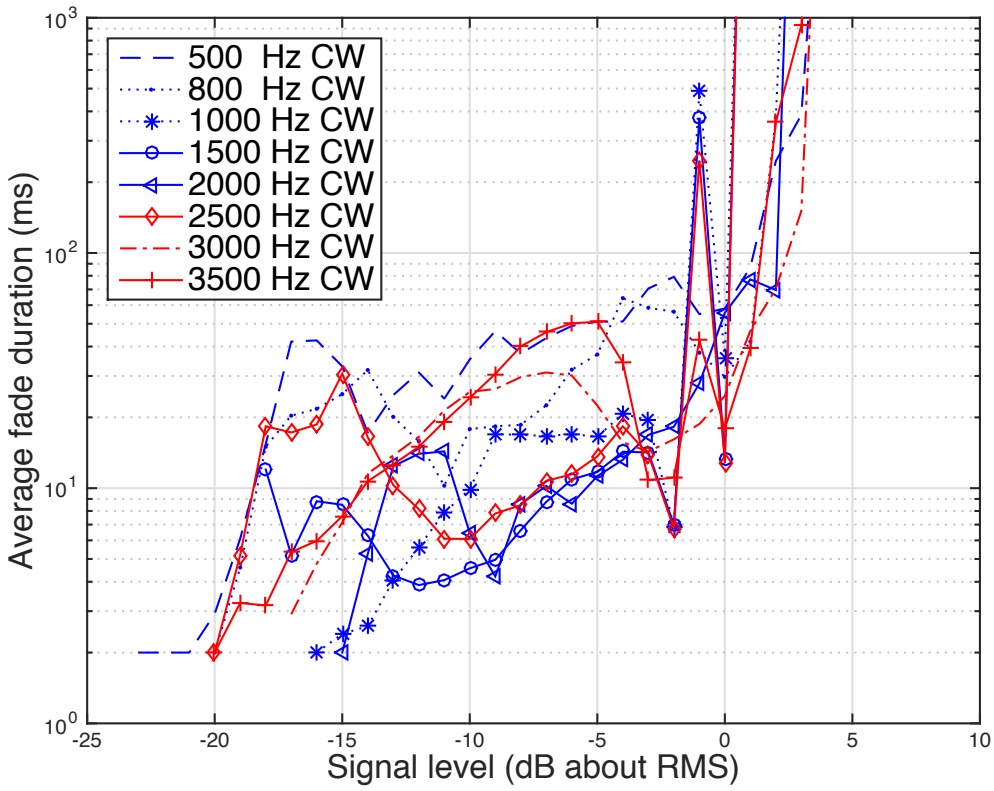

Figure 26: The average fade durations of the CW signals received by the PSAP at different frequencies on the I-75 freeway.

4.5 Conclusion

A testbed is designed and developed to obtain the fading statistics of the EU emergency call channel. Experiments are performed in different environments to obtain the CDF, LCR, and AFD of the received signal. It is found that with probability less or equal to 0.1%, the fading is -19 dB for the CW signal at 500 Hz and -9.5 dB for the CW signal at 2000 Hz, respectively. It is recommended to move the 500 Hz CW signal and the 800 Hz CW signal for detection and synchronization in the 3GPP TS 26.267 standard to around 2000 Hz for minimum fading. This will give 9.5 dB improvement in signal detection and synchronization. Signals in the frequency range [1000, 2500] Hz experience much smaller

fading.

We also found it impossible to demodulate and decode the MSD with two fading gaps in four seconds. The cumulative fading distribution of the channel indicated that strong fading persisted in the GSM voice channel even after power control. The fading statistics indicated that about 0.01% of the received power attenuated 27 dB, 0.1% attenuated over 16 dB, 1% attenuated over 5.8 dB, and 10% attenuated over 4.8 dB. Fading throughout the entire voice channel severely impacted the MSD data transmission in our experiment.

The experiment results have shown that severe fading still exists in the voice channel of the GSM network with power control. The fading explains the substantial delays observed in the NXP road trial of the MSD transmissions employing the 3GPP TS 26.267 system, which was also seen in experiments using this testbed. The fading increases the MSD transmission delay and reduces the success rate of the MSD transmission. The fading should be considered in the future revision of the 3GPP TS 26.267 standard to minimize the MSD transmission delay in emergency call systems.

CHAPTER 5 ERROR PROBABILITY PERFORMANCE EVALUATION FOR THE IN-BAND MODEM

5.1 Introduction

The EU eCall is expected to reduce rescue response time and save thousands of lives every year. However, the test setup, used to select the eCall in-band modem, was simulated between two computers in a laboratory. The impact of various time-variant and non-linear elements in the channel affecting eCall MSD transmissions, such as power control, adaptive echo cancellers, noise cancellers, and transcoding between codecs, was not taken into consideration in the selection. These impairments can affect the performance of the eCall in-band modem, resulting in data errors. Additionally, according to the test results in the previous chapter, fading still exists in the cellular voice channel, even if some anti-fading techniques such as diversity, interleaving, and power control, are applied in the mobile network to eliminate the consequence of multipath propagation and Doppler shift. The fading can increase the error probability and intersymbol interference (ISI), which can reduce the success rate of the received MSD. Furthermore, the spectral broadening caused by Doppler shift, also affects the performance of the eCall data transmission. The probability of bit error rate is a widely used and valuable statistical indicator of performance when estimating the performance of digital communication systems [57].

Fading, in the GSM channel, can notably degrade the MSD signal as it is compressed by the GSM speech coders and voice activity detectors (VAD). Existing methods for the in-band modem over voice channels can be divided into two categories [24]. The first category is to minimize the BER; the second category emphasizes maximizing the transmission speed in an acceptable BER. The error probability performance results will then

be compared to the bipolar 4-PPM modulation scheme used in the EU eCall standard.

5.2 Analytical Expressions for Error Probability Performance

The SNR of a received signal is defined as the ratio of the received signal power Pr to the noise power within the bandwidth of the transmitted signal. The received power Pr is affected by multipath fading, the path loss, shadowing, and the transmitted signal power. The noise power can be calculated by the spectral properties of noise the bandwidth of the transmitted signal [52]. Assuming that the MSD signal passes through the AWGN channel without fading, the received signal by the PSAP is the sum of the transmitted MSD signal and Gaussian white noise $n(t)$, which is a Gaussian random process with zero mean and power spectral density $N_0/2$. Specifically, if the bandwidth of bandwidth of the transmitted signal is $2B$, the total noise power is $N = N_0/2 \times 2B = N_0B$. So the SNR of the received signal [52] is given by

$$\gamma = \frac{Pr}{N_0B} \tag{5.1}$$

Let E_b represent energy per bit, and E_s represent energy per symbol. The quantities $\gamma_s = E_s/N_0$ and $\gamma_b = E_b/N_0$ are called the SNR per symbol and the SNR per bit, respectively. The SNR γ then can be expressed as

$$\gamma = \frac{Pr}{N_0B} = \frac{E_s}{N_0BT_s} = \frac{E_b}{N_0BT_b}, \tag{5.2}$$

where Ts is the symbol time and T_b is the bit time. For M-aray modulation scheme.

$$p_b \approx \frac{P_s}{\log_2 M} \tag{5.3}$$

In the AWGN channel, the probability of symbol error depends primarily on the SNR γ_s of the received signal. In a channel with fading, the SNR is a random variable and changes with the distribution of the fading. Thus, the statistical average SNR of the fading distribution is calculated to estimate the probability of symbol error. The average SNR [52] $\overline{\gamma}$ is,

$$\overline{\gamma} = \int_0^\infty \gamma p_\gamma(\gamma)\, d\gamma. \tag{5.4}$$

Where γ_s denotes the instantaneous SNR per symbol at the receiver output that includes the effect of fading.

It is assumed that γ_s is approximately constant during a symbol time T_s. Then the averaged probability of symbol error $\overline{P_s}$ is calculated by integrating the error probability in AWGN channel over the fading distribution

$$\overline{P_s} = \int_0^\infty P_s(\gamma) p_{\gamma_s}(\gamma)\, d\gamma, \tag{5.5}$$

where $P_s(\gamma)$ is the probability of symbol error in AWGN channel with SNR γ.

The in-band modem used in the eCall system is bipolar 4PPM. The probability of symbol error M-ary PPM [58, 59] can be expressed as,

$$P_s(\gamma) = erfc\left(\frac{1}{2\sqrt{2}}\sqrt{\gamma \frac{M}{2}\log_2 M}\right) \tag{5.6}$$

where $erfc(.)$ is the complementary error function. The fading distribution has been cal-

culated using fading statistics in chapter 4. The results of $p_{\gamma_s}(\gamma)$ and $P_s(\gamma)$ are substituted into the Equation (5.6). Then, the error probability of the in-band modem of the eCall voice channel can be calculated.

5.3 Experimental Procedure and Data Collection

The MSD transmission experiment was conducted with randomly generated MSD data for 500 times in each environment to ensure statistical significance. BER data was collected in the five experimental environments described in Chapter 3. The following test procedure was repeated for each set of test conditions. The IVS recorded the GSM signal strength for each test and the PSAP calculated the bit error rate.

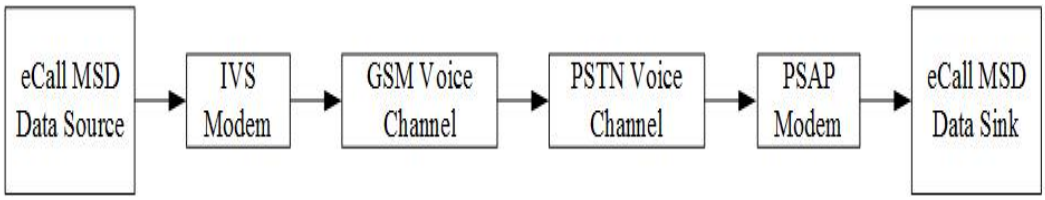

Figure 27: Block diagram of BER performance measurement for the eCall in-band modem.

Bit error performance was evaluated via the following procedure.

The IVS platform is tested and verified by pressing the emergency button to trigger an emergency call. The test procedure is shown in Figure 28. The detailed steps of the test process are.

1. When the emergency button is pressed, the IVS calls the PSAP and a voice call will be established between the IVS and PSAP.

2. When the IVS is running in push mode, an INITIATION message is sent to the PSAP. The INITIATION message is used to tell the PSAP that an emergency call is activated.

3. Upon the detection of the synchronization preamble and when PSAP detects the

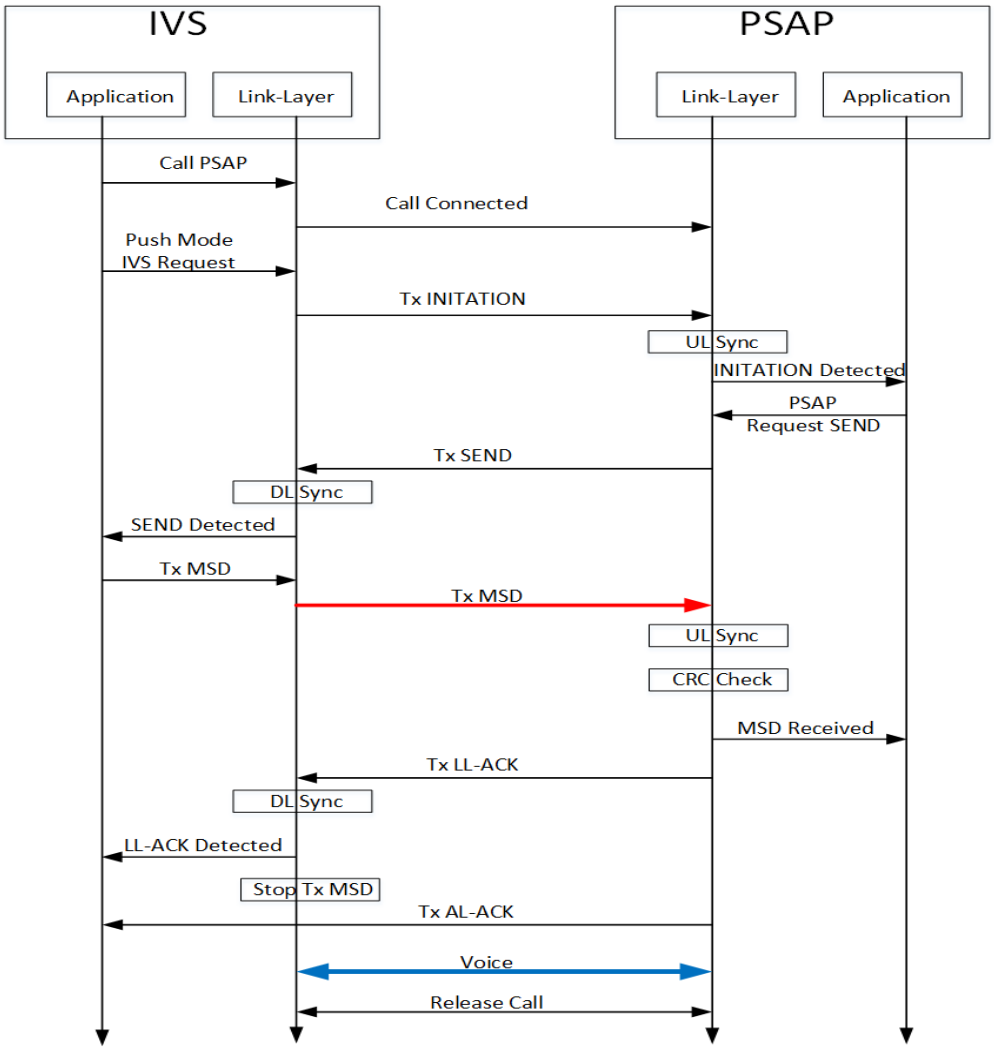

Figure 28: The EU emergency call BER test procedure.

INITIATION message, the PSAP sends a START message to the IVS continuously up to 5 times.

4. Once the IVS has successfully decoded the START message, which indicates that the PSAP is ready to receive the MSD, the IVS begins transmitting one synchronization frame followed by the first redundancy version MSD RV0.

5. If the PSAP does not demodulate and decode the MSD redundancy version RV0, a negative acknowledgment (NACK) message is sent to the IVS.

6. If the IVS receives the NACK message, the IVS then send MSD RV1 to the PSAP.

7. Once the PSAP successfully obtains the MSD, the PSAP sends an application layer ACK, which indicates that the MSD is successfully received by the application layer.

8. The IVS stops sending the MSD when the ACK is received by the IVS.

9. The eCall system is then switched to voice talk. The driver and the PSAP operator start a conversation at this moment.

10. Finally, the original MSD sent by the IVS and the received MSD by PSAP are compared and the error probability is calculated accordingly.

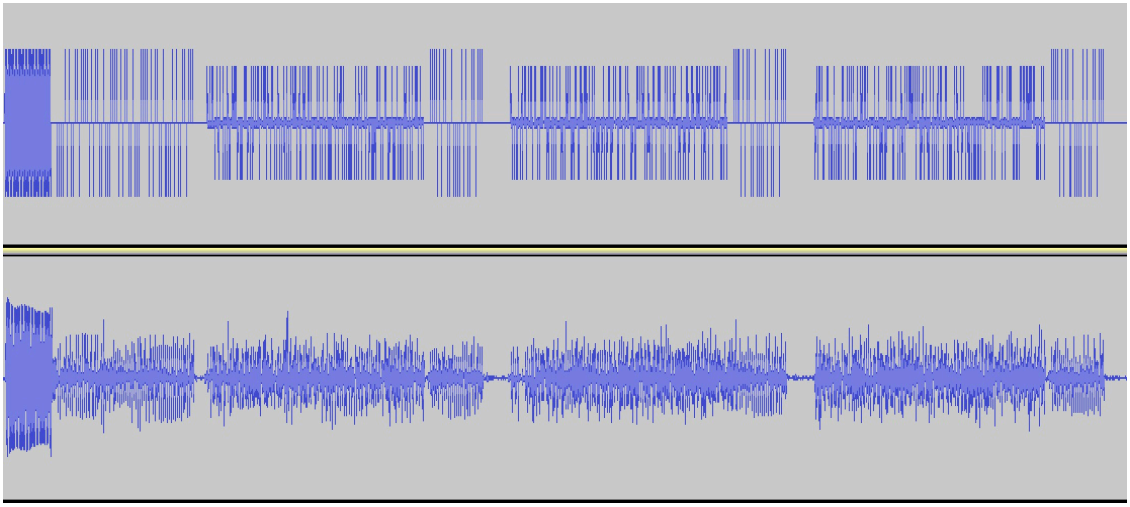

Figure 29: The MSD signal sent by the IVS and the received MSD signal by the PSAP.

Figure 29 shows the MSD signal sent by the IVS and the received MSD signal by the PSAP. Figure 30 shows the original downlink feedback messages sent by the PSAP and the received feedback messages by the IVS.

5.4 Data Analysis and Discussion

Figure 31 shows the probability distribution of the received signal power around its median, under the eCall channel, Gaussian channel, and Rayleigh channel. The curves indicate that the signal power probability distribution in the eCall channel is neither Gaus-

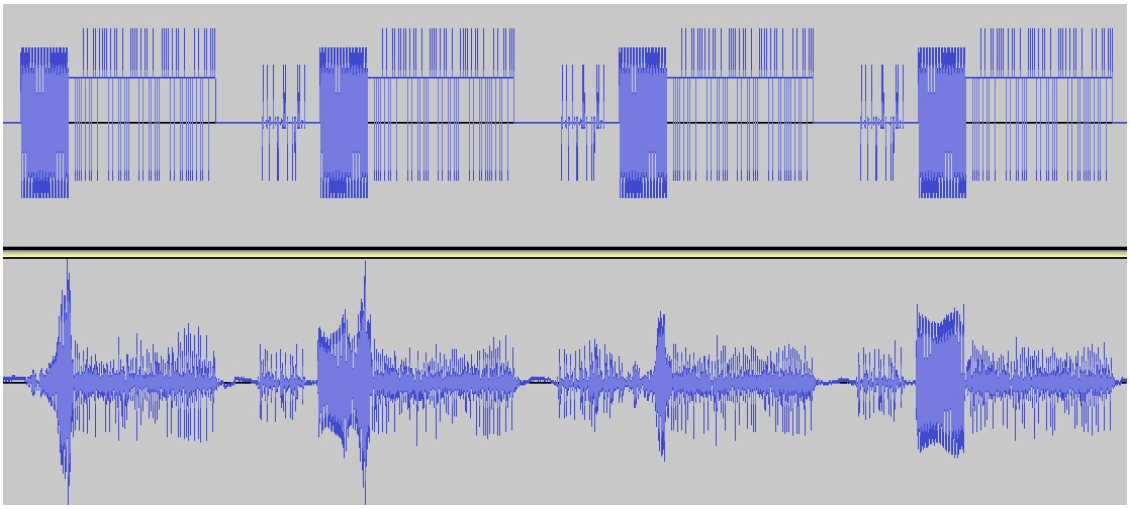

Figure 30: The downlink feedback messages sent by the PSAP and the received feedback messages by the IVS.

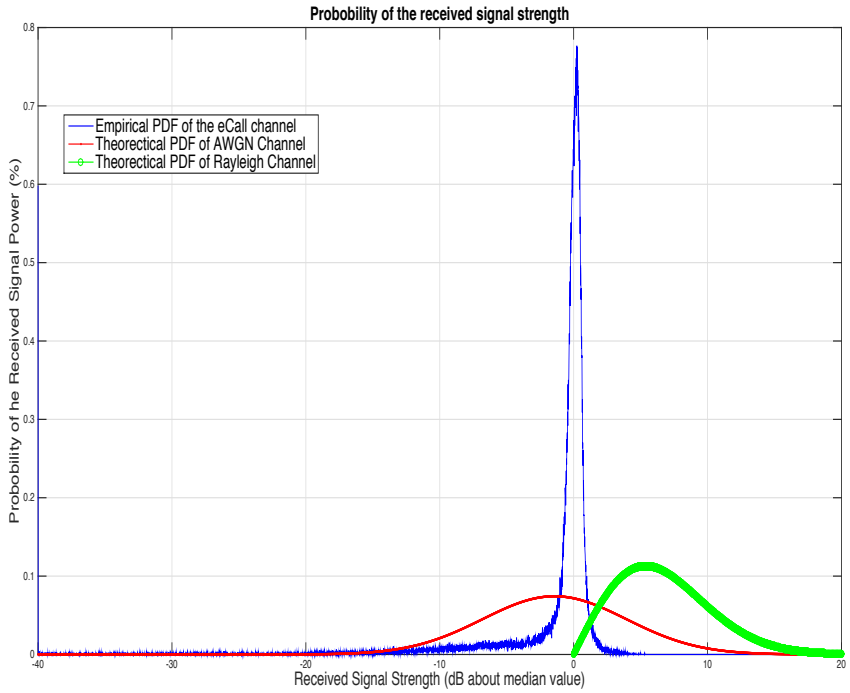

Figure 31: PDFs of the eCall channel, AWGN chanel and Rayleigh fading channel.

sian nor Rayleigh distribution. The figure also shows that the signal fading was mainly concentrated in the -10 to 5 dB range.

Equation (6.6) expresses the BER of the M-array PPM modulation scheme in the

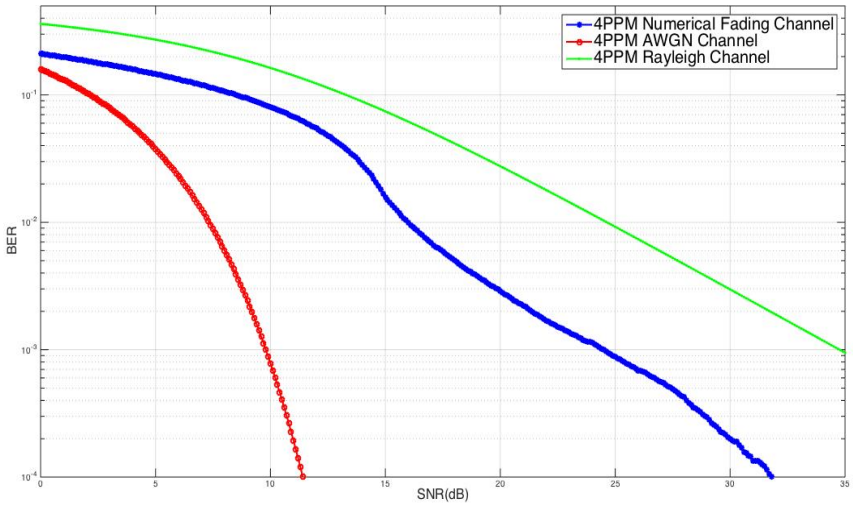

Figure 32: BER performance of 4-PPM under the voice Channel, AWGN channel, and Rayleigh fading channel.

AWGN channel. The BER value can be calculated when the SNR varies from 0 dB to 35 dB, then BER values and the measured probability distribution values can be substituted into Equation (6.7) to calculate the probability distribution in the eCall channel. Figure 5.4 shows the error probability of 4-PPM in the eCall channel, AWGN channel, and Rayleigh fading channel. The required SNR is approximately 9.6 dB to maintain a 10^{-3} bit error rate in the eCall channel, AWGN channel, and Rayleigh fading channel. Conversely, about 24.6 dB SNR is needed to maintain the same error rate in the eCall channel; the SNR should be 35 dB to maintain the same BER performance.

5.5 Conclusion

This chapter presents a straightforward empirical methodology that can be readily used to measure the average bit error rate of the nonlinear time-varying fading channel. Furthermore, this research uses road test to collect realistic error data for both fast mode and robust mode transmissions in the different road environment and calculate BER for bipolar

PPM modulation techniques in fading channels. In fading channels, the received signal power is not constant but changes as the fading of the channel changes. The BER of the fading channel averaged over the different fading states reveals the nature of the system behavior and illustrates the system performance.

CHAPTER 6 TIMING SYNCHRONIZATION PERFORMANCE EVALUATION FOR THE IN-BAND MODEM

6.1 Introduction

Timing synchronization is critical for reliable symbol detection and timing offset estimation, in a wireless communication system. Especially in applications such as in-vehicle eCall systems, reliable timing synchronization is one of the most significant factors for successful emergency data transmission [60]. Acquiring accurate symbol timing is particularly challenging in fading channels because it is very difficult to e estimate signal parameters before demodulation. In this chapter, an experiment is designed to evaluate the performance of the selected synchronization sequence in the eCall system and determine the detection probability of the synchronization preamble.

6.2 Synchronization Signal Generation and Format

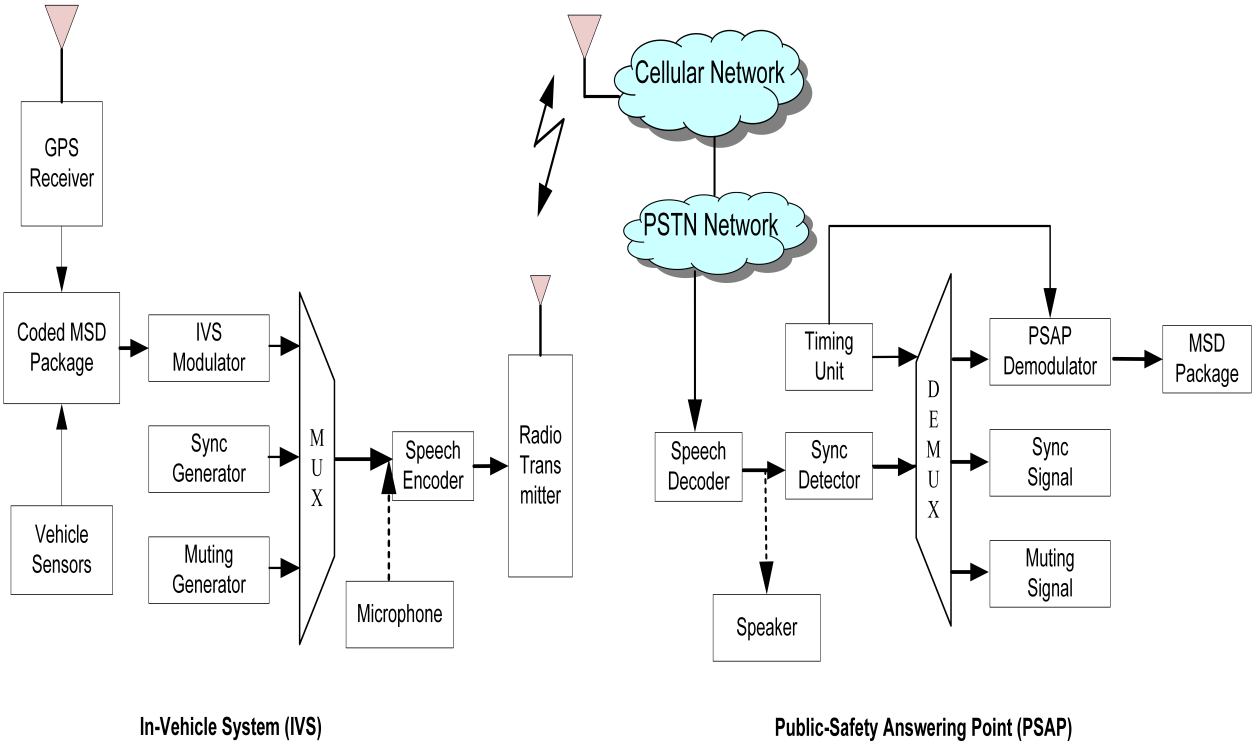

Figure 33: Block diagram of the uplink channel in the 3GPP eCall system.

Figure 33 shows the detailed structure of the IVS modem and PSAP modem. The IVS modem includes a BPPM modulator, a synchronization generator, and a muting signal generator. An MSD multiplexer synthesizes the generated signals and transmits to the PSAP through the uplink channel. The PSAP modem consists of a synchronization detector and a PSAP demodulator. The MSD signal received by the PSAP is identified by the detector to obtain a time synchronization. Simultaneously, the time synchronization signal is provided to the PSAP demodulator, and the modulated MSD signal is demodulated according to the obtained timing information. If the synchronization detector does not detect the time synchronization signal or false alarm detection occurs, the MSD signal cannot be correctly received. As shown in the Figure 34, the IVS starts detecting the START signal, and the PSAP starts detecting the INITIATION signal after an emergency call is established. Once the START signal is successfully detected, the IVS starts sending the uplink signal including the 260 ms synchronization frame and the 8 RVs MSD data frames to the PSAP until the PSAP receives the data. If the miss detection happens at RV0, the IVS needs to resend the second version RV1 with 1.32 s length. It will increase the transmission time of the MSD and affect the real-time transmission. Therefore, synchronous detection is crucial for the real-time transmission of MSD data.

The synchronization frame in the eCall consists of two parts: synchronization tone $s_t(n)$ and synchronization preamble $s_p(n)$. The $s_t(n)$ is a sampled sinusoidal signal with a length of 64 ms. A sinusoidal signal with a frequency of 500 Hz indicates the fast modulator mode and a synchronization tone of an 800 Hz sinusoidal signal is chosen for the robust modulator mode. The $s_t(n)$ includes 8000 * 0.64 = 512 samples when the sampling rate is 8000 samples per second. Each sample is represented by a 16-bit binary.

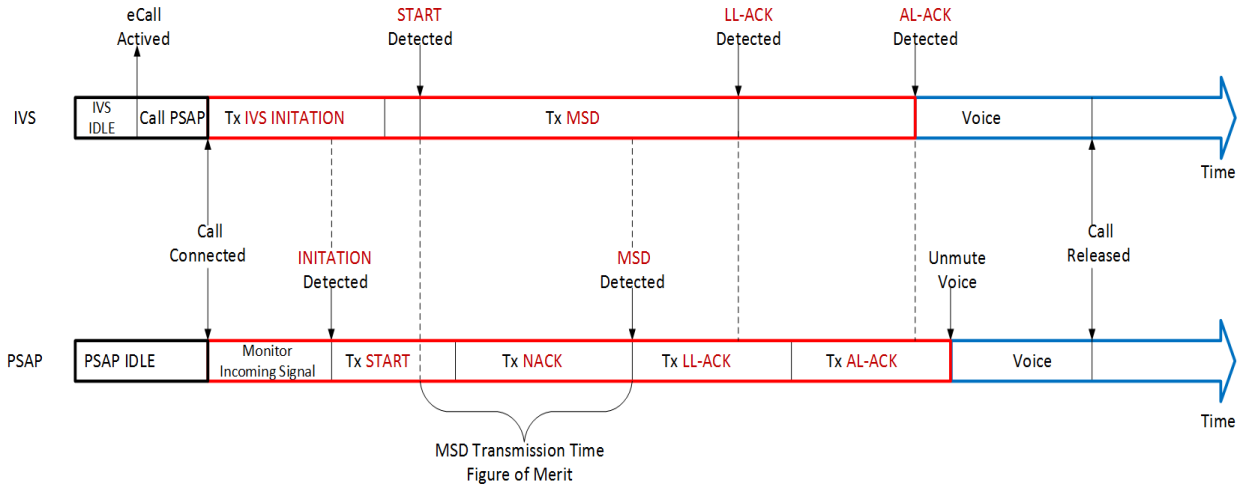

Figure 34: The time line of synchronization process for the eCall system.

The first 512-sample pulses, as shown in Figure 35, represent the synchronization tone. The synchronization tone is followed by the synchronization preamble, whose duration is 196ms; a total of 8000 * 0.64 = 1568 samples.

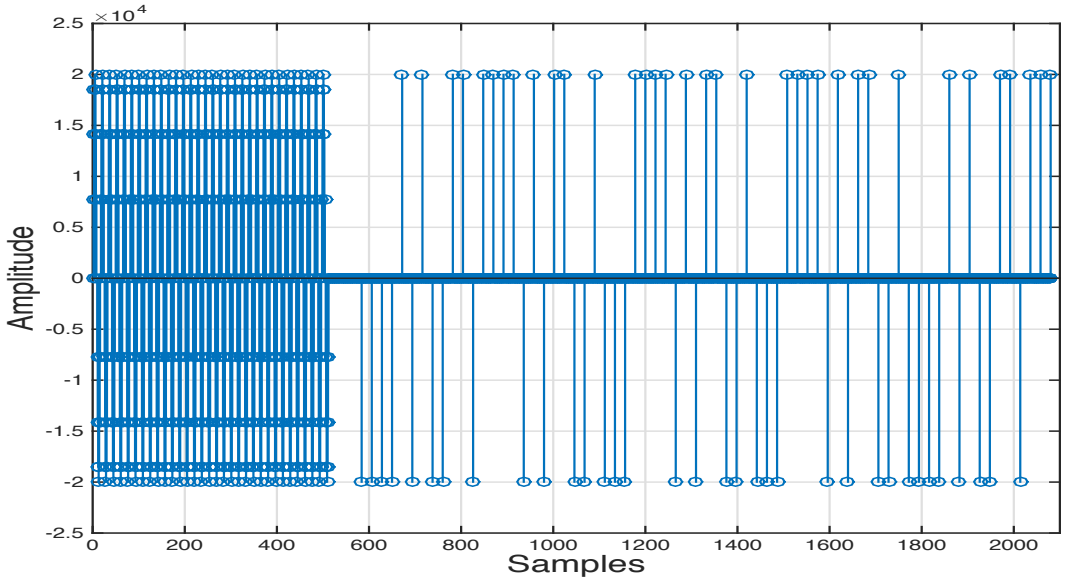

Figure 35: Synchronization frame of the in-band modem.

The synchronization preamble is a sequence of pulses that are known at the receiver. Figure 37 shows the pulse sequence for the synchronization preamble, The synchro-

nization preamble pulse sequence is composed of 5 basic pseudorandom noise (PN) sequences of length 15. The value of the base PN sequence is (1,1,1,1,-1,1,-1,1,1,-1,-1,1,-1,-1,-1). Each '1' represents a signed pulse with an amplitude value of 20,000. The five base PN sequences are numbered from left to right as the number 1 to 5. The first and fifth PN sequences are inverted (i.e., all elements are multiplied by -1), and the last 3 elements of the first inverted PN sequence are the same as the first 3 elements of the second PN sequence. The three overlap elements are transmitted only once. Similarly, the last three elements of the fourth normal phase PN sequence are identical to the first three elements of the fifth inverted PN sequence, and the overlap elements are transmitted only once. Thus, the length of the synchronization preamble pulse sequence is 75 - 3 - 3 = 69 samples. Figure 36 illustrates the method of generating the pulse sequence. Figure 35 shows a generated synchronization preamble pulse sequence with length of 69 samples. The adjacent pulse '1' of the synchronization preamble pulse sequence is then inserted with 21 zero samples, and 71 zero samples are placed before the first pulse to form a synchronization preamble. The resulting $s_p(n)$ has a duration of 71 + 69 + (68 * 21) = 1568 samples, or 196 ms. Therefore, the total length of the synchronization frame is 260 milliseconds or 13 speech frames. The synchronization preamble is an autocorrelation-optimized pulse sequence that is used not only for sync frames, but also for inserting a portion of the sync preamble into the middle of the MSD for uplink synchronization tracking purposes.

6.3 Experiment Design

It is difficult to precisely determine the beginning and end of the preamble due to the fading and distortion of the channel. Further studies are required to design experiments

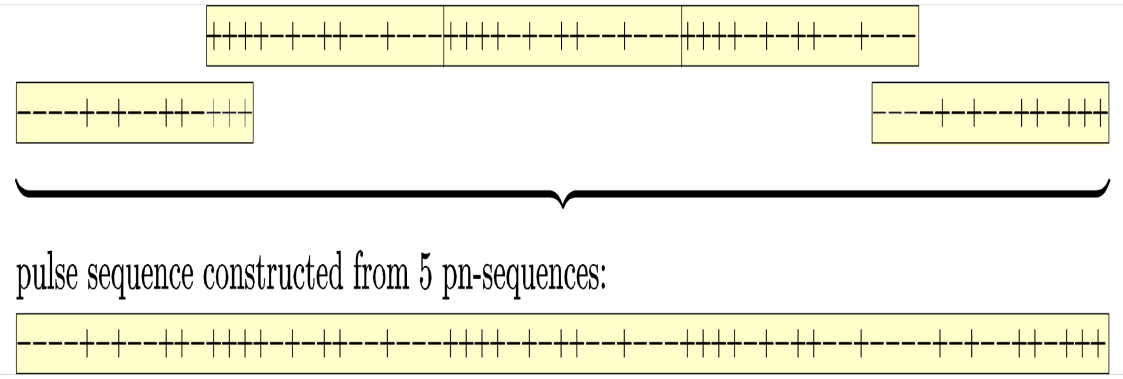

Figure 36: The method of generating the synchronization preamble pulse sequence..

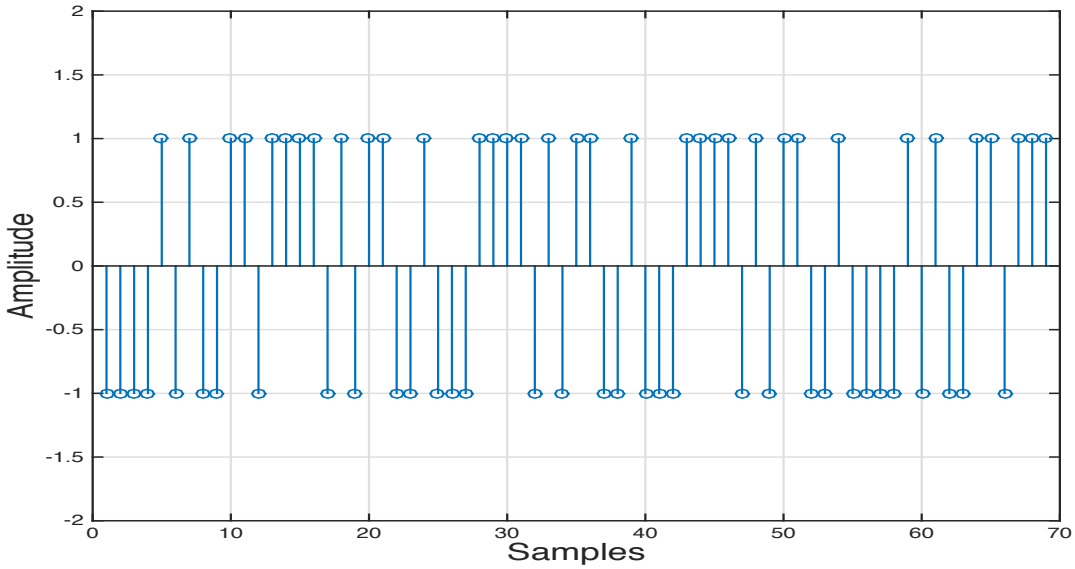

Figure 37: Pulse sequence of the synchronization preamble.

to access the signal synchronization performance for the EU eCall system.

Figure 38 shows a block diagram of the synchronization frame generation, transmission, and detection for the up-link channel in the 3GPP eCall system. In order to evaluate the detection probability of the synchronization signal, the in-band modulator and muting generator were removed from the testing system. The signals generated by the synchronization tone generator and the synchronization preamble generator, are synthesized and passed through the AMR vocoders and AWGN channel, and finally, the synchronization

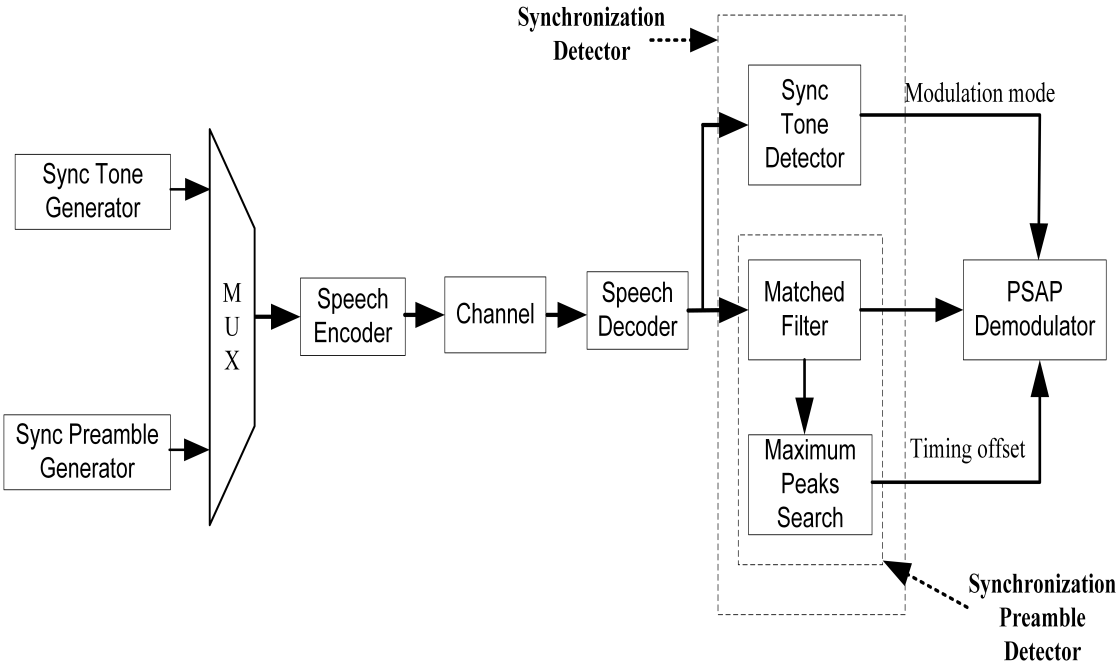

Figure 38: Block diagram of the synchronization frame generation, tansmission, and detection for the up-link channel in the 3GPP eCall system.

preamble is detected at the PSAP synchronization detector.

The synchronization signals pass through vocoders with AMR rates of 4.75 kbps, 5.15 kbps, 6.70 kbps, 7.40 kbps, 10.2 kbps, and 12.2 kbps, respectively. The SNR setting of the AWGN channel is stepped up by 0.5 dB, gradually. The synchronization signal was subjected to 1000 experiments through the AMR vocoder and the AWGN channel corresponding to each SNR value. For each successful detection, the synchronization preamble counter is incremented by 1, and the detection probability is obtained.

6.4 Detection Algorithm and Data Analysis

Figure 39 shows the flow chart of timing synchronization detection algorithm for the in-band modem. The synchronization detector scans the input signal and checks a 500 Hz or 800 Hz sinusoidal signal through the synchronization tone detector. The input sig-

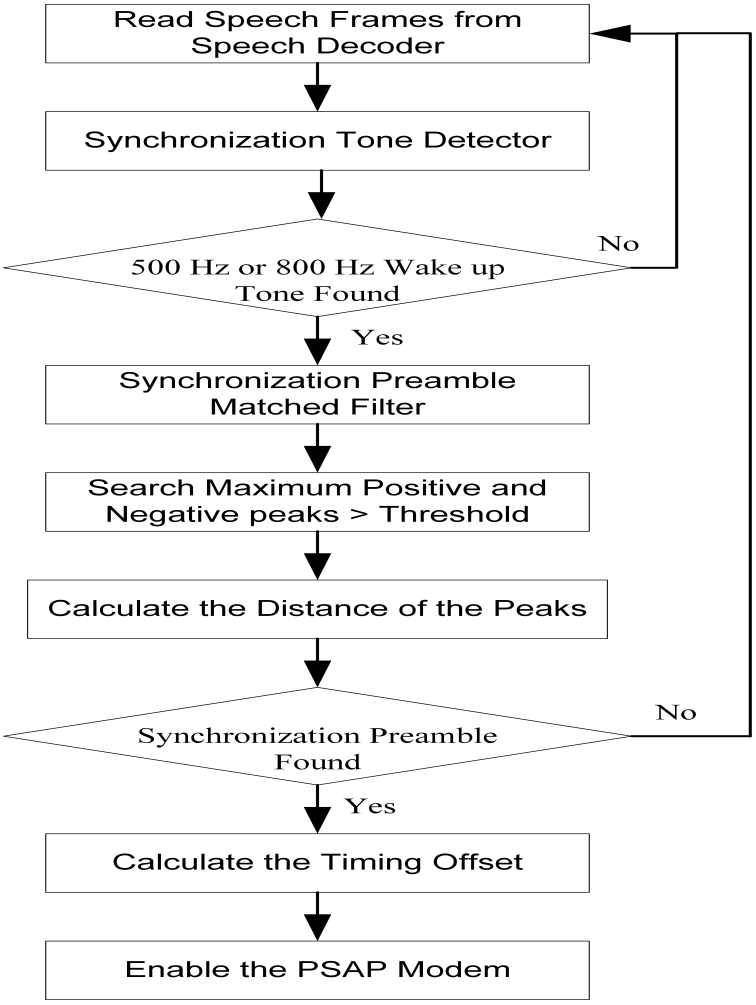

Figure 39: The flow chart of timing synchronization detection algorithm for the in-band modem.

nal arriving at the PSAP correlates with the stored PN sequence at the receiver after the synchronization tone is detected. If the input signal and the PN sequence are autocorrelated, the matched filter outpus five correlation peaks. Finally, the five peaks along with the distances between the peaks are used to identify the starting position and timing offset of the data frame according to the detection algorithm. The autocorrelation property of the pulse sequence is shown in Figure 40.

The detection algorithm determines the synchronization preamble and timing offset by checking the matching of the distance between the five correlation peaks and the number

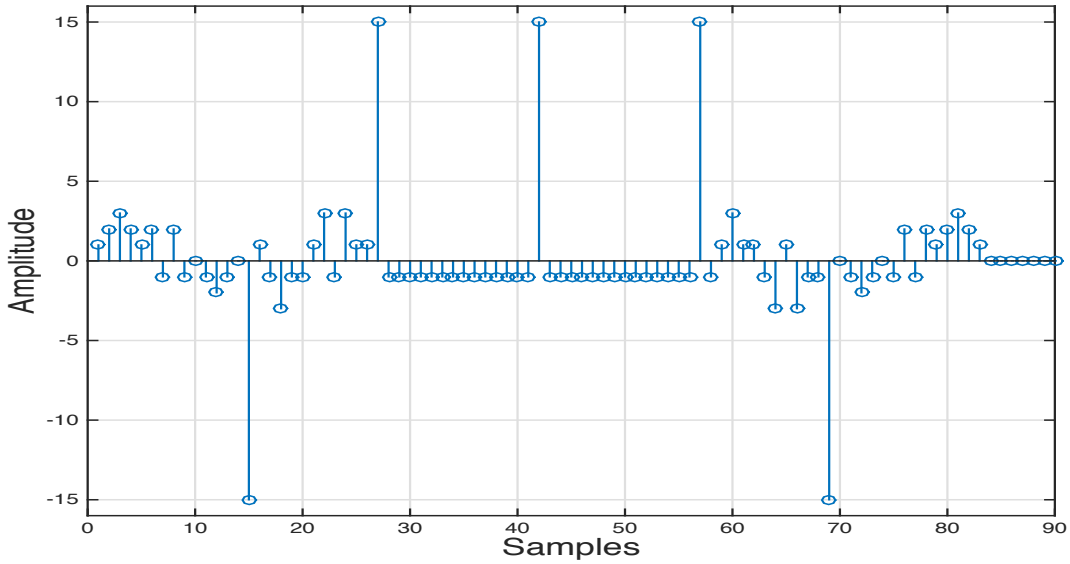

Figure 40: Autocorrelation of the synchronization preamble pulse sequence.

of detected peaks. The PN sequence at the receiver is correlated with the received sync preamble to generate five main peaks (1 negative peak, 3 positive peaks and 1 negative peak) , as shown in Figure 40. The timing offset is determined by any of the three detected peaks and the corresponding time distance between the peaks. The combination of the three detected peaks and the corresponding time distance is always unique. Table shows the combination of the detected peaks . The correlation peaks in Table 1 use '- ' to indicate a negative peak and '+' to indicate a positive peak. If only a pair of peaks (2, 4) or a pair of peaks (1, 5) is detected and the distance is correct between each other, the preambles are considered to be detected as long as they satisfy a certain amplitude constraint. Their average value should not be less than half of the global maximum synchronous filter output, or an additional peak can be identified to obtain timing. After the synchronization detector obtains the timing signal, the PSAP modem is enabled to complete the demodulation of the MSD. The advantage of this detection algorithm is that the synchronization detector

can reliably detect the synchronization preamble even if the signal quality is poor on a channel, or the loss of the speech frame may result in the loss of the correlation peak.

Table 6.1 shows the combination of three peaks detected, each of which lost two peaks after passing through the matched filter. Each entry in Table 6.1 represents a unique mode peaks and the time distance between peaks. The sync signal can be reliably detected.

Figure 41 shows the performance of the synchronization preamble through various AMR vocoders and AWGN channel. As shown in Figure 41, when the synchronization signal only passes through the AWGN channel without the AMR encoder and the SNR is -3.8 dB, the detection probability can reach 100%. When the SNR is -5 dB, the detection probability can achieve 94% can be achieved. When the synchronization signal passes through the AMR vocoder of 10.2 kbps or 12.2 kbps, their performances are pretty close to that of the AWGN channel, which indicates that the synchronization performance of the in-band channel is close to that of the Gaussian channel when high rate vocoders are used. The lowest detection probability occurs in the case when an AMR vocoder rate of 4.75 kbps is used, indicating that the low coding rate has a significant influence on the

Table 1: Detected correlation peaks for the timing synchronization

Cases	1	2	3	4	5
Case1		+		+	
Case2	-				-
Case3			+	+	-
Case4		+		+	-
Case5		+	+		-
Case6		+	+	+	
Case7	-			+	-
Case8	-		+		-
Case9	-		+	+	
Case10	-	+			-
Case11	-	+		+	
Case12	-	+	+		

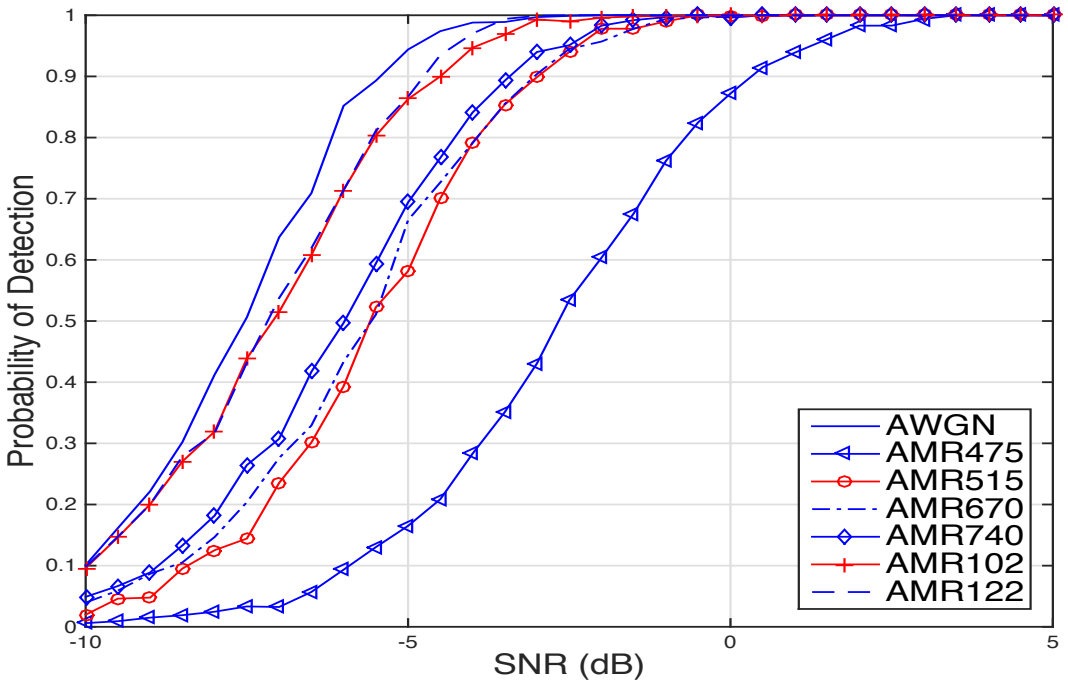

Figure 41: Comparison of the detection probability of the synchronization preamble through various AMR vocoders and AWGN channel.

synchronization signal. To achieve a 90% detection probability, the required SNR of the AMR vocoder of 4.75 kbps has to be 6.0 dB more than the SNR of the AWGN channel. When the SNR is greater than 3.5 dB, the probability of detection for all test cases can reach 100%. Therefore, in order to ensure the correct detection of the synchronization signal, the SNR of the input signal received at the PSAP receiver is recommended to be more than 3.5 dB.

6.5 Conclusion

The synchronization preamble of the in-band modem is particularly critical for reliable detection and precise delay estimation. This chapter presents the generation of the synchronization preamble and introduces a simple approach and procedure for the performance evaluation. Finally, timing estimation performance and synchronization detec-

tion probability are obtained by transmitting the synchronization preamble through various adaptive multi-rate vocoders and additive white Gaussian noise channel.

CHAPTER 7 CHANNEL FADING MEASUREMENT AND STATISTICS FOR UAS COMMUNICATIONS

7.1 Introduction

Recently the unmanned aerial system industry has experienced a strong growth. They have been employed in numerous applications including agriculture, wildfire management, disaster monitoring, remote sensing, wind estimation, filmography, traffic control, search and rescue, medical aid and inspection of infrastructure, railroad, road and power line [1, 61, 2, 62]. “Unmanned aerial systems (UAS) [63, 64], sometimes referred to as drones, are multi-use aircraft controlled from a licensed operator on the ground.” The Association for Unmanned Vehicle Systems International estimates that the unmanned aircraft services will have a $82 billion impact on the global economy from 2015 to 2025 [1]. A radio link between the UAS and the operator is required by the FAA for real-time UAS ID tracking, command and control [3]. The Aviation Rulemaking Committee recommends a maximum total latency of 6.5 seconds and update rate greater or equal to 1 Hz for UAS ID tracking. This is a tighter requirement than the automatic dependent surveillance - broadcast (ADS-B) system for manned aircraft and the ADS-B system has not achieved this performance yet. The FAA Part 107 requires a UAS weighing less than 55 pounds (or 25 kg) to fly below 400 feet (or 122 m) above ground level (AGL) unless under special waiver. In Europe, it is 120 m. When a loss of aircraft power occurs at 400 feet above ground level, it takes 5 seconds for the UAS to hit the ground through a free fall. Therefore, the round trip latency of the command and control link should be less than 5 seconds for safety reasons, a requirement very difficult to satisfy in beyond-visual-line-of-sight (BVLOS) operations.

Current radios being tested for real-time tracking and command of UAS include cellular

radio, satellite radio, and telemetry radio. Cellular radio infrastructure including 2G/3G/4G provide the most extensive coverage, and the cost of a user terminal is low. All of the data channels in digital cellular systems were originally designed using IP, with a random data transmission latency greater than 6.5 seconds. How to transmit real-time data through the existing digital cellular infrastructure remains a world challenge. Satellite radio is of larger size and higher cost. Its coverage for commercial applications is much smaller than the digital cellular infrastructure. In [65], it was reported that ”pilots routinely deal with a five to eight-second delay on their controls when flying beyond-line-of-sight (BLOS) due to encryption overhead and the time it takes to relay commands via satellites. ” Telemetry radio is point-to-point with the smallest coverage currently available. For mass deployment of UAS beyond-visual-line-of-sight (BVLOS) operations, telemetry radios fail to meet the same coverage capability of cellular networks or satellites. Satellites or long-range communication systems are expensive and slow for UAS applications [66].

In [67], LTE network in San Diego was tested for UAS applications. The mobility route was at 5 m/s with 0.5 Mbps UDP uplink throughput requested. The maximum flight altitude was 400 feet AGL. Three bands were tested including PCS, AWS and 700 MHz. Strong fading existed in the downlink and the uplink (Figure 2-8, Figure 2-13, [67]). On the ground, the reference signal received power (RSRP) in the downlink was in the range [-105, -65] dBm in the PCS band, [-100, -60] dBm in the AWS band and [-95, -55] dBm in the 700 MHz band. The uplink transmission power was in the range [-22, 15] dBm per resource block in the 700 MHz band. The median of the Signal to Interference and Noise Ratio (SINR) received by the UAS at altitude was 5 dB lower than on the ground. This means that it is challenging for the cellular radio to maintain link availability during a full UAS flight.

Worldwide, GSM has the most extensive coverage. The coverage of 3G networks is more extensive than 4G LTE. 5G networks are currently in the research and development stage [68]. It is interesting to obtain fading statistics in 2G/3G networks for UAS communications through the measurement of cellular signals. Knowing fading statistics is necessary to design a communication system that meets the requirements of link reliability and delay [69, 70, 71].

In [72], key challenges and requirements for UAS communication links were discussed. The study showed that high availability, chaining and multi-priority design are required for UAS communication links. The work suggested that communication links using both multi-carrier modulation and time division multiplexing would be suitable for UAS communications.

In [66], meshed airborne communication networks were considered for UAS. Authors claimed that only meshed ad hoc networking can meet the communication demands for mass deployment of UAS. Feasibility was shown through experiments. The ability of airborne UAS networks with controlled mobility was discussed to improve performance.

In [73], a multi-objective path planning method was proposed for UAS to employ joint offline and online search. Based on the static safety index map, the offline search reduced the travel time and avoided static obstacles. The online search was based on the dynamic safety index map of unexpected obstacles to bypass unexpected obstacles. The effectiveness of the proposed method was verified through an experiment in a dynamic urban environment.

In [74], the researchers studied flying Ad Hoc network (FANET) for UAS application. Two routing algorithms were compared for optimized link-state routing (OLSR) and pre-

dictive OLSR. UASs with fixed wings were employed in experiments. It was shown that the predictive OLSR gave better performance.

In [75], a field experiment was conducted to collect data using UAS. It was shown that flying at higher altitude helped to improve UAS communication performance. In [76], a modified airframe was used for navigation, image acquisitions, and payload delivery. The work focuses on the onboard image processing, autonomous operation and rescue mission.

7.2 System Model

Consider measuring the power of the received signal for both uplink and downlink in cellular systems. For data channels, the modem input is data stream, and output is decoded bits. There is no way to measure power directly for data channels. For a voice channel, both of the channel input and output are analog signals. Because the carrier frequency is the same, the physical fading process is the same for both voice channel and data channel. Data channels utilize more advanced power control algorithms and were expected to experience smaller variance of fading at the power control loop output. Therefore, fading statistics measured in the voice channel can serve as the benchmark in UAS communications through cellular networks.

Figure 42 is the block diagram of the communication system designed for this UAS communication experiment. A UAS is installed with a UAS radio consisting of an electronic control unit (ECU), a cellular transceiver and a GPS receiver. The ECU is interfaced with a flight controller. The ECU can generate signal $s(t)$ to be transmitted over the voice channel of the cellular network using the cellular transceiver. The UAS radio establishes a full duplex communication link with the operation center through cellular network and public

switched telephone network (PSTN). It transmits the generated signal to the operation center through the uplink channel. The transceiver in the operation center detects the signal and records the waveform, and transmits another signal through the downlink to the UAS. The UAS records the received signal on the downlink for processing and analysis.

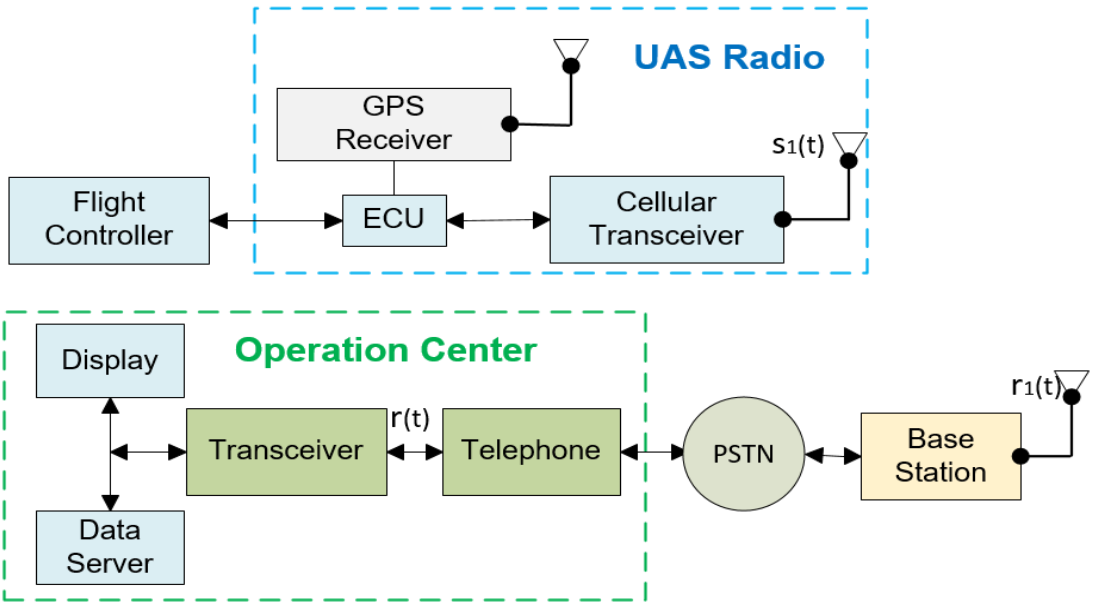

Figure 42: Block diagram of the full duplex UAS communication system.

The ECU transmits a continuous wave (CW) signal of 1500 Hz to the receiver in the operation center through the uplink so that the receiver can measure the power of the received for the uplink. The output signal of the ECU is fed into a cellular transmitter. The output signal of the cellular transmitter is transmitted through a cellular network and PSTN to the operation center. The channel between the UAS and the cellular base station is a multi-path fading channel. The uplink channel impulse response can be modeled as [30]

$$c(t;\tau) = \sum_{k=1}^{L} \alpha_k(t)\delta(t-\tau_k) \tag{7.1}$$

where $\alpha_k(t)$ is the attenuation factor of the kth path and τ_k is the time delay of the kth path. The transmitted signal by the UAS radio is $s_1(t)$. The received signal $r_1(t)$ by the base station receiver can be written as

$$r_1(t) = \sum_{k=1}^{L} \alpha_k(t) s_1(t - \tau_k) + n(t) \tag{7.2}$$

where $n(t)$ is additive white Gaussian noise (AWGN). The base station sends the baseband signal through the PSTN network to the transceiver in the operation center. The receiver in the operation center receives the baseband analog signal $r(t)$, performs sampling at 8 kHz sampling rate, and records the signal at 16 bits per sample. The recorded signal is analyzed to obtain fading statistics of the uplink channel.

For the downlink, the transmitter in the operation center sends a CW signal to the UAS radio. The receiver in the UAS radio performs sampling and recording of the downlink signal. The recorded signal is analyzed to obtain fading statistics of the downlink channel. The communications between the UAS radio and transceiver in the operation center is full duplex in real time.

Power control was a major task in designing cellular networks [29, 28]. Power control algorithms were implemented in all of 2G/3G/4G networks. A thorough literature search did not find paper to analyze radio signal power distribution after power control in 2G/3G/4G networks. In [67, 77], it was shown that large fading still exists after power control in 4G LTE networks. Because the power control algorithms in 2G/3G cellular networks are not as strong as those in the 4G cellular network, it is expected that fading after power control in 2G/3G cellular networks are worse than that in the 4G cellular network.

Before accurate theoretical results become available, communication researchers and engineers have to design a testbed to measure cellular radio signals in order to understand fading statistics.

7.3 UAS Communication Testbed and Measurements

A testbed was designed and built to support full duplex real-time UAS communications using cellular channels. It was applied to measure the fading characteristics of cellular channels for UAS communication. A communication terminal was installed in a UAS consisting of a radio board and a cellular transceiver and a GPS receiver. Figure 43 shows the UAS flying during the experiment with the radio board and the cellular transceiver and the GPS receiver inside the pink box. One cellular antenna was placed at the bottom of the UAS pointing toward the ground. One GPS antenna was installed on top of the UAS looking into the sky. A transceiver located in the operation center supported full duplex communications. Time and altitude were obtained through the GPS receiver and recorded during flight.

The radio board contained a Freescale i.MX 6 automotive grade board as the ECU and a u-Blox GSM module LEON-G200 and a GPS module LEA-6S. For the uplink, the Freescale i.MX 6 processor generated CW signal $s(t)$ and fed it into the GSM module. The radio signal was transmitted through the GSM antenna and sent to a base station. The signal received by the base station was transmitted through the PSTN network to a telephone recording box located inside the operation center. The signal received by the receiver at the operation center was sampled and recorded by a sound card inside the operation center at 8 kHz sampling frequency and 16 bits per sample. The digital signal was stored on a server for processing. For the downlink, the transmitter inside the operation

Figure 43: The UAS flying during the experiment with the radio transceiver and the GPS receiver inside the pink box. The radio antenna pointed down.

center generated a CW signal. The signal was received by the Freescale i.MX 6 processor and recorded on an SD card for processing. Software and drivers were designed and developed in C programming language to run each experiment automatically.

7.3.1 Test Cases

Experiments have been carried out in different environments. The following test cases were studied.

Case 1 was conducted at Wayne State University parking structure 2. The experiment was carried out from 11:00 a.m. to 1:00 p.m. on December 8, 2017. There was NW wind at 16 mph. The UAS took off from the top of the parking structure which is not surrounded by tall buildings. The UAS hovered for 15 minutes at each of the following altitudes: 50

Figure 44: The UAS flying above the Wayne State University parking structure.

feet, 100 feet, 200 feet, 300 feet and 400 feet AGL. There was a line-of-sight propagation path between the radio antenna and the cellular base station. Figure 44 shows the UAS was flying above the parking lot.

Figure 45: The UAS flying in the front yard of a house.

Case 2 was conducted in the front yard of a house. The experiment was carried out from 9:30 a.m. to 11:00 a.m. on December 9, 2017. The UAS took off from the front yard of the house located at Bagley street in Detroit. The surrounding structures were two-story homes and are not overshadowed by tall buildings. The UAS hovered for 15 minutes at each of the following altitudes: 50 feet, 100 feet, 200 feet, 300 feet and 400 feet above the front yard. Figure 45 shows the UAS was flying in the front yard of the hous.

Case 3 was conducted in the parking lot of Whole Foods Market on Mack Avenue in Detroit. The experiment was carried out from 3:30 p.m. to 5:30 p.m. on December 9, 2017. The UAS took off from the sidewalk close to the market. The UAS hovered for 15 minutes at each of the following altitudes: 50 feet, 100 feet, 200 feet, 300 feet and 400 feet above the Whole Foods Market. Figure 43 shows the UAS was flying in the parking lot of Whole Foods Market.

Figure 46: The UAS flying above a CVS pharmacy store.

Case 4 was conducted at a CVS pharmacy store on Warren Avenue in Detroit. The

experiment was carried out from 2:00 p.m. to 3:00 p.m. on December 16, 2017. The UAS took off from the sidewalk of the store. The UAS hovered for 15 minutes at each of the following altitudes: 50 feet, 300 feet and 400 feet above the store. Figure 46 shows the UAS was flying above a CVS pharmacy store.

Case 5 was conducted to test the UAS flying at 300 feet and 400 feet over the downtown Detroit area. There are many 20-30 story buildings in the downtown Detroit area. The experiment was carried out from 2:30 p.m. to 3:30 p.m. on December 8, 2017. The UAS took off from the top of a 3-story parking lot between Cass Avenue and Woodward Avenue in Detroit. The UAS flew about 15 minutes at each of the following altitudes: 300 feet and 400 feet over downtown Detroit.

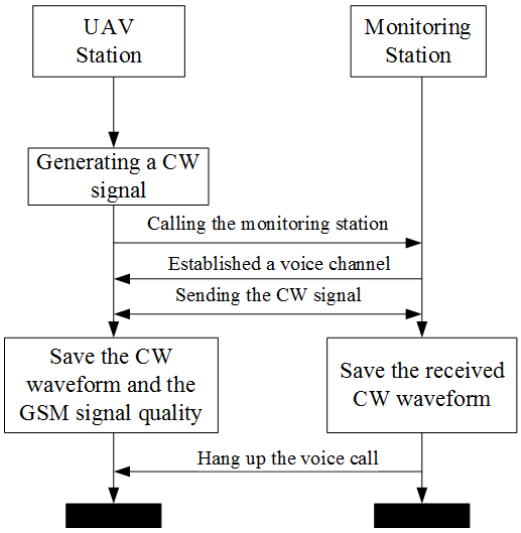

Figure 47: The procedure to measure CW signal strength.

Case 6 was conducted to test the UAS flying at 300 feet and 400 feet over the I-94 freeway. The experiment was carried out from 4:00 p.m to 5:30 p.m. on December 8, 2017. The UAS took off from the top of Wayne State University parking structure 2. The UAS flew for 15 minutes at each of the following altitudes: 300 feet and 400 feet over the

I-94 freeway. The UAS took off from the top of Wayne State University parking structure 2. The UAS flew for 15 minutes at each of the following altitudes: 300 feet and 400 feet over the I-94 freeway.

7.3.2 Measurement Procedure

The procedure to measure the power of received signals for full-duplex real-time UAS communications using cellular channels is shown in Figure 47. The amplifier gain was set to 0 dB for the UAS radio and the operation center. The UAS radio dialed a call. The operation center answered the incoming call. After the full-duplex voice call was established, the UAS radio sent a 1500 Hz CW signal for 10 seconds. The receiver at the operation center recorded the received signal at 8 kHz sampling rate and 16 bits per sample for the uplink. Meanwhile, the transmitter in the operation center sent a CW signal to the UAS through the downlink. The UAS radio saved the CW waveform into the SD card on the radio board. The experiments repeated the procedure for 30 times at each height for the six test cases. These data and waveforms were analyzed and discussed in the next subsection.

7.4 Fading Statistics for Unmanned Aerial System

Finding fading statistics of cellular channels for UAS communications is necessary. After the statistics are found, the communication system can be designed and evaluated properly in detection, synchronization, modulation and coding [78, 79]. Link availability and transmission delay can also be found with the fading statistics. This subsection finds CDF of the received signal power and average fading duration for both the uplink and the downlink in UAS communications using the cellular channel. The results are compared

with a signal with Rayleigh fading.

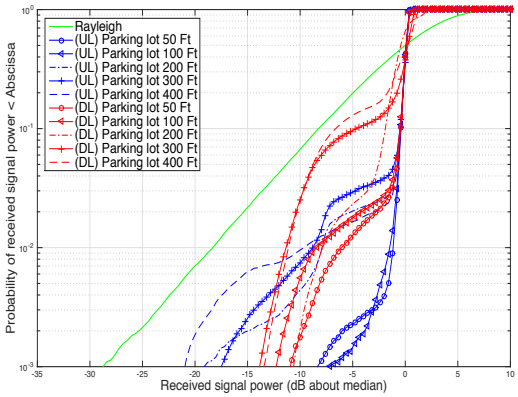

(a) Above the parking lot

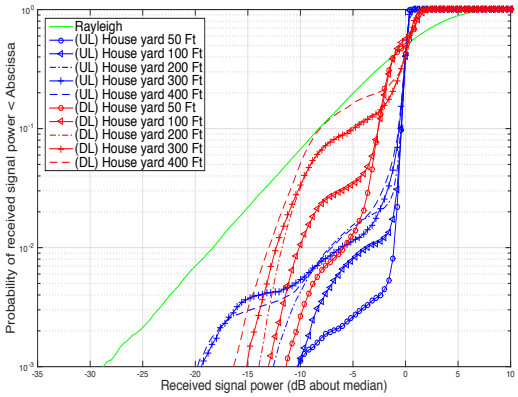

(b) Above the house front yard

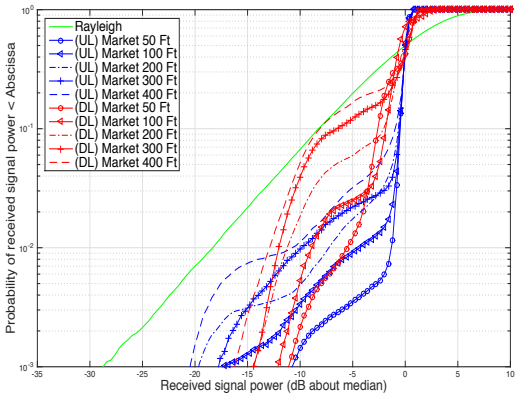

(c) Above the Whole Foods Market

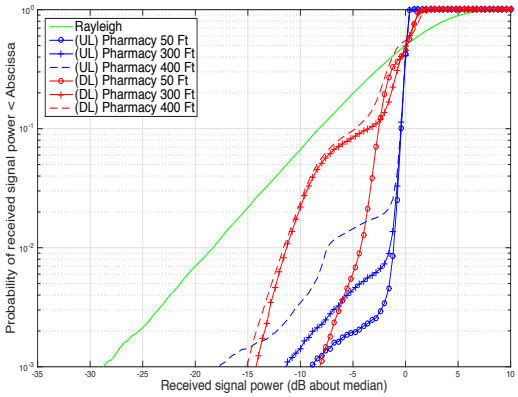

(d) Above the CVS pharmacy

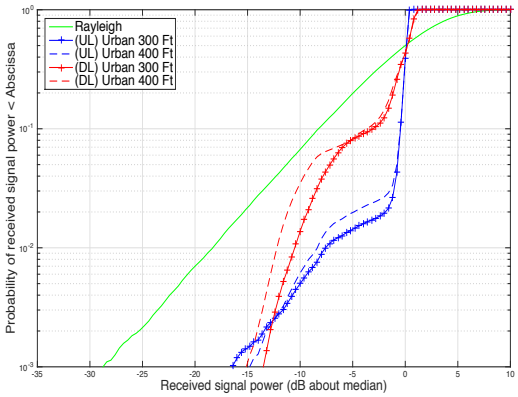

(e) Flying over Detroit urban area

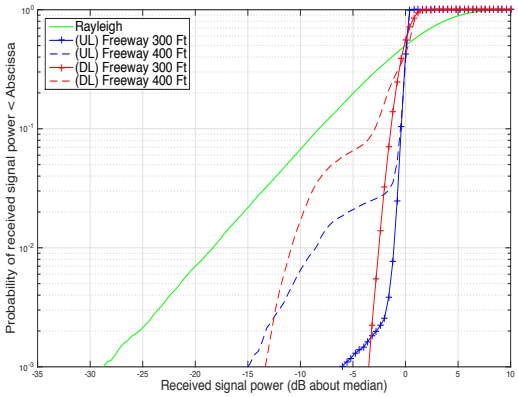

(f) Flying over the I-94 freeway

Figure 48: The uplink and downlink CDFs at 50 feet, 100 feet, 200 feet, 300 feet and 400 feet above the six test locations. Rayleigh distribution is plotted for comparison.

The blue curves in Figure 48 show CDFs of the uplink signals received by the receiver in the operation center for the six test locations. Rayleigh fading is plotted for comparison. It can be seen that the uplink channel fading was less significant at a flight altitude of 50 feet AGL. Approximately 0.1% of the received CW signal fading was more than 10 dB about the median and 1% of the fading exceeded 1 dB about the median.

Figure 48(a) shows the CDF of the received signal power when the UAS was flying above the roof of Wayne State University Parking Structure 2 at 50 feet (15.24 m), 100 feet (30.48 m), 200 feet (60.96 m), 300 feet (91.44 m) and 400 feet (121.92 m) AGL. The parking structure is a 6-floor building. For the uplink, at probability less or equal to 10^{-3}, the fading was -8 dB below the median of the receiver signal power at 50 feet AGL, or -7.5 dB below the median at 100 feet AGL, or -19 dB below the median at 200 feet AGL, or -17.5 dB below the median at 300 feet AGL, or -21 dB below the median at 400 feet AGL. The uplink fading became -10 dB worse as the UAS elevation increased from 50 feet AGL to 200 feet AGL. This might be because the cellular base station antenna looks down at the ground, and any elevation higher than 200 feet AGL would make the UAS loose line-of-sight to the base station. For the downlink, at probability less or equal to 10^{-3}, the fading was -11 dB below the median of the receiver signal power at 50 feet AGL, or -12.5 dB below the median at 100 feet AGL, or -10.8 dB below the median at 200 feet AGL, or -14 dB below the median at 300 feet AGL, or -13.5 dB below the median at 400 feet AGL. At 50 feet AGL, at probability less or equal to 10−3, the fading in the downlink was -3 dB worse than the fading in the uplink. At any elevation, the fading in the downlink was worse than that in the uplink. The downlink fading at 300 feet AGL was close to the fading at 400 feet AGL.

Figure 48(b) shows the CDF of the received signal power when the UAS was flying above the front yard of the house on Bagley street in Detroit at 50 feet (15.24 m), 100 feet (30.48 m), 200 feet (60.96 m), 300 feet (91.44 m) and 400 feet (121.92 m) AGL. For the uplink, at probability less or equal to 10^{-3}, the fading was about -10 dB below the median of the receiver signal power at 50 feet AGL or 100 feet AGL, or -12.5 dB below the median at 200 feet AGL, or -19.5 dB below the median at 300 feet AGL, or -20 dB below the median at 400 feet AGL. The uplink fading became -7 dB worse as the UAS elevation increased from 200 feet AGL to 300 feet AGL. For the downlink, at probability less or equal to 10^{-3}, the fading was -11.5 dB below the median of the receiver signal power at 50 feet AGL, or -13 dB below the median at 100 feet AGL, or -14 dB below the median at 200 feet AGL, or -15 dB below the median at 300 feet AGL, or -16 dB below the median at 400 feet AGL. At 50 feet AGL, at probability less or equal to 10^{-3}, the fading in the downlink was -1.5 dB worse than the fading in the uplink. The fading at 300 feet AGL was close to the fading at 400 feet AGL.

Figure 48(c) shows the CDF of the received signal power when the UAS was flying above the parking lot of the Whole Foods Market on Mack Avenue in Detroit at 50 feet (15.24 m), 100 feet (30.48 m), 200 feet (60.96 m), 300 feet (91.44 m) and 400 feet (121.92 m) AGL. For the uplink, at probability less or equal to 10−3, the fading was about -10.5 dB below the median of the receiver signal power at 50 feet AGL, or -12.5 dB at 100 feet AGL, or -13 dB below the median at 200 feet AGL, or -19.5 dB below the median at 300 feet AGL, or -20.5 dB below the median at 400 feet AGL. The uplink fading became -11 dB worse as the UAS elevation increased from 50 feet AGL to 100 feet AGL. The uplink fading became worse as the UAS elevation increased. For the downlink, at probability less or

equal to 10^{-3}, the fading was -11 dB below the median of the receiver signal power at 50 feet AGL, or -12 dB below the median at 100 feet AGL, or -14.5 dB below the median at 200 feet AGL, or -14.5 dB below the median at 300 feet AGL, or -16 dB below the median at 400 feet AGL. At 50 feet AGL, at probability less or equal to 10^{-3}, the fading in the downlink was -0.5 dB worse than the fading in the uplink.

Figure 48(d) shows the CDF of the received signal power when the UAS was flying above the parking lot of the CVS pharmacy store on Warren Avenue in Detroit at 50 feet (15.24 m), 300 feet (91.44 m) and 400 feet (121.92 m) AGL. For the uplink, at probability less or equal to 10^{-3}, the fading was about -9 dB below the median of the receiver signal power at 50 feet AGL, or -11 dB below the median at 300 feet AGL, or -18 dB below the median at 400 feet AGL. The uplink fading became -7 dB worse as the UAS elevation increased from 300 feet AGL to 400 feet AGL. For the downlink, at probability less or equal to 10^{-3}, the fading was -8 dB below the median of the receiver signal power at 50 feet AGL, or -14 dB below the median at 300 feet AGL, or -15 dB below the median at 400 feet AGL.

Figure 48(e) shows the CDF of the received signal power when the UAS was flying in downtown Detroit up to 400 feet AGL. The area was crowded with many buildings between 20 to 30 stories. For the uplink, at probability less or equal to 10^{-3}, the fading was about -16 dB below the median at 300 feet AGL, or -15 dB below the median at 400 feet AGL. For the downlink, at probability less or equal to 10^{-3}, the fading was -14 dB below the median at 300 feet AGL, or -15 dB below the median at 400 feet AGL.

Figure 48(f) shows the CDF of the received signal power when the UAS was flying above the I-94 freeway up to 400 feet AGL. For the uplink, at probability less or equal to

10^{-3}, the fading was about -12 dB below the median at 300 feet AGL, or -15 dB below the median at 400 feet AGL. For the downlink, at probability less or equal to 10^{-3}, the fading was -12 dB below the median at 300 feet AGL, or -13.5 dB below the median at 400 feet AGL.

Figure 48(a) shows that about 0.1% of the received signal fading was more than 8 dB, and 1% of the fading exceeded 1.2 dB. Figure 48(a), Figure 48(b), and Figure 48(c) show that about 0.1% of the signal fading was more than 20 dB at flight altitudes above 300 feet. Figure 48(e) shows that about 0.1% of the signal fading was more than 15 dB at 300 feet and 400 feet when the UAS flew over the urban area. Figure 48(f) shows that the fading impact was the least at the flight altitude of 300 feet among the six test environments. Only about 0.1% of the signal fading was more than 6 dB. Observing Figure 48(a), Figure 48(b), Figure 48(c) and Figure 48(d), one can conclude that the uplink signal quality was better at 50 feet or 100 feet AGL than the signal quality at 300 or 400 AGL.

The red curves in Figure 48 show CDFs of the downlink signals received by the UAS for the six test cases. As it can be seen from the Figure 48(a), Figure 48(b), Figure 48(c), and Figure 48(d), about 0.1% of the received downlink signal was faded 11 dB, 1% of the received signals was faded more than 5 dB when the UAS radio was at 50 feet above the test site. Similarly, Figure 48(a) shows that about 0.1% of the received power was faded 13 dB when the UAS flew at 300 feet above the university parking lot. Figure 48(b) shows that about 0.1% of the received power was attenuated 15 dB when the UAS flew at 300 feet AGL in the front yard of the house. Figure 48(c) and Figure 48(d) show that about 0.1% of the received signal faded more than 14 dB, when the UAS was hovering above the market and the pharmacy. Figure 48(e) shows that about 0.1% of the received signal

faded more than 13 dB at 300 feet and 400 feet above the urban area. Figure 48(f) shows that the received signal had minimum fading impact flying over the freeway and 0.1% of the received signal was faded only about 3.8 dB.

The fading impact is less severe when the flight height of the UAS is between 50 feet and 200 feet AGL. Flying UAS at 300 feet above the freeway gives the least fading. This may be a good choice for a UAS to deliver parcels in long distance. UAVs can choose to fly 50 to 200 feet above the ground when it is close to the destination.

For the uplink the worst fading was -21 dB at probability less or equal to 10−3 which occurred at 400 AGL on the rooftop of the Wayne State University Parking Structure 2. For the downlink the worst fading was -16 dB at probability less or equal to 10−3 which occurred at 400 AGL above the front yard of the house in Detroit and the parking lot of the Whole Foods Market in Detroit. For both the uplink and the downlink, the fading became worse as the UAS elevation increased. In all of the test cases, the fading was apparently less severe than Rayleigh fading. Therefore, the fading of UAS communications using the GSM network is huge and needs to be handled.

Level crossing rate is the number of fades for a given time interval. It shows how often the fades occur for a given threshold. The blue curves in Figure 49 show LCRs of the uplink for the six test locations. The red curves in Figure 49 show LCRs of the downlink signals received by the UAS for the six test cases. It can be seen that the downlink LCRs were larger than the uplink LCRs. Figure 49(a) shows the maximum downlink LCR occurred at 400 feet above the parking lot. The LCR was 55 fades per second when the fade fell below -8 dB. The maximum uplink LCR occurred at 300 feet above the parking lot. The LCR was 10 fades per second when the fade fell below -7 dB. Figure 49(b) shows the maximum

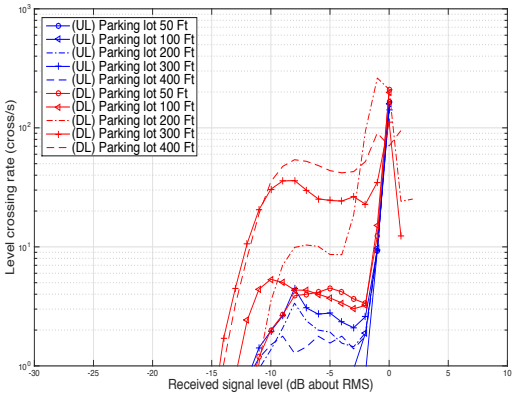

(a) Above the parking lot

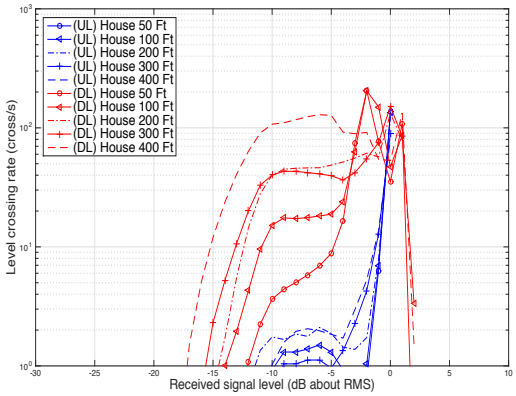

(b) Above the house front yard

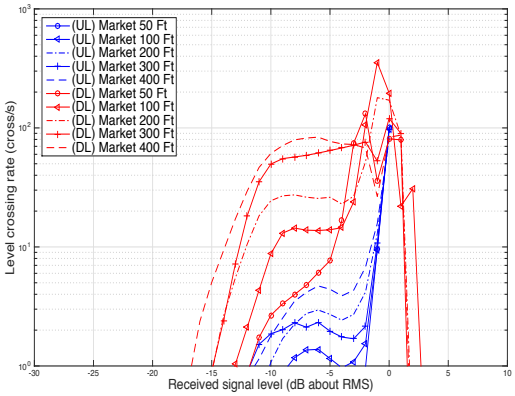

(c) Above the Whole Foods Market

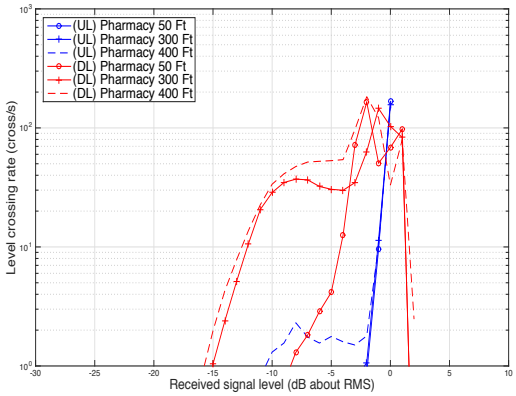

(d) Above the CVS pharmacy

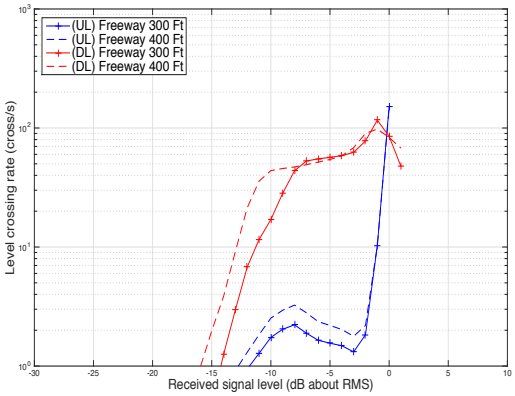

(e) Flying over Detroit urban area

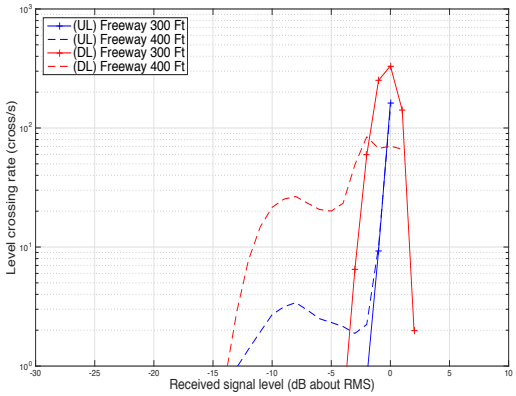

(f) Flying over the I-94 freeway

Figure 49: The uplink and downlink LCRs at 50 feet, 100 feet, 200 feet, 300 feet and 400 feet above the six test locations.

downlink LCR occurred at 400 feet above the front yard of the house. The LCR was 103 fades per second when the fade fell below -5 dB. The maximum uplink LCR occurred at 400 feet above the front yard of the house. The LCR was 2 fades per second when the fade fell below -7.5 dB. Figure 49(f) shows the downlink LCR was 11 fades per second When the fade fell below -10 dB at the height of 400 feet above the freeway. The uplink LCR was 3 fades per second when the fade fell below -10 dB. Figure 49(c), Figure 49(d), Figure 49(e), and Figure 49(f) also show the maximum downlink and uplink LCR occurred at 400 feet above the test locations.

The blue curves in Figure 50 show AFDs of the uplink signals received by the receiver inside the operation center above the six test locations. Figure 50(a) shows that the uplink AFD was 3 ms at 50 feet above the parking structure when the received signal level was 15 dB below the RMS value. If the data rate is 2000 bit/s, three bits data would be lost. When the UAS flight altitude was 200 feet, the uplink AFD could reach 20 ms. There would be more data bits loss when flying at 200 feet or higher. Figure 50(b) shows that the AFD was 2 ms at 50 feet above the house front yard when the received signal level was 15 dB below the RMS value. The uplink AFD was 8 ms when the flight altitude was 200 feet. Figure 50(c) shows that the AFD was 7 ms at 50 feet above the market and the AFD was about 10 ms when the flight altitude was 100 feet. The uplink AFD was about 50 ms when the flight altitude was 200 feet. Figure 50(d) shows the uplink AFD was 4 ms at 50 feet and 100 feet above the CVS pharmacy when the received signal level was 15 dB below the RMS. At 200 feet, the AFD was 28ms. Therefore, the uplink AFD was minimum at the university parking structure, the residential area, the market, and the CVS pharmacy when the flight altitude was 50 feet to 100 feet above the ground. Figure 50(e) shows the

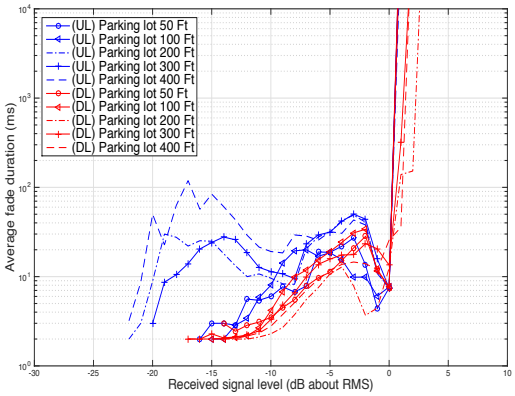

(a) Above the parking lot

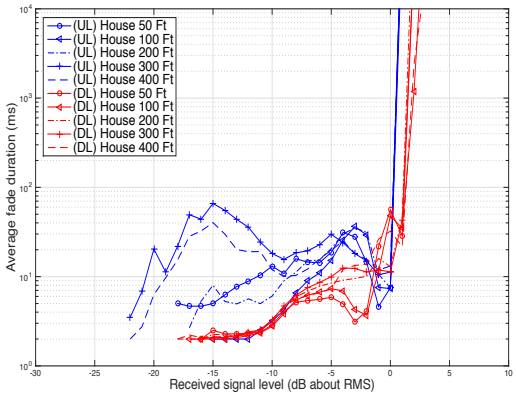

(b) Above the house front yard

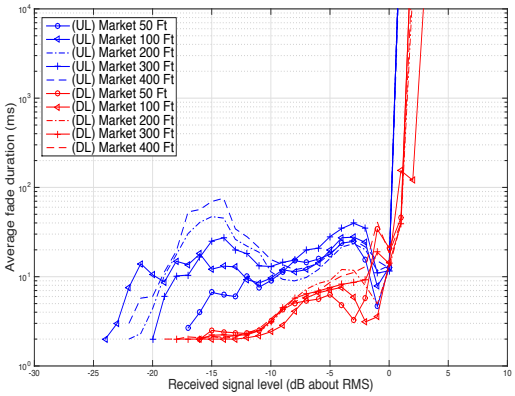

(c) Above the Whole Foods Market

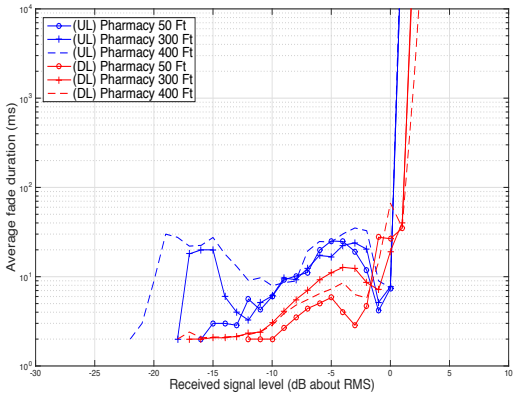

(d) Above the CVS pharmacy

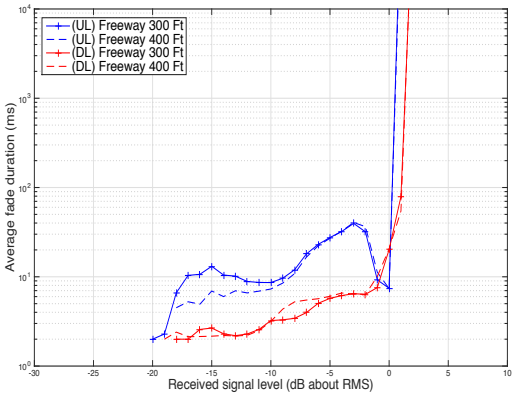

(e) Flying over Detroit urban area

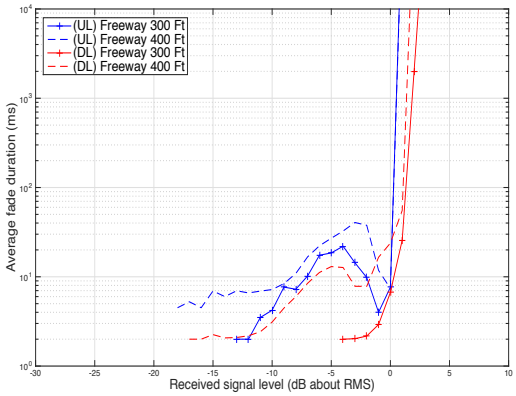

(f) Flying over the I-94 freeway

Figure 50: The uplink and downlink AFDs at 50 feet, 100 feet, 200 feet, 300 feet and 400 feet above the six test locations.

uplink AFD was about 10 ms at 300 feet above the urban area when the received signal level was 15 dB below the RMS. Figure 50(f) shows the uplink AFD was about 2 ms when the UAS flew at 300 feet above the freeway.

The red curves in Figure 50 show AFDs of the downlink signals received by the UAS above the six test locations. Observing Figure 50(a), Figure 50(b) and Figure 50(c), one can conclude that the AFD was 2 ms at 50 feet, 100 feet, and 200 feet when the received signal level was 15 dB below the RMS level. Figure 50(d) shows that the downlink AFD was 2 ms at 50 feet or 300 feet. Figure 50(e) and Figure 50(f) show the downlink AFD was also 2 ms at 300 feet and 400 feet above the ground when the received signal level was 15 dB below the RMS value. In summary, the AFD of the downlink was smaller than the AFD of the uplink at the same flight altitude. The AFD was smaller when the flight altitude was between 50 feet and 100 feet above the university, the residential area, the market, and the CVS pharmacy. When flying over the freeway, 300 feet AGL is a good choice.

In all of the test cases, the downlink fading was smaller than the uplink fading. Therefore, UAS ID tracking using the uplink is more difficult to achieve than command and control using the downlink.

7.5 Conclusion

A testbed is designed and developed to support full duplex UAS communications using cellular networks. The testbed is applied to measure signal power for uplink and downlink. A novel method is proposed to measure the power of cellular networks and obtain fading statistics for full-duplex real-time UAS communications. UAS test flights are realized and data is collected for six test sites. Cumulative distribution function and average fading duration are obtained for six test sites. The statistics of the cellular network can be directly

applied to design full duplex real time UAS communication systems and evaluate system performance including detection, synchronization, modulation and coding.

For the uplink, the worst fading was -21 dB at probability less or equal to 10^{-3} which occurred at 400 AGL on the rooftop of the Wayne State University Parking Structure 2. For the downlink, the worst fading was -16 dB at probability less or equal to 10^{-3} which occurred at 400 AGL above the front yard of the house in Detroit and the parking lot of the Whole Foods Market in Detroit. This means that real-time UAS ID tracking is more difficult to achieve using the uplink than command and control using the downlink. For both the uplink channel and the downlink channel, the fading became worse as the UAS elevation increased. In all of the test cases, the fading was less severe than Rayleigh fading. Therefore, the fading of UAS communications using GSM network is vast and needs to be handled.

CHAPTER 8 CONCLUSION AND FUTURE WORK

8.1 Conclusion

In this dissertation, a testbed is designed and developed to obtain the fading statistics of the in-band channel for the 3GPP emergency call system and unmanned aerial systems. Experiments are performed in different environments to obtain the CDF, LCR, and AFD of the received signal. It is found that with probability less or equal to 0.1%, the fading is -19 dB for the CW signal at 500 Hz and -9.5 dB for the CW signal at 2000 Hz, respectively. It is recommended to move the 500 Hz CW signal and the 800 Hz CW signal for detection and synchronization in the 3GPP TS 26.267 standard to around 2000 Hz for minimum fading. This will give 9.5 dB improvement in signal detection and synchronization. The longest fade duration observed is 540 ms. The 64 ms synchronization signal in the current standard is insufficient to handle the fading. It is shown that fading is minimized in the frequency range [1000, 2500] Hz for the 3GPP TS 26.267 system.

The experiment results have shown that severe fading still exists in the voice channel of the GSM network with power control. The fading is one of the reasons that explain the road test results of the HeURO project. The fading increases the MSD transmission delay and reduces the success rate of the MSD transmission. In the future revision of the 3GPP TS 26.267 standard, the statistics obtained in this dissertation can be employed to design a better system including detection, synchronization, modulation, and coding. The results can be employed to minimize the MSD transmission delay in emergency call systems.

Furthermore, the fading results are used to calculate the BER performance for the in-band modem. Timing estimation performance and synchronization detection probability are obtained by transmitting the synchronization preamble through various adaptive multi-

rate vocoders and the additive white Gaussian noise channel. The results of the fading statistics, synchronization, and BER can be directly applied to design real-time communication systems and evaluate system performance including detection, synchronization, modulation and coding.

The testbed is also applied for full-duplex real-time unmanned aerial system communications using cellular networks. The testbed is applied to measure the power of signals received by the UAS in flight for the downlink and by the receiver in the operation center for the uplink, respectively. The method is proposed to measure the power of cellular networks and obtain fading statistics for full duplex real-time UAS communications. Field experiments are carried out by flying a UAS above a university campus, the front yard of a house, the parking lot of Whole Foods Market, the parking lot of CVS pharmacy, downtown Detroit and I-94 freeway. Results of flying UAS in snow is reported for the first time. Received signals are recorded for both the uplink and the downlink in real time. UAS test flights are realized and data is collected for six test sites. Cumulative distribution function and level cross rate and average fading duration are obtained for all of the test cases. For the uplink the worst fading was -21 dB at probability less or equal to 10^{-3} which occurred at 400 AGL on the rooftop of the Wayne State University Parking Structure 2. For the downlink, the worst fading was -16 dB at probability less or equal to 10^{-3} which occurred at 400 AGL above the front yard of the house in Detroit and the parking lot of the Whole Foods Market in Detroit. This means that real-time UAS ID tracking is more difficult to achieve using the uplink than command and control using the downlink. For both the uplink and the downlink, the fading became worse as the UAS elevation increased. In all of the test cases, the fading was less severe than Rayleigh fading.

8.2 Future Work

The MSD transmission success rate of the eCall system has a great potential to be improved and the delay of the MSD transmission can be reduced, based on the HeURO test results. Future research efforts should focus on such challenges. When the channel fading is severe or the channel quality is bad, the PSAP may miss the synchronization signal and hence the MSD data is not detectable. This results in low transmission success rate and increases transmission time. In future work, the PSAP should measure the fading and signal strength of the received signal. When the fading exceeds a specific threshold, a feedback signal should be sent to the IVS. The IVS switches the robust transmission mode to implement adaptive modulation, which can improve the success rate and real-time performance.

REFERENCES

[1] L. Gupta, R. Jain, and G. Vaszkun, “Survey of important issues in UAV communication networks,” *IEEE Communications Surveys Tutorials*, vol. 18, no. 2, pp. 1123–1152, Secondquarter 2016.

[2] A. Cho, J. Kim, S. Lee, and C. Kee, “Wind estimation and airspeed calibration using a UAV with a single-antenna GPS receiver and pitot tube,” *IEEE Transactions on Aerospace and Electronic Systems*, vol. 47, no. 1, pp. 109–117, January 2011.

[3] ARC Committee, “UAS identification and tracking (UAS ID) aviation rulemaking committee (ARC) ARC recommendations final report,” September 2017.

[4] “Digital cellular telecommunications system (Phase 2+) (GSM); Universal Mobile Telecommunications System (UMTS); eCall data transfer; In-band modem solution; General description,” 3GPP Technical Specification Group Services and System Aspects, Valbonne, France, Jul. 2018.

[5] R. Öörni and A. Goulart, “In-vehicle emergency call services: eCall and beyond,” *IEEE Communications Magazine*, vol. 55, no. 1, pp. 159–165, Jan. 2017.

[6] European Parliament. (2015, Apr.) Automatic emergency call devices in all new car models from spring 2018. [Online]. Available: http://www.europarl.europa.eu/news/en/news-room/20150424IPR45714/automatic-emergency-call-devices-in-all-new-car-models-from-spring-2018

[7] “Global status report on road safety 2015,” World Health Organization, Tech. Rep., 2015.

[8] R. Öörni, E. Meilikhov, and T. O. Korhonen, “Interoperability of eCall and ERA-

GLONASS in-vehicle emergency call systems," *IET Intelligent Transport Systems*, vol. 9, no. 6, pp. 582–590, Aug. 2015.

[9] M. Nader and J. Liu, "Developing modulator and demodulator for the EU eCall in-vehicle system in FPGAs," in *Proc. 2016 International Conference on Computing, Networking and Communications*, Feb 2016, pp. 1–5.

[10] European Commission. (2016, March) 2015 road safety statistics: What is behind the figures? [Online]. Available: http://europa.eu/rapid/press-release_MEMO-16-864_en.htm

[11] "Impact assessment on support for an EU-wide eCall service in electronic communication networks for the transmission of in-vehicle emergency calls based on 112 ('eCalls')," Jun. 2011.

[12] (2016, Jan.) eCall: Time saved = lives saved. [Online]. Available: https://ec.europa.eu/digital-single-market/en/ecall-time-saved-lives-saved

[13] (2013, Mar.) eCall connected cars can help save lives. [Online]. Available: https://www.ericsson.com/res/region_RLAM/press-release/2013/2013-03-22-ecall-en.pdf

[14] eSafety initiative. (2006, Jun.) esafety: the use of information and communication technology (ICT) for road safety. [Online]. Available: http://eur-lex.europa.eu/legal-content/IT/TXT/?uri=uriserv:l31102

[15] eSafety Forum eCall Driving Group. (2004, May) Memorandum of understanding for realisation of interoperable in-vehicle ecall. [Online]. Available: https://ec.europa.eu/digital-single-market/sites/digital-agenda/files/invehicle_ecall_mou_1.pdf

[16] GSM Europe. (2006, Apr.) Options for ecall msd signalling. [Online]. Available: http://www.ecall.fi/Appendixes/Appendix_11.pdf

[17] *Cellular text telephone modem; General description (Release 8)*, 3GPP Technical Specification Group Services and System Aspects Technical Specification TS 26.226, Rev. 8.0.0, Sep. 2007.

[18] European Parliament, “Automatic emergency call devices in all new car models from spring 2018,” *Press Release*, Apr. 28, 2015.

[19] Y. Li and J. Q. Liu, “Fading statistics of voice channel for the European Union emergency call,” in *Proc. IEEE Vehicular Technology Conference*, Sep. 2016, pp. 1–5.

[20] M. Werner, C. Pietsch, C. Joetten, C. Sgraja, G. Frank, W. Granzow, and J. Huang, “Cellular in-band modem solution for eCall emergency data transmission,” in *Proc. IEEE Vehicular Technology Conference*, Apr. 2009, pp. 1–6.

[21] J. C. Brandenburg and J. Q. Liu, “Uncoded bit error rate of eCall modem through AMR codec and AWGN channel,” in *Proc. IEEE Global Communications Conference*, Dec. 2013, pp. 4055–4060.

[22] R. Öörni and T. O. Korhonen, “eCall minimum set of data transmission-results from a field test in Finland,” *IET Intelligent Transport Systems*, vol. 8, no. 8, pp. 639–647, Nov. 2014.

[23] R. Kazemi, M. Boloursaz, S. M. Etemadi, and F. Behnia, “Capacity bounds and detection schemes for data over voice,” *IEEE Transactions on Vehicular Technology*, vol. 65, no. 11, pp. 8964–8977, Nov. 2016.

[24] B. T. Ali, G. Baudoin, and O. Venard, “Data transmission over mobile voice channel based on M-FSK modulation,” in *Proc. Wireless Communications and Networking Conf.*, 2013, pp. 4416–4421.

[25] B. Kotnik, Z. Mezgec, J. Svečko, and A. Chowdhury, “Data transmission over GSM voice channel using digital modulation technique based on autoregressive modeling of speech production,” *Digital Signal Processing*, vol. 19, no. 4, pp. 612–627, 2009.

[26] *Intelligent transport systems - ESafety - eCall high level application requirements (HLAP) using GSM/UMTS circuit switched networks*, European Committee for Standardization Std. EN 16 062, Apr. 2015.

[27] M. Hentschinski, M. Grzebellus, and A. Rooke, “Final results of the tests with lessons learnt, conclusions and recommendations,” Harmonized eCall European Pilot (HeERO), Jun. 2015.

[28] T. S. Rappaport, S. Y. Seidel, and R. Singh, “900-MHz multipath propagation measurements for US digital cellular radiotelephone,” *IEEE Transactions on Vehicular Technology*, vol. 39, no. 2, pp. 132–139, May 1990.

[29] B. Bjerke, J. Proakis, K. Lee, and Z. Zvonar, “A comparison of GSM receivers for fading multipath channels with adjacent and co-channel interference,” *IEEE Journal on Selected Areas in Communications*, vol. 18, no. 11, pp. 2211–2219, Nov. 2000.

[30] J. G. Proakis, *Digital Communications*, 5th ed. New York: McGraw-Hill, 2008.

[31] T. D. Novlan, H. S. Dhillon, and J. G. Andrews, “Analytical modeling of uplink cellular networks,” *IEEE Transactions on Wireless Communications*, vol. 12, no. 6, pp. 2669–2679, Jun. 2013.

[32] P. Guan and M. D. Renzo, “Stochastic geometry analysis and optimization of uplink cellular networks with fractional power control and optimum combining,” in *Proc. IEEE International Conference on Communications (ICC)*, May 2016, pp. 1–6.

[33] M. S. Alouini and A. J. Goldsmith, “Capacity of Rayleigh fading channels under different adaptive transmission and diversity-combining techniques,” *IEEE Transactions on Vehicular Technology*, vol. 48, no. 4, pp. 1165–1181, Jul. 1999.

[34] A. Stefanov and T. M. Duman, “Turbo-coded modulation for systems with transmit and receive antenna diversity over block fading channels: system model, decoding approaches, and practical considerations,” *IEEE Journal on Selected Areas in Communications*, vol. 19, no. 5, pp. 958–968, May 2001.

[35] *Intelligent transport systems - eSafety - eCall minimum set of data (MSD)*, European Committee for Standardization Std. EN 15 722, Apr. 2015.

[36] *Intelligent transport systems - eSafety - Pan-European eCall operating requirements*, European Committee for Standardization Std. EN 16 072, Apr. 2015.

[37] M. Grzebellus, M. Stapelfeld, A. Paul, K. Yeadon, and A. Rooke, “Final results of the tests with lessons learnt, conclusions and recommendations,” Harmonized eCall European Pilot (HeERO), Dec. 2014.

[38] “eCall data transfer in-band modem solution - general description,” 3GPP Technical Specification Group Services and System Aspects, Valbonne, France, Mar. 2017.

[39] M. Werner, C. Pietsch, C. Joetten, C. Sgraja, G. Frank, W. Granzow, and J. Huang, “Cellular in-band modem solution for ecall emergency data transmission,” in *Proc. IEEE Vehicular Technology Conference*, Apr. 2009, pp. 1–6.

[40] M. Nader, Y. Li, and J. Liu, “Chip design for Turbo encoder module for in-vehicle system,” in *Proc. IEEE Annual Computing and Communication Workshop and Conference*, Jan. 2018, pp. 389–393.

[41] J. C. Brandenburg and J. Q. Liu, “Uncoded error performance of ecall modem through AMR codec and AWGN,” in *Proc. IEEE Vehicular Technology Conference*, Sep. 2013, pp. 1–4.

[42] R. Ghosh, B. Chatterjee, D. Dey, S. Dalai, and S. Chakravorti, “Remote monitoring of power frequency electrical signals employing gsm network,” in *Proc. Applications and Innovations in Mobile Computing Conference*, Feb. 2014, pp. 81–84.

[43] H. Suzuki, “A statistical model for urban radio propogation,” *IEEE Transactions on communications*, vol. 25, no. 7, pp. 673–680, Jul. 1977.

[44] J. M. Romero-Jerez, M. Ruiz-Garcia, and A. Diaz-Estrella, “Effects of multipath fading on ber statistics in cellular cdma networks with fast power control,” *IEEE Communications Letters*, vol. 4, no. 11, pp. 349–351, Nov 2000.

[45] B. Rohani, H. Hosseini, and H. Zepernick, “Combined AMR mode adaptation and fast power control for GSM Phase 2+,” in *Proc. Asia-Pacific Conference on Communications*, Oct. 2005, pp. 411–415.

[46] M. Werner, T. Junge, and P. Vary, “Quality control for AMR speech channels in GSM networks,” in *Proc. IEEE International Conference on Acoustics, Speech, and Signal Processing*, May 2004, pp. 1076–1079.

[47] J. M. Romero-Jerez, M. Ruiz-Garcia, and A. Diaz-Estrella, “Effects of multipath fading

on BER statistics in cellular CDMA networks with fast power control," *IEEE Communications Letters*, vol. 4, no. 11, pp. 349–351, Nov. 2000.

[48] *Radio subsystem link control*, 3GPP Technical Specification Group GSM/EDGE Radio Access Network Std. TS 05.08, Rev. 8.23.0, Nov. 2005.

[49] Y. Li, M. Nader, and J. Liu, "In-vehicle system design for the European Union emergency call," in *Proc. IEEE International Conference on Electro/Information Technology*, May 2018, pp. 908–912.

[50] T. Zhao, Q. Wang, W. Jiang, and Y. Ni, "System design and development of parallel-hybrid electric vehicle based on CAN bus," in *International Conference on Electrical Machines and Systems*, Sept. 2005.

[51] F. Man and W. Lenan, "Research on anti-fading performance of ebpsk system," in *2009 Second International Symposium on Information Science and Engineering*, Dec 2009, pp. 561–564.

[52] A. Goldsmith, *Wireless Communications*. Cambridge University Press, 2005.

[53] T. S. Rappaport, *Wireless Communications: Principles and Practice*. NJ: PTR Prentice-Hall: Upper Saddle River, 2002.

[54] X. Dong and N. Beaulieu, "Average level crossing rate and fade duration of maximal ratio diversity in unbalanced and correlated channels," in *Proc. IEEE Wireless Communications and Networking Conference*, Mar. 2002, pp. 762–767.

[55] P. H. Leong, T. A. Lamahewa, and T. D. Abhayapala, "Framework to calculate level-crossing rate and average fade duration in two-dimensional and three-dimensional scattering environments," *IET Communications*, vol. 6, no. 15, pp. 2474–2479, October 2012.

[56] S. Lin and D. J. Costello, *Error Control Coding*. New Jersey: Prentice Hall, 2004.

[57] S. Zakhem, J. Liu, and J. Brandenburg, “Performance of eCall modem with Turbo codes in AWGN and AMR,” in *Proc. IEEE 86th Vehicular Technology Conference*, Sept. 2017, pp. 1–5.

[58] H. Li, H. Liu, and S. Vafi, “Bipolar chaotic pulse position modulation communication system based on cyclic LDPC,” *EURASIP Journal on Wireless Communications and Networking*, vol. 11, no. 1, pp. 1–9, 2014.

[59] T. Y. Elganimi, “Performance comparison between OOK, PPM and pam modulation schemes for free space optical (FSO) communication systems: analytical study,” *International Journal of Computer Applications*, vol. 79, no. 11, 2013.

[60] M. Nader, Y. Li, and J. Liu, “Preamble detection for the in-vehicle system receiver,” in *Proc. IEEE International Conference on Electro/Information Technology*, May 2018, pp. 902–907.

[61] L. Afonso, N. Souto, P. Sebastiao, M. Ribeiro, T. Tavares, and R. Marinheiro, “Cellular for the skies: Exploiting mobile network infrastructure for low altitude air-to-ground communications,” *IEEE Aerospace and Electronic Systems Magazine*, vol. 31, no. 8, pp. 4–11, Aug 2016.

[62] R. Z. Homma, O. Sohn, and R. C. Bose, “Analysis of the recognition and localisation techniques of power transmission lines components in aerial images acquired by drones,” *CIRED - Open Access Proceedings Journal*, vol. 2017, no. 1, pp. 29–32, Oct. 2017.

[63] Federal Highway Administration. (2018, Sep.) Unmanned Aerial Systems. [Online]. Available: https://www.fhwa.dot.gov/uas/

[64] I. Colomina and P. Molina, “Unmanned aerial systems for photogrammetry and remote sensing: A review,” *ISPRS Journal of Photogrammetry and Remote Sensing*, vol. 92, pp. 79–97, April 2014.

[65] J. Poss, “It’s the data link, stupid,” March 2017.

[66] E. W. Frew and T. X. Brown, “Airborne communication networks for small unmanned aircraft systems,” *Proceedings of the IEEE*, vol. 96, no. 12, pp. 2008–2027, Dec 2008.

[67] Qualcomm Technologies, Inc., “LTE unmanned aircraft systems,” May 2017.

[68] C.-P. Li, J. Jiang, W. Chen, T. Ji, and J. Smee, “5G ultra-reliable and low-latency systems design,” in *Proc. European Conference on Networks and Communications*, June 2017, pp. 1–5.

[69] Z. Chen, Q. Wang, D. O. Wu, and P. Fan, “Two-dimensional evolutionary spectrum approach to nonstationary fading channel modeling,” *IEEE Transactions on Vehicular Technology*, vol. 65, no. 3, pp. 1083–1097, March 2016.

[70] M. Chiani, M. Z. Win, and A. Zanella, “On the capacity of spatially correlated MIMO Rayleigh-fading channels,” *IEEE Transactions on Information Theory*, vol. 49, no. 10, pp. 2363–2371, Oct. 2003.

[71] H. Liu, Y. Song, and R. Qiu, “The impact of fading correlation on the error performance of MIMO systems over Rayleigh fading channels,” *IEEE Transactions on Wireless Communications*, vol. 4, no. 5, pp. 2014–2019, Sep. 2005.

[72] R. Jain and F. Templin, “Requirements, challenges and analysis of alternatives for wireless datalinks for unmanned aircraft systems,” *IEEE Journal on Selected Areas in Communications*, vol. 30, no. 5, pp. 852–860, June 2012.

[73] C. Yin, Z. Xiao, X. Cao, X. Xi, P. Yang, and D. Wu, “Offline and online search: UAV multi-objective path planning under dynamic urban environment,” *IEEE Internet of Things Journal*, no. 99, pp. 1–13, June 2017.

[74] S. Rosati, K. Kruzelecki, G. Heitz, D. Floreano, and B. Rimoldi, “Dynamic routing for flying Ad Hoc networks,” *IEEE Transactions on Vehicular Technology*, vol. 65, no. 3, pp. 32–37, Mar 2015.

[75] D. Palma, A. Zolich, Y. Jiang, and T. A. Johansen, “Unmanned aerial vehicles as data mules: An experimental assessment,” *IEEE Access*, vol. 5, pp. 24 716–24 726, Nov. 2017.

[76] D. Erdos, A. Erdos, and S. E. Watkins, “An experimental UAV system for search and rescue challenge,” *IEEE Aerospace and Electronic Systems Magazine*, vol. 28, no. 5, pp. 32–37, May 2013.

[77] R. Amorim, H. Nguyen, P. Mogensen, I. Z. Kovacs, J. Wigard, and T. B. Sorensen, “Radio channel modeling for UAV communication over cellular networks,” *IEEE Wireless Communications Letters*, vol. 6, no. 4, pp. 514–517, Aug 2017.

[78] W. Medina-Pazmino, A. Jara-Olmedo, and D. Valencia-Redrovan, “Analysis and determination of minimum requirements for a data link communication system for unmanned aerial vehicles-UAV’s,” in *IEEE Ecuador Technical Chapters Meeting*, Oct. 2016, pp. 1–6.

[79] G. N. Solidakis, F. M. Tsokas, M. C. Batistatos, N. C. Sagias, G. V. Tsoulos, D. A. Zarbouti, and G. E. Athanasiadou, “An Arduino-based subsystem for controlling UAVs through GSM,” in *2017 6th International Conference on Modern Circuits and Systems Technologies*, May 2017, pp. 1–4.

ABSTRACT

CHANNEL FADING STATISTICS FOR REAL-TIME DATA TRANSMISSION IN EMERGENCY CALL SYSTEMS AND UNMANNED AERIAL SYSTEMS

by

YUNRUI LI

December 2018

Advisor: Dr. John Liu

Major: Electrical Engineering

Degree: Doctor of Philosophy

The Third Generation Partnership Project (3GPP) selected an in-band modem to transmit emergency data over cellular voice channel for the European Union emergency call (eCall) system. However, the road test results presented by the Harmonized eCall European Pilot project showed that the success rate of data delivery was only 71%, indicating that there is significant potential to improve its performance.

In this dissertation, a testbed is designed for the eCall system that satisfies the 3GPP TS 26.267/268/269 standards. A method is proposed to measure the power of the received signal that passes through the in-band channel. Experiments are performed with the in-vehicle system testbed in a laboratory or a car travelling in city, suburb, country- side, or freeway. Fading statistics of the received signal after power control are found and discussed, together with cumulative distribution function (CDF), level crossing rate (LCR), and average fade duration (AFD). It is found that with probability less than or equal to 0.1%, fading and attenuation can vary from -19 dB for the continuous wave (CW) signal at 500 Hz to -9.5 dB for the CW signal at 2000 Hz. This dissertation recommends moving the CW signals at 500 Hz and 800 Hz for

detection and synchronization in the 3GPP standard to 1500 Hz and 2000 Hz, respectively. This will give 9.5 dB improvement in detection and synchronization.

The fading results are used to calculate the bit error rate (BER) performance for the eCall in-band modem. Synchronization detection probability are obtained by transmitting the synchronization preamble through various adaptive multi-rate vocoders and an additive white Gaussian noise channel.

The testbed and proposed method are also used to measure the power of signals received by an unmanned aerial systems (UAS) and by the receiver in the operation center, respectively. Field experiments are carried out by flying the UAS above different locations. Statistics, including CDF, LCR, and AFD, are calculated for the six test-sites. The results of the fading statistics, synchronization detection probability, and BER can be directly applied to design real-time communication systems, including detection, delay estimation, modulation and coding.

AUTOBIOGRAPHICAL STATEMENT

Yunrui Li received his B.S. degree and M.S. degree from Beijing University of Chem- ical Technology in China. He is currently a Ph.D. candidate in the Advanced Communica- tions Research Lab at Wayne State University under the supervision of Dr. John Liu. His research focuses on in-vehicle emergency call system, embedded system design, channel fading model and statistics. He has published several research articles in peer-reviewed international conferences and journals. He is an active student member of IEEE.